The Role of BRCA2 in the Maintenance of Genome Stability in Response to Replication Stress

---

Dissertation

zur

Erlangung der naturwissenschaftlichen Doktorwürde
(Dr. sc. nat.)

vorgelegt der

Mathematisch-naturwissenschaftlichen Fakultät

der

Universität Zürich

von

Sofija Mijic

von

Arbedo-Castione TI

Promotionskommission

Prof. Dr. Massimo Lopes (Vorsitz und Leitung der Dissertation)

Prof. Dr. Alessandro Sartori

Prof. Dr. Martin Pruschy

Zürich, 2017

Dedicated to my family.

Our greatest weakness lies in giving up.
The most certain way to succeed is always to try just one more time.

Thomas A. Edison

Zusammenfassung

Eine fundamentale Eigenschaft des lebenden Organismus ist die akkurate Replikation des Genoms, um die exakte Weitergabe der genetischen Information über mehrere Zellteilungen zu gewährleisten. Die molekulare Maschinerie, die für die Replikation der DNA verantwortlich ist und an der sog. Replikationsgabel agiert, kann des Öfteren gestört werden durch sowohl extrazelluläre als auch intrazelluläre Hindernisse; dazu gehören zum einen Chemikalien oder UV-Strahlung, zum anderen Kollisionen der Replikationsmaschinerie mit anderen zellulären Prozessen wie zum Beispiel der Transkription. Diese Komplikationen können zur Verlangsamung oder zum Pausieren der Replikationsgabel führen, ein Phänomen, das wir Replikationsstress nennen.

Zellen haben eine Vielzahl von Mechanismen - definiert als Teil der sog. DNA Damage Response (DDR) - entwickelt, die ermöglichen, auf diesen Replikationsstress zu reagieren. Versagen dieser DDR Antwort kann zu DNA Schäden und letztendlich zu genomischer Instabilität führen, eine der treibenden Kräfte der Tumorgenese. Des Weiteren kann Replikationsstress gezielt durch Chemotherapeutika induziert werden, um die absolute Abhängigkeit der schnell replizierenden Zellen vom eigentlichen Replikationsprozess auszunutzen. Die Untersuchung der Mechanismen hinter dem Phänomen Replikationsstress hat sich deshalb als einer der Schlüsselansätze entwickelt, die Hintergründe der Krebsentstehung zu verstehen und neue therapeutische Ansätze zu entwickeln.

Unser Labor hat vor kurzem gezeigt, dass die Behandlung von Zellen mit genotoxischen Substanzen zu einer Verlangsamung, sowie zu einer Umgestaltung der Replikationsgabeln hin zu einer Four-way-Junction, einer sog. Reversed Fork, führt. Diese transiente molekulare Transaktion wird als eine Schutzreaktion angesehen, die den Bruch der Replikationsgabel in Stresssituationen verhindern kann. Des Weiteren hat unser Labor gezeigt, dass diese Umgestaltung der Replikationsgabel nicht nur durch exogene genotoxische Einflüsse ausgelöst werden kann, sondern auch durch endogene molekulare Prozesse, die bekanntlich die genomische Integrität gefährden, wie z.B. die Aktivierung (Überexpression oder Amplifikation) von zellulären Proto-Onkogenen.

In dieser Thesis präsentiere ich unsere Bemühungen zu verstehen, was die Umgestaltung der Replikationsgabel hin zur Reversed Fork in verschiedenen Kontexten auslöst und welches die Faktoren sind, die zu dieser Umgestaltung beitragen.

Im ersten Teil beschreibe ich unsere Strategien, neue induzierbare Überexpressionsystemen für Onkogenen in verschiedenen zellulären Modellen zu etablieren, mit dem Ziel, die Konsequenzen der Aktivierung verschiedener Onkogene auf ihre Gemeinsamkeiten und Unterschiede zu vergleichen. Auf Grund von hauptsächlich technischen Schwierigkeiten in der Etablierung von

effizienten und robusten Induktionssystemen für Onkogene hat dieser Teil der Arbeit bis jetzt nicht zu eindeutigen Ergebnissen führen können. Die Wichtigkeit dieser Frage (Onkogen-induzierter Replikationsstress in der Tumorgenese) bedarf einer Fortführung der Arbeit, mit besonderem Augenmerk auf dem Fine-tuning der Techniken, die eine zeitlich kontrollierbare Onkogen-Überexpression ermöglichen.

Im zweiten Teil dieser Thesis konnte ich erfolgreich erarbeiten, welche Funktion Proteine aus der homologen Rekombination (HR), vor allem die Tumorsuppressoren RAD51 und BRCA2, in der Umgestaltung der Replikationsgabel erfüllen. Neben ihrer bereits etablierten Rolle in der Reparatur von Doppelstrangbrücken (DSB) via HR sind RAD51 und BRCA2 bekannt dafür, pausierende Replikationsgabeln vor umfangreichem nukleolytischen Abbau zu schützen. Die Bedeutung dieser alternativen Funktion dieser Proteine wird durch die Beobachtung untermauert, dass Defekte im Schutz der Replikationsgabel zu chromosomaler Instabilität führen und, über einen unbekannten Mechanismus, zur Sensitivität von BRCA2-defekten Tumoren gegenüber Chemotherapeutika beitragen.

Unsere Ergebnisse zeigen, dass RAD51 an der Umgestaltung hin zur Reversed Fork beteiligt ist. Zudem haben wir erarbeitet, dass diese Strukturen in Abwesenheit von BRCA2 (BRCA2 Mutationen, die zum Funktionsverlust führen, sind eine Gemeinsamkeit vieler Tumorarten) zunehmend abgebaut werden. Inhibierung der Nukleaseaktivität oder ihre Rekrutierung zur Reversed Fork kann die Integrität der Reversed Fork wiederherstellen und den chromosomalen Abbau verhindern. Wird der Abbau der Reversed Fork jedoch dadurch verhindert, dass die Umgestaltung der Replikationsgabel an sich blockiert ist, führt dies zu einer Häufung an chromosomalen Brüchen in BRCA2-defekten Zellen, die die genomische Stabilität gefährden. Zusammenfassend zeigt unsere Studie, dass die Umgestaltung der Replikationsgabel hin zur Reversed Fork eine bedeutende physiologische Rolle im Schutz der genomische Stabilität gegen Replikationsstress spielt, und dass ein komplexes Zusammenspiel von HR Faktoren benötigt wird, um die DNA Replikationsgabel umzugestalten und zu stabilisieren.

Summary

A fundamental aspect of living organisms is the accurate replication and maintenance of the genome to ensure the high-fidelity inheritance of genetic information throughout many cell generations. The molecular machinery that replicates the DNA – acting at the so-called replication fork – can be frequently hindered by obstacles of both extracellular and intracellular origin, such as chemicals or UV radiations on one hand, and collision with other processes occurring on the DNA, like gene transcription, on the other. These challenges to DNA replication may lead to transient slowing or stalling of replication forks: we refer to this as replication stress.

Cells evolved a variety of mechanisms, which fall under the definition of DNA damage response, that allow them to respond to replication stress. Failure of these mechanisms can lead to DNA damage, and ultimately result in genomic instability, a major driving force of cancer. On the other hand, many chemotherapeutic compounds are designed to induce replication stress, exploiting the stringent requirement of highly replicating cancer cells to continuously replicate their genome. Therefore, investigating the mechanisms underlying replication stress has emerged as a key tool to both understand cancer onset, and to develop new therapeutic approaches.

Our laboratory has recently reported that, upon cellular exposure to genotoxic treatments, replication forks slow down and are frequently remodeled to form a detectable four-way junction at the replication fork, called reversed fork. This transient molecular transaction is considered to be a protective response, required to limit fork breakage in conditions of replication stress. In addition, our laboratory reported that, besides exogenous genotoxic treatments, fork reversal frequently occurs also in response to endogenous molecular processes, which are known to undermine genomic integrity, such as the activation (overexpression or amplification) of cellular proto-oncogenes.

In the current thesis, I will present our efforts to understand what triggers reversed fork formation in different contexts, and what are the factors that contribute to its formation and stability.

In the first part, I describe strategies we designed for the generation of new inducible oncogene overexpression systems in different cellular models, with the aim of describing the common or different molecular consequences downstream of aberrant activation of different oncogenes. This part has led to date to inconclusive results, mainly due to technical difficulties in establishing an efficient and robust oncogene induction system. The importance of this question (oncogene-induced replication stress in cancer) demands additional future work, and fine-tuning of the techniques for a time-controlled oncogene overexpression.

In the second part, I successfully investigated the function in replication fork remodeling of the proteins involved in homologous recombination, with particular attention on the tumor suppressors RAD51 and BRCA2. Besides their established role in double strand break repair via homologous recombination, RAD51 and BRCA2 were in fact known to protect stalled replication

forks from extensive nucleolytic degradation. Underlying the importance of this alternative function for these genes, defects in fork protection lead to chromosomal instability, and contribute to the sensitivity of BRCA2-defective tumors to chemotherapeutics by yet-unknown mechanisms. Our results showed that RAD51 contributes to reverse fork formation. Moreover, we found that these structures are progressively degraded in the absence of BRCA2 (loss-of-function mutations in BRCA2 are a common feature of many cancer types). Inhibiting MRE11 nuclease activity or its recruitment to the reversed fork can restore fork integrity and prevent chromosomal breakage. On the contrary, preventing fork degradation by impairing the formation of reversed forks, leads to increased chromosomal breakage in BRCA2-defective cells, being thus detrimental for genome stability. Collectively, our study reveals that fork reversal has a crucial physiological relevance in protecting genome stability upon replication stress, and that a complex interplay of HR factors co-operate to remodel and stabilize stalled DNA replication forks.

1. Introduction

The year 2015 was a very exciting year for the DNA repair field. Three scientists - Tomas Lindahl, Paul Modrich, and Aziz Sancar - were awarded the Nobel Prize in Chemistry for their pioneering studies on biochemical mechanisms in three of the major DNA repair pathways: base excision repair, mismatch repair and nucleotide excision repair, respectively. Moreover, the prestigious Albert Lasker Basic Medical Research Award honored Evelyn M. Witkin and Stephen J. Elledge for their discoveries concerning the DNA damage response, the mechanism that protects the genomes of all living organisms.

The importance of these discoveries is emphasized by the fact that every human cell faces the daunting task of faithfully replicating the 6×10^9 nucleotides of genomic information which is stored into DNA molecules and packaged as chromatin. However, during the life of any organism, the genome is constantly challenged by exogenous and endogenous factors, which can damage DNA, generating approximately 10^4-10^6 lesions per day. Although genetic variation is important for evolution, the survival of the individual demands genetic stability.

Mistakes in DNA replication introduce mutagenic DNA lesions or genomic instability, both of which have been linked to the onset of many diseases, including cancer. Cells respond to DNA lesions by activating the DNA damage checkpoint and by using different repair pathways. The coordinated action of both processes is known as the DNA damage response (DDR).

1.1 DNA Replication in Eukaryotes

Cellular proliferation is an essential process during the development and maintenance of an organism. Every cell division cycle requires the faithful duplication of the entire genome to assure high-fidelity transmission of genetic information from parental cell to daughter cells. Therefore, it is of prime importance that the genome is replicated once and only once and then segregated equally to the daughter cells. This mechanism, conserved from prokaryotes to eukaryotes, is known as semiconservative DNA replication and it is broken down into separate steps - initiation, elongation, and termination - that are carried out at distinct cell cycle stages and depend on a set of tightly regulated factors.

DNA replication starts with the assembly of the replisome complex at genomic sites that are termed origins of replication (Ori)[1]. Origins are selected through binding of the origin recognition complex (ORC), which consists of six proteins ORC1-ORC6. During G1 phase, DNA replication

factor 1 (CDT1) and cell division cycle 6 (CDC6) proteins associate with Ori sites throughout the genome and facilitates the recruitment and loading of inactive double-hexameric mini-chromosome maintenance 2–7 (MCM2-7) helicase. This results in the generation of a prereplication complex (pre-RC), which licenses the origin to fire in the following S phase. Many of the licensed origins will not fire during normal replication but provide backup origins in case of replication slow down or failure (Figure 1).

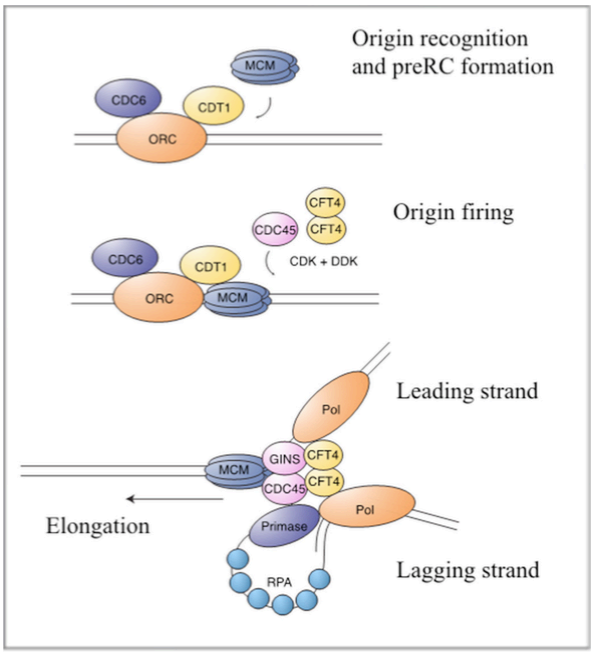

Figure 1 Schematic representation of replication initiation, origin firing and elongation. Origin recognition and formation of pre-RC complex implicates binding of ORC to DNA and subsequent loading of MCM2-7 helicase complex via the action by Cdc6 and CDT1. CDK and DDK-dependent activation of pre-RC components leads to Cdc45 loading, resulting in origin firing. Helicases and associated proteins unwind DNA. ORC, Cdc6 and Cdt1 dissociate from DNA and the chain elongation starts. Modified from (Claus Storgaard Sørensen, 2011).

At the onset of S phase, origin firing is brought about by the activity of cyclin-dependent kinase 2 (CYCE-CDK2) and Dbf4/Drf1-dependent CDC7 kinase (DDK). DDK and CDKs phosphorylate several replication factors like CDC45, GINS and DNA polymerase ε (POL ε) to promote their loading on origins[2]. MCM2–7 double hexamer is also phosphorylated and together with CDC45 and GINS form the active helicase (CMG) required for DNA unwinding. At this point, replication protein A (RPA) binds to single strand DNA (ssDNA) to stabilize the replication fork[3]. The topological tension generated by DNA helix unwinding is released by topoisomerase, which cuts either one (topoisomerase I, TOP1) or both (topoisomerase II, TOP2) strands of DNA double helix and re-anneals them. DNA polymerases must use a 3'-OH of a nucleoside as a primer and synthesize DNA in the 5'-3' direction. Since DNA consists of antiparallel strands, they are copied differently, with one strand synthesized continuously (leading strand) and the opposite strand copied in short segments (Okazaki fragments), which are joined together postreplicatively (lagging strand). Both the leading strand and every Okazaki fragment on the lagging strand are primed by a short RNA primer synthesized *de novo* by polymerase α-primase. The latter is replaced by DNA polymerase δ and ε to continue synthesizing the complementary strand of DNA in the lagging strand and the leading strand respectively. Replication factor C (RFC) and proliferating cell nuclear antigen (PCNA) regulate the switch between polymerase α-primase and

replicative polymerases δ and ε and act as loading platform for DNA ligase I and flap endonuclease I (FEN-1) for maturation of Okazaki fragments[4].

Little is known about termination process of DNA synthesis. Since multiple origins are fired on each chromosome, termination of replication occurs when two opposing replication forks meet and the nascent DNA from the two forks is ligated together. This process involves completion of DNA synthesis, decatenation of daughter molecules and replisome unloading. Resolution of steric hindrances of the merging forks and topological constrains requires TOPII[5]. The mechanism of replisome disassembly is still under investigation. Recent studies have identified factors that regulate unloading of MCM2-7: MCM-BP[6] or p97/VCP/CDC48 protein remodeler[7,8].

1.2. Replication stress and DDR

Even before the discovery of the DNA structure in 1953, researchers have showed that exogenous agents, such as irradiations or chemicals can cause genetic alterations that might lead to cancer[9]. Many years after DNA structure has been defined, researchers discovered that DNA could be damaged also from endogenous sources during normal metabolism like reactive oxygen species (ROS)[10] or stochastic misincorporation of nucleotides. In addition to these lesions, intrinsic replication-fork obstacles such as unusual DNA structures or transcription complex can interfere with the progression of DNA replication, thereby causing the forks to slow down or stall. This phenomenon is defined as replication stress and is among the primary cause of genome instability and tumorigenesis.

To preserve genome integrity, cells have evolved sophisticated mechanisms, collectively known as DDR[11]. Via these mechanisms cells can detect DNA lesions and promote cell cycle arrest. This allows the cells to either repair or bypass the damage. When the repair of the lesion is not possible or is incomplete, DDR triggers senescence or programmed cell death.

In 2005, work from Halazonetis[12] and Bartek[13] groups showed that most cancers, in their early state, display varying degrees of replication stress, accompanied by activation and increased expression of various DDR components. A failure in DDR activation, or mutations in DDR factors, causes tumor progression. These findings established replication stress as a causative event in cancer and the DDR as an important barrier against tumor formation and progression.

It is important to note that, even though replication stress can be a prominent cause of tumorigenesis, it also has the potential of being a target for cancer therapy. In fact, when replication stress occurs at low to mild levels, it can fuel tumorigenesis. Conversely, current cancer chemotherapies are meant to induce high levels of replicative stress, which causes cancer cell death through mitotic catastrophe, thereby counteracting cancer progression.

1.2.1 Sources of replication stress

Faithfull DNA replication requires processive and stable replication forks, which however encounter many obstacles on their path[14]. Template unwinding by helicases can be impaired by topological constraints, such as DNA secondary structures like hairpins or G-quadruplexes, intra-strand crosslinks or tightly DNA bound proteins. Progression of DNA polymerases can be directly impaired by unrepaired DNA lesions (nicks and gaps, misincorporated ribonucleotides, DSB or bulky base-adducts) or by shortage of replication machinery components and nucleotides. Additionally, during S phase DNA polymerases compete for the same template with other enzymes like RNA polymerases. Although cells have evolved a spatio-temporal segregation to

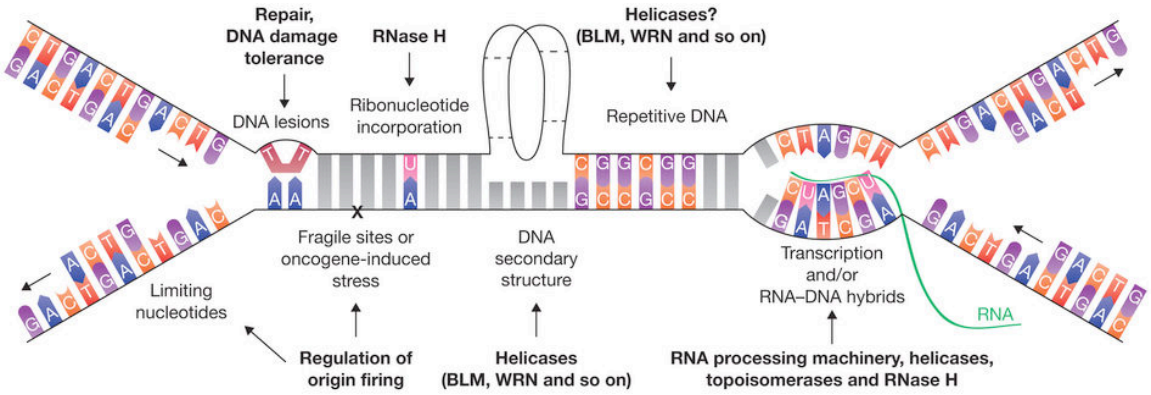

Figure 2 Sources of replication stress. Schematic representation of obstacles that can impair replication fork progression and induce replication stess. Modified from (Zeman and Cimprich, 2014).

minimize replication-transcription conflict, certain conditions like RNA polymerase blockage or unresolved R-loops can cause these two machineries to collide, thus inducing replication stress[15]. Finally, overexpression or constitutive activation of oncogenes increases origin firing, which depletes nucleotide pools and decreases replication speed, resulting in replication fork collapse. As described in more details below, by perturbing the timing of replication initiation and progression, oncogenes can disrupt spatio-temporal separation that normally prevents collision between transcription and replication (Figure 2).

Oncogene activation. Many oncogenes have been reported to cause replication stress when activated[12,13,16]. In pre-neoplastic lesions, the DDR signaling is constitutively activated, providing a natural barrier that delays or prevents malignant transformations through the induction of senescence or apoptosis. Interestingly, analogous constitutive DDR activation can be recapitulated *in vitro* by overexpression of various oncogenes such as CYCE, E2F1 and cell division cycle 25 homolog A (CDC25A), linking oncogene-induced replication stress and tumorigenesis[13,17,18]. The DDR activation has been attributed to unspecified alterations of bulk DNA replication and DSB accumulation, particularly in regions intrinsically difficult to replicate[19,20]. Despite the accumulated evidence indicating that oncogene-induced replication stress is a major driving force in the early stages of tumorigenesis, its molecular basis is still largely unclear. A widespread consequence of oncogene activation is the overriding of cell-cycle checkpoints before the S phase, thereby forcing cell proliferation. Two opposite mechanisms have been proposed: insufficient or excessive usage of replication origins[21]. Overexpression of CYCE can impair MCM2-7 binding to the chromatin resulting in a reduced number of replication origins that are licensed during G1. Consequently, replication stress increases in S-phase due to the shortage of back-up origins to cope with stalled forks[22]. In contrast, the overexpression of certain oncogenes (c-MYC, H-RAS, CYCE, CYCD2) can have the opposite effect and generally increase the origin

firing or origin reactivation within the same cycle of replication by deregulating CDK activity or gene expression of origin licensing factors like CDT1 or CDC6. In particular c-MYC has been found to transcriptionally regulate the expression of cell-cycle-related genes and to directly interact with components of pre-RC at DNA replication origins. Increase in origin firing can drive an unscheduled proliferative burst and/or re-replication of the DNA that result in replication slow down and stalling, due to increased replication-transcription collisions and/or the depletion of nucleotides pool[23,24]. This is supported by the fact that supplementing cancer cells with exogenous nucleotides or inhibiting transcription helps preventing genomic instability. However, it remains unclear how these perturbations at the replication forks results in DSB formation that promotes chromosomal rearrangements.

In our laboratory, we studied the molecular basis of the oncogene-induced replication stress and the DNA breakage, focusing on the conditional overexpression of two well-characterized oncogenes: i) CYCE, the regulator of replication initiation in complex with CDK2, and ii) CDC25A, a phosphatase involved in DNA damage response and activation of CDKs throughout the cell cycle[25]. Both oncogenes substantially slowed down replication fork progression as reported earlier, and surprisingly also induced the accumulation of reversed forks (four-way junction structures discussed in detail in section early after their activation). Despite similar rapid effects on the replication process, the two oncogenes induced DNA damage with different kinetics and penetrance. CYCE-expressing cells showed slow and mild accumulation of DSBs because they could transiently delay mitotic entry and resolve the unusual replication structures. Cells overexpressing CDC25A, on the other hand, entered mitosis prematurely and rapidly accumulated massive DNA breakage and activated full DDR due to unscheduled processing of reversed forks by MUS81.

In another study in our laboratory, we deregulated origin licensing by early mitotic inhibitor 1 (EMI1) depletion to induce and study DNA re-replication, a specific alteration of DNA replication frequently found upon oncogene activation[26]. By directly visualizing replication intermediates at electron microscopy (EM), we observed DDR-blind accumulation of ssDNA during the first replication round. Uncontrolled reactivation of replication origins, in this context, triggered chromosomal breakage when re-replication forks approached discontinuities on the template.

It is currently unknown whether the molecular events described for CYCE and CDC25A can be proposed as a general model for other oncogenes that induce replication stress through different mechanism of action and can be correlated with their diverse tumorigenic potential, in particular H-RAS and c-MYC. H-RAS is a G protein whose activity is regulated by the binding of guanine nucleotides. Following activation by upstream receptor tyrosine kinases, RAS proteins exchange GDP with GTP and activate several effector pathways involved in cell cycle regulation and transcription, the best characterized of which are rapidly accelerated ribrosarcoma (RAF), Phosphoinositid-3-Kinasen (PI3K) and RAL guanine nucleotide exchange factors (RAL-GEFs).

Cancer-associated mutations in *H-RAS* genes generally act by locking the RAS proteins in the GTP-bound constitutively active state, and such mutations are frequently found in human cancers[27,28]. C-MYC is a transcription factor of the helix-loop-helix/leucine zipper class of proteins that heterodimerize with myc-associated factor X (MAX) protein and bind specific DNA sequences known as E-boxes[29]. MYC regulates a complex biological program by transcriptionally activating and repressing its numerous target genes. As such, MYC is a master regulator of key cellular functions, including cell cycle entry, DNA replication, ribosome biogenesis, and metabolism[30,31]. Additionally, c-MYC has also a non-transcriptional control of DNA replication by interacting with pre-replicative complex[32]. The *MYC* oncogene was first implicated in Burkitt's lymphoma[33] and later showed to be mutated in nearly all types of human cancers[34].

1.2.2 Cellular response to replication stress

DDR is a complex arsenal of interacting pathways that, similarly to developmental molecular cascades, has signal sensors, transducers, and effectors[11].

Contrary to the signaling pathways that are triggered by ligands of receptor kinases, the DDR is activated by unusual DNA structures formed in response to DNA damage or DNA replication stress. The main regulators of the DDR belong to the family of the phosphatidylinositol 3-kinase-like protein kinase (PIKK), which includes, in particular, ataxia-telangiectasia mutated (ATM), and ATM-and-RAD3-related (ATR). ATM triggers a response to various stimuli, but most prominently to DNA double strand breaks (DSBs). In contrast, ATR is activated upon ssDNA and is therefore the major kinase mediating the response to replication stress[14].

Impediments on the DNA that specifically stall the DNA polymerase lead to physical uncoupling of the polymerase from the replicative helicase, which continues unwinding and generates extended ssDNA at the replication fork. ssDNA is also generated during DNA repair, as a of controlled nuclease-dependent resection of DSBs during the S- and G2-phase. In both cases, the ssDNA is readily coated by RPA, which recruits and activates ATR through the action of its associated factor ATR-interacting protein (ATRIP). The importance of this mechanism is emphasized by the fact that loss of ATR and other components of the pathway is embryonically lethal, while hypomorphic mutations cause developmental disorders, like ATR-Seckel syndrome[35]. Once activated, ATR amplifies the DNA damage signal by phosphorylating several repair and checkpoint proteins at Ser/Thr-Glu motifs. Among the latter are checkpoint kinase 1 (CHK1), histone H2AX and tumor protein p53. CHK1 himself triggers a second wave of phosphorylation events aiming to promote resolution of the stress and to ensure the completion of DNA synthesis. Locally, ATR-CHK1-mediated signaling regulates different components of the replisome to slow DNA synthesis, stabilize and restart stalled forks, and suppress recombination. Globally, the ATR-CHK1 pathway inhibits cell-cycle progression and prevents late origin firing[36].

ATM is activated upon DSB formation. ATM mutations lead to a neurodegenerative and cancer-prone disorder called ataxia telangiectasia[37]. Its effector kinase is checkpoint kinase 2 (CHK2), which similarly to CHK1 phosphorylates proteins that regulate cell cycle and DNA damage repair. Mild cancer-relevant replication stress has been largely uncoupled from DSB formation[25,26,38–40], therefore ATM is considered to have a less prominent role during replication. Nevertheless, ATM pathway also slows DNA replication in response to DNA damage, stabilizes and repairs damaged replication forks[11].

It must be noted that not all sources of replication stress lead to long ssDNA formation. Along the same line, replication stress is not necessarily associated with detectable checkpoint activation. There is not yet a well-defined set of cellular markers that characterize all types of replication stress and the outcomes in the cell are not entirely understood. As a result the definition of replication stress is still evolving[14].

Stabilization of the stalled replication forks. In eukaryotic cells, replication fork breakdown constitutes a major source of genomic instability and it is therefore important to preserve its integrity, especially during replication stalling. Immunoprecipitation experiments in yeast showed that ATR-CHK1 pathway stabilizes the replisome at stalled forks[41], but this view has been later challenged by biochemical studies showing that replisome stability upon fork stalling is independent from checkpoint kinases[42]. One way to interpret these conflicting data is to postulate that the replisome does not disassemble, but moves away from the site of DNA synthesis, and that the role of ATR-CHK1 pathway is to control exonuclease and endonuclease activities that potentially process unprotected DNA at stalled forks.

In addition to checkpoint factors, also homologous recombination (HR) proteins appear to be involved in the protection of arrested forks. Studies in vertebrates have shown that breast cancer 1 and 2 (BRCA1/2) and Fanconi Anemia (FA) proteins stabilize RAD51 filaments at stalled forks, thereby protecting nascent strands from excessive Meiotic recombination 11 (MRE11)-dependent degradation[39,40,43]. This process will be extensively discussed in the section 1.3.3.

Mechanisms of replication fork processing and restart. Several cellular mechanism have been described to explain the processing and the restart of stalled replication forks and their relevance vary depending on the cause of fork arrest and genetic background[44] (**Figure 3**):

(i) unreplicated regions caused by the stalling of a fork can be synthesized by the neighboring active replication fork; (ii) activation of the dormant origins in the proximity of stalled forks further promotes replication completion; (iii) re-priming DNA synthesis downstream of an obstacle and filling the ssDNA gap left behind; (iv) activating the DDT pathway that permits bypassing the lesion by recruiting specialized DNA polymerases (also known as ‘translesion DNA synthesis’) or by using the sister chromatid as alternative template via recombination-based and post-replicative

repair mechanisms (template switch); (vi) structure-specific endonucleases such as MUS81 and Essential Meiotic Structure-Specific Endonuclease 1 (EME1) can generate one-ended DSB and the DNA synthesis is then reinitiated by a HR variant called break induced replication (BIR); (vii) the replication fork can be remodeled to form a more stable four-way junction structure called reversed fork.

Despite the relative importance of each of the above-mentioned pathways, investigating the molecular events underlying the replication fork reversal constitutes the founding rationale of the work presented in this thesis.

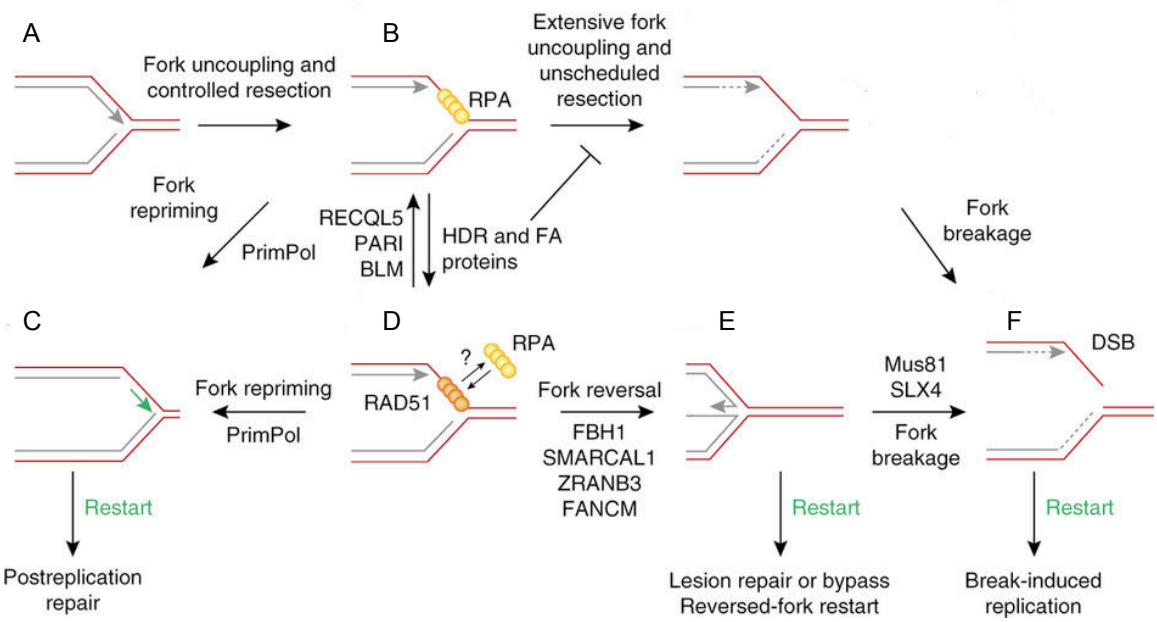

Figure 3 Mechanisms of replication fork processing and restart. (A-B) Replication-fork uncoupling through functional dissociation of helicase from polymerase leads to ssDNA accumulation at the fork. Alternatively, ssDNA may result from nuclease-mediated resection of stalled forks. ssDNA is rapidly coated by RPA (yellow spheres). (C) DNA synthesis can be re-primed (green arrow) and reinitiated ahead of the lesion. The resulting gaps are repaired post replicatively by a recombination-based mechanism or by specific translesion synthesis (TLS) polymerases. (D) RAD51 (orange spheres) binds to ssDNA at stalled forks and drives fork reversal. (E) Fork reversal prevents collisions between the moving fork and the lesion, allowing the time for the repair of the lesion. (F) Prolonged fork stalling promotes fork cleavage by structure-specific endonucleases. Broken forks resume DNA synthesis by the error-prone BIR mechanism. Modified from (Berti and Vindigni, 2016).

1.2.3 Replication fork reversal

Besides replication slowdown, ssDNA gaps and γH2AX foci, there is a peculiar feature that accompanies replication stress at the DNA level: replication fork reversal[45].

Replication fork reversal is defined as the conversion of the replication fork into a stable paused four-way junction structure by the unwinding of newly synthesized strands from their template, the re-annealing of the parental strands and the annealing of the newly synthesized strands to each

other, to form a fourth regressed arm at the fork elongation point (Figure 4). This DNA transaction structure was first proposed in 1976[46], and for a long time it was found only in prokaryotes and specific yeast mutants[47].

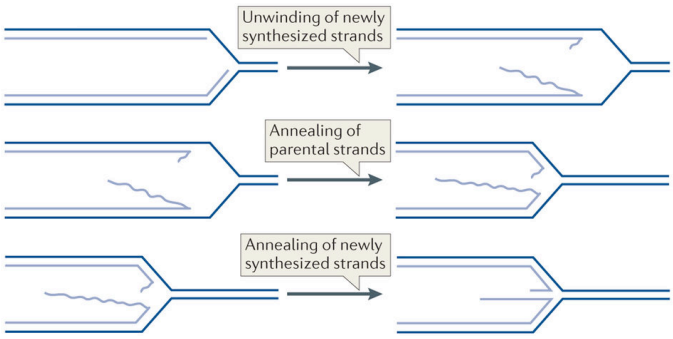

Figure 4 The process of replication fork reversal. During fork reversal, the three-way junction at the replication fork is converted into a four-way junction and is backtracked along the replicating DNA molecule. This includes the unwinding of newly synthesized strands, annealing of the parental strands and annealing of the newly synthesized strands. Modified from (Neelsen and Lopes, 2015).

First piece of evidence that supported the physiological relevance of the replication fork reversal during replication stress in human cells arose from studies in our lab using TOP1 inhibitors like camptothecin (CPT)[38]. Here, it was shown that, upon TOP1 inhibition, replication forks undergo rapid slowdown and frequent reversal to prevent the collision with the damaged DNA ahead of the fork, thereby limiting DSB formation. Further studies identified replication fork reversal in response to oncogene activation[25], deregulated origin licensing[26], secondary DNA structures[48] and to a full set of chemotherapeutic treatments[49], suggesting fork remodeling in eukaryotes as a general physiological strategy to cope with different types of replication stress. Poly (ADP-ribose) polymerases (PARP) inhibition, one of the most promising chemotherapy treatment for breast cancer and ovarian cancer[50,51], was the first condition found to impair effective fork reversal[38], suggesting that the molecular determinants orchestrating fork remodeling may be novel attractive target for combinatorial cancer chemotherapy.

Extensive effort from our laboratory, in collaboration with other groups, allowed the identification of an initial set of human factors involved in the formation, processing or restart of reversed replication forks. Although many DNA translocases, like SWI/SNF-related matrix-associated actin-dependent regulator of chromatin subfamily A-like protein 1 (SMARCAL)[52] or helicase like transcription factor (HLTF)[53], can drive fork reversal *in vitro*, a clear *in vivo* function has been so far confirmed by direct visualization of reversed forks only for the helicases F-box DNA helicase 1 (FBH1)[54] and zinc finger RANBP2-Type containing 3 (ZRANB3)[55].

Moreover, increasing evidence suggests that several HR factors possess a DSB repair-independent role in replication stress response. In particular, the recombinase RAD51 is required to drive fork reversal in response to mild genotoxic treatments[49]. Thorough analysis of the replication intermediates isolated from challenged cells revealed accumulation of extended ssDNA at the fork junctions, reflecting uncoupling between DNA polymerase and the helicases involved at the fork. Importantly, there is a marked correlation between the frequency of fork

reversal and the extent of ssDNA regions at the fork[49]. By analogy to DSB repair (see Chapter 3.2), the recombinase RAD51 is proposed to be recruited to the extended ssDNA where, by recombinational strand exchange, contributes to the conversion of uncoupled forks into reversed forks. Intriguingly, this appears to be true not only for treated cancer and primary cell lines, but also for unperturbed mouse embryonic cells[56]. In these cells fork reversal is very frequent, and it is possibly required for coping with high levels of replication stress caused by fast cell cycle progression. Also in this context RAD51 is required for fork remodeling and its loss leads to marked chromosomal breakage. These findings implicate that such fork remodeling function, rather than its well-known role in DSB-repair, may represent the essential role of RAD51 during early embryogenesis. We speculate that this might possibly be the case for other HR factors.

However, our mechanistic understanding of the role of HR factors in replication fork remodeling is still very limited. In principle, HR-mediated transactions can be envisaged in both steps of fork remodeling, fork reversal and fork restart[45] (**Figure 5 a**).

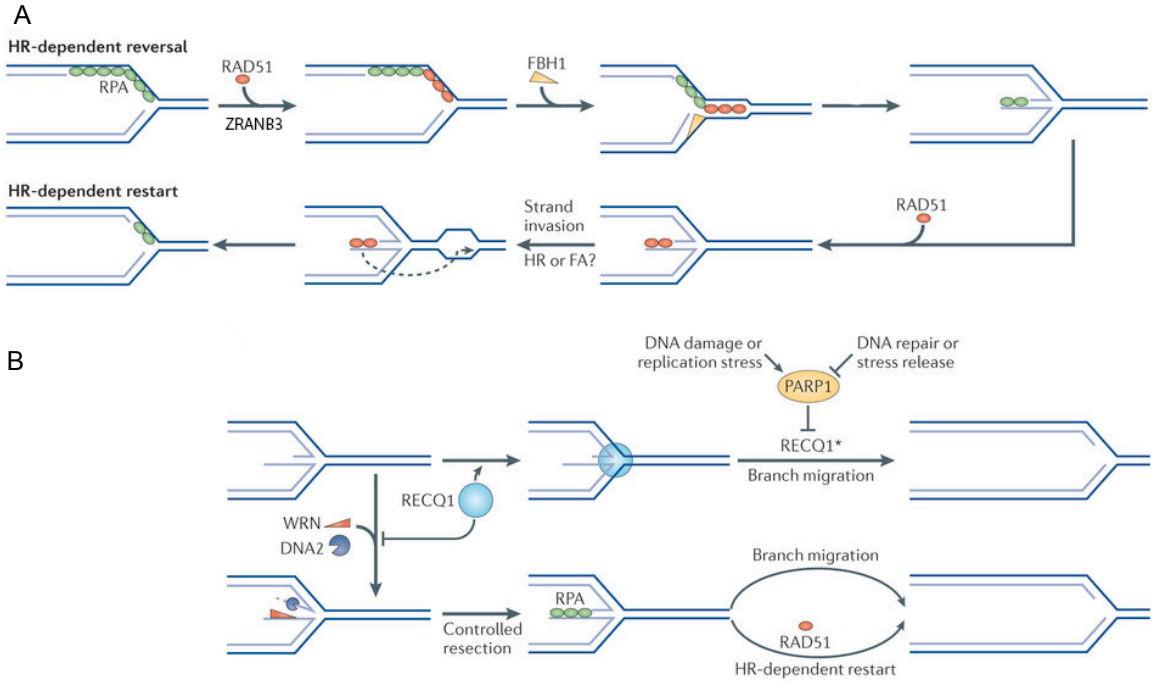

Figure 5 Role of homologous recombination factors in replication fork remodelling. (a) The top panel shows that following replication stress and fork uncoupling, RAD51 binds to extended ssDNA regions at the fork. Assisted by ZRNB3 and FBH1, RAD51 mediates fork reversal. Once reversed fork is formed, the regressed arm is processed by the controlled action of DNA2 and WRN to recruit RAD51 (bottom panel), promote homology-driven invasion of the re-annealed template strands and drive recombination-mediated fork restart. (b) RECQ1 binds to reversed fork and primes the restart through branch migration mechanism. PARP1 stabilizes reversed forks by transiently inhibiting RECQ1. When the DNA is repaired and replication stress released, PARP is inactivated. RECQ1 binding at the reversed forks inhibits the fork restart via DNA2/WRN mechanism. The resected regressed arm may recruit and alternative branch migration factors, or promotes homologous recombination-dependent restart. Modified from (Neelsen and Lopes, 2015).

While strand exchange events are indeed required to drive fork reversal, controlled resection of the regressed arm – remarkably similar to a DSB - may also prime RAD51-dependent homology search and strand exchange reactions with the duplex ahead of the fork and provide one of the mechanisms to restart reversed forks once the stress is released. In condition of RecQ-like 1 (RECQ1) loss, the nucleolytic resection of the regressed arm to form a 3' overhang is mediated by the combined activity of Werner (WRN) and DNA replication ATP-dependent helicase-like homolog (DNA2). Here, the role of DNA2 is independent of the DSB resection activities of proteins such as (CTBP interactin protein) CtIP, MRE11 or exonuclease 1 (EXO1)[57]. Further mechanisms of regressed arm processing in pathological conditions, like upon BRCA2 mutation, are extensively discussed in the section 1.3.3. Resection of the regressed arm in physiological conditions is still largely unknown.

Several important questions are still open: which co-factor assist RAD51 loading at stalled forks upon replication stress? Is loading of RAD51 different during formation and restart of reversed forks? What is the role of HR factors that are involved in maintaining the stability of the stalled forks, like BRCA1 and BRCA2, in fork remodeling? These questions need to be tackled to fully understand the events underlying fork remodeling, especially considering that many of these factors involved are tumor suppressor genes often mutated in human syndromes displaying genomic instability.

Besides a recombination-mediated fork restart, a branch migration-assisted reestablishment of a functional replication fork has been described. Here, the human RECQ1 helicase drives the restart of reversed forks, and its activity is strictly limited by PARP1-mediated ADP ribosylation, until the damage is repaired[58] (**Figure 5 b**)

When the damage persists and the fork fails to resume, the reversed forks might represent a preferred substrate for structure-specific nucleases. Indeed, MUS81 is linked to chromosomal breakage after prolonged fork stalling, and more recently it was shown to cleave reversed forks upon oncogene-induced replication stress[25,59]. Similarly, SLX4 targets replication forks regressed by SMARCAL1 following nucleotide depletion[60]. Normally, these nucleases act in late-S or G2 phases of cell cycle, thus their activation could represent the last attempt to complete the replication before the cell division.

How cells choose between these apparently redundant mechanisms of replication fork processing and restart is still unknown. Moreover, mechanistic understanding of the turnover and position of the replisome components and specific chromatin marks during fork reversal is currently very limited.

1.3. BRCA2: from DNA damage repair to replication fork protection

BRCA1 and BRCA2 are tumor suppressors that participate in a variety of DDR and genome stability processes - in particular DSBs repair, interstrand DNA crosslink repair via the FA pathway, DNA damage checkpoint activation and protection of DNA replication forks upon replication stress[61].

BRCA1 and *BRCA2* were identified as genes mutated in hereditary breast and ovarian cancer in 1994[62] and 1995[63], respectively. The average cumulative risks by age 70 years for *BRCA1* carriers is estimated to be 60% for breast cancer and 59% for ovarian cancer. For *BRCA2* carriers, the corresponding risks are 55% for breast cancer, 16.5% for ovarian cancer[64]. The numbers are frighteningly high.

BRCA-mutated tumors are defective in DNA repair and display genetic instability. This opens a therapeutic window by making tumor cells exquisitely sensitive to DNA damaging drugs, like crosslinking agents (e.g.cisplatin) and PARP inhibitors[65]. In the latter case it is exploited the genetic concept of synthetic lethality[66]. It describes the situation in which defects in either one of two genes individually is compatible with life, but simultaneous loss of both genes results in cell death. Inhibition of PARP1 has been shown to be synthetically lethal with deficiency of BRCA genes. PARP1 is involved in various DNA repair pathways, including ssDNA repair pathway[67]. It was proposed that PARP inhibitors caused an increase of single-strand breaks, which are converted to DSBs during replication. Replication-associated DSBs are irreparable in the absence of HR, and are therefore toxic in the context of BRCA deficiency. Cells carrying *BRCA* mutations are up to 1,000 times more sensitive to PARP inhibitors than wild-type cells, therefore PARP inhibitors such as Olaparib continue to be among the most promising and attractive treatment options for BRCA-deficient tumors[50,51,66].

Given the malleable nature of cancer cells, unfortunately even tumors carrying mutations in *BRCA* genes acquire resistance. Understanding the fine mechanistic detail of BRCA functions and mechanisms that drive chemoresistance in mutant tumors will open new opportunities for clinical applications.

The work presented in this thesis is focused on the role of the BRCA2 protein.

1.3.1 BRCA2 functional domains

BRCA2 is a large protein of 384 kDa, composed of 27 exons and exist predominantly as a homodimer [61]. Several key domains have been identified in BRCA2 in the past two decades (**Figure 6**). Through these domains, BRCA2 forms complexes with several proteins, implicating

BRCA2 in multiple cellular functions such as DNA repair, DNA replication, telomere homeostasis and cell cycle progression. N-terminus interaction with partner and localizer of BRCA2 (PALB2) connects BRCA2 to BRCA1: the formation of this tripartite complex is critical for its role in HR (see paragraph 1.3.2). The central part contains eight conserved BRC repeats, required for RAD51 binding. Interactions between the BRC repeats and RAD51 occur through the ATPase core of RAD51, and these interactions maintain RAD51 in a form that is mostly monomeric. Downstream of the BRC repeats there is a DNA-binding domain (DBD), which consists of a helical domain (H), three oligonucleotide binding (OB) folds, and a tower domain (T). Their combined action facilitates BRCA2 binding to both single-stranded DNA and double-stranded DNA. The C-terminal part of BRCA2 contains a nuclear localization signal (NLS) critical for its cellular localization and a TR2 domain, an additional RAD51 binding site. This binding is crucial in response to DNA damage, when RAD51 is delivered to sites of DNA damage and interaction between the C-terminal region of BRCA2 and RAD51 serve to stabilize the filaments on ssDNA. Of note, BRCA2 is post-translationally modified by CDK and other DNA Damage dependent kinases (ATM/ATR, CHK1/2) in a cell cycle-dependent fashion. Among the multiple phosphorylation sites there is S3291, whose phosphorylation abrogates BRCA2-RAD51 interaction at G2/M[68].

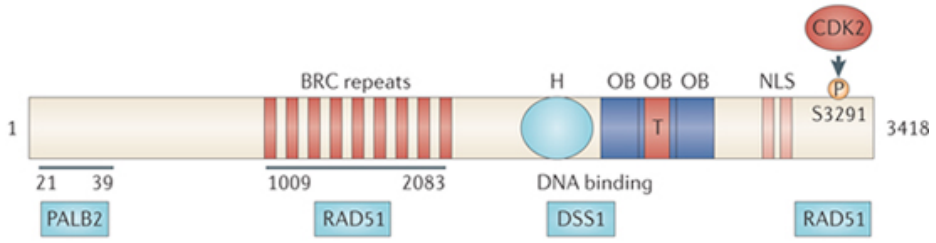

Figure 6 Structure of BRCA2. The N terminus of BRCA2 mediates PALB2 binding. Its central BRC repeats and C-terminal domain interact with RAD51. The BRCA2 DNA binding domain contains oligonucleotide binding (OB) domain, helical domain (H) and a tower domain (T) and mediates BRCA2 interaction with ssDNA and dsDNA. This region also binds deleted in split-hand/split-foot syndrome (DSS1). CDK phosphorylation site at S3291 is indicated.

1.3.2 BRCA2 is a key factor in DSB repair by HR

Among DNA types of damage, DSBs are the most menacing lesions for a cell. If left unrepaired, they may cause mutations or broader chromosomal aberrations, both of which are hallmarks of cancer[11].

DSB are induced by DNA-damaging agents such as irradiation (IR) and DNA topoisomerase inhibitors (e.g. CPT), or arise spontaneously due to endogenously generated reactive oxygen species or collapsing DNA replication fork. Although most DSBs are not desirable, cells possess

specific enzymes that can introduce breaks in important physiological processes, like meiotic recombination or maturation of the immune system (e.g. the class-switch and V(D)J recombination in B- and T-lymphocytes).

In higher eukaryotes, classical nonhomologous end joining (c-NHEJ) and HR are the main DSB repair pathways. Importantly, while the first acts throughout the cell cycle and rely on rapid ligation of the two ends with little-to-no DNA end processing, the second is restricted to the S/G2 phase and requires extensive DNA resection. The regulation of DSB resection, therefore, acts as the key determinant in committing the repair of DSB to C-NHEJ or to HR pathway. These two pathways are described in more detail in the sections below.

Which pathway to choose is a critical step for repairing DSBs[69]. Two fundamental regulators of this choice have been identified: tumor suppressor p53 binding protein 1 (53BP1) and BRCA1. 53BP1 promotes NHEJ by antagonizing resection of DSBs, whilst BRCA1 channels DSB repair into HR[70]. In G1 phase, 53BP1 inhibits the resection of DSBs by recruiting the two effectors Pax transactivation domain-interacting protein (PTIP), and RAP1-interacting factor 1 (RIF1). PTIP and RIF1 bind to sites of 53BP1 that are phosphorylated by ATM. 53BP1-RIF1 complex acts under both physiological (Class switch recombination) and pathological conditions, while 53BP1-PTIP pathway functions only under pathological conditions to promote NHEJ[71,72]. These interactions repress the recruitment of the pro-resection factor BRCA1. Indeed, in RIF1- or 53BP1-depleted cells, BRCA1 can form foci in G1. Antagonistically, in coordination with CtIP during S/G2 phase, BRCA1 prevents the accumulation of 53BP1, RIF1 and PTIP at the break sites. There are additional layers of control that regulate the choice of the repair pathway at DSBs. Some examples are the DNA end protection by Ku heterodimer[73], which blocks resection in G1, or the TONSL-MMS22L complex, which recognizes de novo loaded histone H4 during replication to mark post-replicative chromatin, and favor HR[74]. HR is further supported by CDK activity, which targets multiple end processing factors, such as CtIP and EXO1 to stimulate end resection[75].

Classical nonhomologous end joining. Shortly, during NHEJ, DSBs are rapidly recognized and bound by the Ku heterodimer (Ku70 and Ku80), as a consequence of its extremely high affinity for DNA ends[76]. The most prominent function of Ku is to protect DSB and recruit DNA-dependent protein kinase (DNA-PK)[77]. DNA-PK phosphorylates an array of DDR proteins and most importantly auto-phosphorylates itself on two distinct regions: the so-called PQR and ABCDE phosphorylation clusters. Auto-phosphorylation of the ABCDE residues dampens the interaction between DNA-PK and the DNA ends, thereby facilitating end joining. In contrast, auto-phosphorylation at PQR cluster inhibits DSB processing, which in turn blocks DSB repair via HR[78]. At this point, a nuclease called ARTEMIS is recruited at the DNA ends, resulting in nucleotide gaps subsequently filled by DNA polymerases μ, λ and TdT. DNA ends ligation can then be executed by the essential DNA ligation complex DNA ligase IV/XRCC4/XLF. In C-NHEJ

the sequence at DSB might not be faithfully restored: this could lead to loss of information and/or chromosomal rearrangements[79].

Homologous recombination. HR has a primary role in the S/G2 phases, when the sister chromatids are available as template. HR can therefore promote error-free DSB repair. HR can be divided into 3 stages: presynapsis, synapsis and post synapsis[11]. Presynapsis is initiated by the MRE11-RAD50-NBS1 (MRN) complex that recognizes the breaks and, together with CtBP-interacting protein (CtIP), starts the short-range DNA end resection. Subsequently, extensive resection is carried out by the combined action of EXO1, DNA2, and the Bloom syndrome helicase (BLM). However, MRE11, the nuclease within the MRN (MRE11-RAD50-NBS1) complex, exhibits 3′-5′ exonuclease activity, which is the exact opposite of what is required to generate 3′ ssDNA overhangs for HR promotion. Emerging evidence indicates that CtIP activates MRN endonuclease activity to generate an incision in a single strand close to the DSB. This is followed by bidirectional resection catalyzed by MRN, in the 3′ to 5′ direction, and EXO1, in the 5′ to 3′ direction[80,81]. As the degradation occurs, the ssDNA is promptly coated by the ubiquitous and abundant RPA. At this step, BRCA1 recruits PALB2 and BRCA2 to the DSB. BRCA2, in turn, binds and dismantles native RAD51 heptamers and facilitates the loading of RAD51 monomers onto ssDNA, replacing RPA. In mammalian cells this process is assisted by other factors, like RAD52 and RAD51 paralogs.

Once the RAD51-ssDNA nucleoprotein filament is formed, RAD51 initiates the search for an homologous DNA template by invading the sister chromatid, and resulting in the formation of a D-loop structure called synapsis. Here, the invading 3' end acts as a primer for DNA polymerization. Finally, in the postsynapsis phase, the D-loop is resolved by different mechanisms, all yielding to intact and repaired DNA molecules. In mitotic cells, most frequently, the D-loop is resolved by anti-recombinases helicases, such as regulator of telomere elongation helicase 1 (RTEL1). The 3' invading strand is disengaged after DNA synthesis and re-annealed to the second end of the break in a pathway called synthesis-dependent strand annealing (SDSA). In meiotic cells instead, the second end of the break is captured by the D-loop to form a double Holliday junction (HJs) structure. The junction can then be processed by the activity of endonucleases MUS81-EME1, SLX1-SLX4 or GEN1 into either non-crossover or crossover products. Alternatively, HJs can be dissolved by the BLM-TOPIII- RMI1-RMI2 (BTR) complex, leading to either crossover (CO) or non-crossover (NCO) products[82].

1.3.3 BRCA2 maintains genomic stability upon replication stress

While our understanding of the exact mechanism by which resection contributes to the processing of stalled replication forks is limited, both its loss and its uncontrolled activity are detrimental for replication fork restart and genome stability. Controlling stalled fork resection therefore represents an important barrier to prevent genome instability.

A role for BRCA2 in stabilizing stalled forks was firstly reported by Venkitaraman and colleagues in 2003[83]. This study showed that Y-shaped DNA junctions - stalled replication forks are detected in 2D gel electrophoresis - disappear during hydroxyurea (HU)-induced replication arrest in BRCA2-deficient mouse cells. The explanation for this puzzling observation came from a later study, showing that BRCA2 protects stalled forks from extensive MRE11-dependent degradation[39]. They used the so-called DNA fiber assay, in which the newly synthesized DNA is sequentially pulse-labeled for equal amount of time with different nucleotides analogues. These modified nucleotides are then recognized by fluorescently labelled antibodies. This setup allows measuring the stability of stalled replication forks based on the length of newly synthesized labeled DNA. By exploiting several BRCA2-deficient mammalian cell lines, the authors observed that the nascent strands were significantly shorter, demonstrating that BRCA2 protects nascent DNA at stalled replication forks. The nuclease responsible for this form of fork instability in absence of BRCA2 is MRE11. This conclusion could also confirm previous results obtained by EM analysis in RAD51-depleted *Xenopus laevis* extracts, that showed a high frequency of MRE11-dependent ssDNA gaps at replication forks[43].

Mutational analysis revealed that BRCA2 does not prevent the degradation by directly binding the DNA, but through its ability to load and stabilize RAD51 filaments by its conserved C-terminus domain. Interestingly, BRCA2 mutants like Ser3291Ala that disrupt the C-terminal interaction with RAD51, are defective for protection against HU-triggered nascent strand resection, leave unperturbed BRCA2 role in repairing DSB via HR. These mutants provide strong evidence of genetically separated functions of BRCA2 in these two processes[39].

Additional factors blocking uncontrolled fork resection. FA is a disorder characterized by severe developmental abnormalities, bone marrow failure, cancer predisposition, and sensitivity to crosslinking agents. RAD51, BRCA1 and BRCA2 are part of the 18 genes of FA that encode for proteins that coordinate multiple repair processes and checkpoint signaling events necessary for the accurate removal of ICL lesions. The central event of FA pathway involves monoubiquitination of FANCD2 and FANCI proteins by the FA core complex, and promote ICL unhooking via DNA incision. The resulting lesion is then accurately repaired by translesion synthesis (TLS) and HR protein[84]. Interestingly, FA/BRCA protein network is also activated by

replication stalling agents (aphidicolin, HU) that do not require a physical removal of the lesion[85]. Moreover, FANCD2 and BRCA2/RAD51 functionally interact and co-localize in DNA damage-induced foci[86,87]. These findings prompted the authors to extend their studies by examining the possible involvement, in fork stability, of other HR components and FA proteins[40]. Perhaps not surprisingly, they found that FANCD2- and BRCA1-defective cell show a dramatic MRE11-dependent degradation of the nascent strand, and an increase in chromosomal aberrations upon replication fork stalling induced by HU treatment. These results unite breast cancer and FA susceptibility genes in one common pathway, whose function is to protect stalled replication forks from extensive degradation, thereby counteracting genomic instability.

Many other proteins have been shown to protect nascent DNA by regulating the formation and the stabilization of RAD51 nucleofilaments. In particular, helicase/nuclease WRN[88] and its binding partner Werner helicase interacting protein 1 (WRNIP1)[89], TLS polymerase REV1[90] and RAD51 paralogs[91], were recently shown to promote resistance to replicative stress in BRCA-deficient cells.

Intriguingly, it has been reported that high levels of RAD51 expression causes genome instability. Moreover, RAD51 appears to be frequently overexpressed in cancers[92]. Thus beside the mechanisms that support RAD51 activity, proteins must exist that will limit the genotoxic effect of RAD51 to promote the proper balance between its activities. Possibly via direct interaction with FANCD2 and BRCA2, a newly identified protein biorientation of chromosomes in cell division 1 like (BOD1L) promotes stalled fork protection through the stabilization of RAD51 by suppressing the anti-recombinogenic and pro-resection activities of FBH1 and BLM[93].

Cells have additional ways of fine-tuning RAD51 function through negative regulation. Recently, a protein called RADX was shown to protect the stalled forks by antagonizing the activity of RAD51[94]. Indeed, its inactivation results in excessive RAD51 activity and fork collapse; on the other hand, in cancer cells lacking BRCA2, RADX deletion is sufficient to restore fork protection and genome stability. Thus, by modulating RAD51 binding at the fork, RADX provides a finely tuned regulatory mechanism to yield the right amount of nascent strand resection.

Factors promoting stalled fork resection. MRE11, CtIP, DNA2, and EXO1 nucleolytic activity have been extensively studied in the context of DSBs processing. As discussed in the section 3.2, MRE11 and CtIP start the short-range resection, while EXO1 and DNA2 act independently to execute extensive resection to facilitate RAD51 loading.

These proteins have also been implicated in nucleolytic processing of stalled forks that leads to increased genome instability[39,40,57,88,95]. MRE11 was the first nuclease to be described acting at stalled forks, and its uncontrolled resection has been observed in the absence of many factors, including functional FA/HR pathways[39,40]. However, MRE11 has limited nucleolytic activity, and is unlikely to be the only nuclease responsible for degrading several kilobases of DNA in

pathological conditions. The proteins DNA2 and EXO1 are also implicated in fork over-resection. DNA2 downregulation, but not depletion of EXO1 or MRE11, has been shown to alleviate fork processing after HU administration[57]. Furthermore, DNA2 loss in FA/HR deficient cells rescues their hypersensitivity to ICLs and limits excessive over-resection of the DNA at stalled forks[93,96,97]. EXO1 knockdown reduced fork over-processing in WRN exonuclease mutant cells[88]. In addition, it has been recently shown that, together with MRE11, EXO1 contributes to extensive fork degradation in BRCA-deficient cells and that this process is initiated by CtIP[98].

The involvement of other proteins regulating resection of stalled forks adds an additional level of complexity. This group of proteins, while not directly possessing a nuclease activity, modulates the recruitment of nuclease enzymes at the stalled forks. PARP1 for example, has been implicated in various DNA repair pathways and in the maintenance of genomic stability[67]. High-throughput analysis of protein dynamics at replication forks revealed the presence of PARP1 at normal and at stalled forks[99]. Beside its role in fork reversal, PARP1 has been shown to interact with and recruit MRE11 to stalled forks[100,101]. Indeed, in the context of BRCA deficiency, in which replication forks become highly unstable upon stalling, PARP1 inhibition prevents excessive fork degradation by limiting MRE11 access to the forks[95,101,102]. In addition, chromatin-remodeling factors, PTIP and Chromodomain Helicase DNA Binding Protein 4 (CHD4) mediate the recruitment of MRE11 to the DNA, thereby their downregulaton impairs MRE11 enzymatic nuclease activity at the forks[102,103].

The discovery of this multitude of factors that contribute to positively or negatively regulate the resection of stalled forks, suggests that this process is astonishingly more complex than initially anticipated.

Clinical relevance of fork protection mechanisms. Resistance to drugs of BRCA-mutant tumors continues to be a major problem in oncology affecting the majority of cancer patients. Besides reduced uptake and increased efflux of drugs, the most well described mechanism that drives chemotherapeutic resistance in BRCA1/2-deficient tumors is through the re-establishment of HR due to secondary mutations[104]. Surprisingly, last year, André Nussenzweig and Shyam Sharan groups described a new mechanism for resistance to BRCA-targeted therapy[101,102]. They found that the central functions of BRCA1/2 in fork protection underlies the sensitivity of BRCA1/2-deficient cells to genotoxic drugs. In fact, loss of PTIP, PARP1 and CHD4 impair recruitment of MRE11 nuclease at stalled replication forks and confers resistance to a variety of DNA-damaging agents. Resistance to PARPi and cisplatin both in primary and in tumour cells grown *in vitro* or *in vivo* correlates with protection from replication fork degradation and is independent of the restoration of classical HR-dependent DSB repair. Clinically, these findings are of particular relevance, as the expression of these proteins appears to be an indicator of patient response to chemotherapy.

Loss of Brca2, as well as other HR factors like BRCA1, in ESCs is incompatible with cell survival[105]. By inactivating PARP1 or PTIP before BRCA2 loss, the above-mentioned groups were able to rescue the lethality of $Brca2^{-/-}$ mESC[101,102]. Importantly, these cells displayed stable replication forks compared to cells carrying Brca2 hypomorphic mutant, but lacked irradiation-induced RAD51 foci, indicating that HR was not restored. Thus, suppression of uncontrolled degradation of stalled forks rescues the lethality of $Brca2^{-/-}$ ESCs without restoring HR repair.

2. Aims

Oncogene-induced replication stress is as a crucial, early event in tumorigenesis. Despite its clinical relevance, the molecular bases of this process have been poorly characterized.
Research in our laboratory has uncovered that overexpression of CyclinE and Cdc25A rapidly (after 8h) induced the formation of reversed forks in osteosarcoma cell line (U2OS), and uncontrolled processing of these structures leads to genomic instability. However, whether this is a general consequence of oncogene activation occurring in cancers, remains an important open question.
The first aim of my doctoral research is to investigate the consequences of overexpressing two frequently mutated oncogenes, c-MYC and H-RAS. This, together with the previous work on CYCE and CDC25A, might enable us to uncover what are the conserved mechanisms occurring downstream of oncogene activation both in cancerous and in untransformed cells, possibly revealing future new therapeutics options to target oncogene-addicted cancer cells.

Extensive work has contributed to our understanding of the mechanism and the factors involved in replication fork reversal. Replication fork reversal has emerged as a global, protective response to genotoxic stress in cancer and untransformed cells. Surprisingly, this transaction was recently found to be extremely frequent in unperturbed fast-replicating mouse embryonic stem cells (mESC).
This molecular transaction at replication forks requires the central recombinase RAD51, suggesting a crucial genome protective role of HR factors in replication fork remodeling.
In addition, several laboratories have uncovered a role for BRCA2, as well as other HR and FA factors, in protecting stalled replication forks from extensive nucleolytic degradation. This is important, as it represents an entirely new function of HR factors, that appears uncoupled from their classical role in double-strand break repair and - most importantly –underlies both the early embryonic lethality and the exquisite sensitivity to genotoxins (e.g. PARP inhibitors) associated with BRCA2 loss.
In light of these recent findings, we have focused, in the second part of the research described in this thesis, on the role of the tumor suppress gene *BRCA2*. More specifically, we have planned to assess the contribution of BRCA2 to fork remodeling, monitoring fork stability and architecture - by fiber analysis and EM, respectively - upon BRCA2 loss in different cellular systems. We envisioned to unveil the structures that are protected by HR factors from extensive nucleolytic degradation, and that are fundamental to preserve genome stability. The elucidation of this mechanism will possibly explain the essential function of HR proteins during early embryogenesis and, more importantly, the specific sensitivity (and acquired resistance) to chemotherapeutic treatments of *BRCA2*-mutant tumors.

Of note, we initially planned to study the role of BRCA2 in fork remodeling upon oncogene activation. However, the experimental system we tested to overexpress c-MYC and H-RAS (tamoxifen-inducible expression of ER-oncogene fusions) still requires refinement and validation, in order to ascertain its suitability for these studies. Thus, inspired by recent publications, we set out to study the role of BRCA2 in fork remodeling, using mainly TOP1 inhibition (CPT) and nucleotide depletion (HU) (instead of oncogene overexpression) as a source of replication stress[38,39,49].

3. Results

3.1 Oncogene-induced replication stress

3.1.1 Selection of the model system

To study the molecular events during the early phases of c-MYC or H-RAS^{V12}-induced replication stress, the selection of two experimental parameters is of crucial importance: 1) an adequate set of cellular systems, and 2) the technology to timely control the overexpression of the genes.

We analyzed the cell cycle distribution of two hTERT-immortalized cell lines, experiencing CPT-induced replication stress: BJ cell line, derived from human foreskin, and RPE-1 cells derived from retinal pigment epithelium; U2OS cells have been used as control[25] (Figure 7 **a**). As observed in U2OS, RPE-1 cells rapidly accumulated in S/G2 phase after CPT treatment, indicative of a relatively high fraction of cells undergoing S-phase. BJ cells in contrast, showed an accumulation in G1. We hypothesized that this could be due to a very low replication rate in the latter cell line, rendering it less suitable to study early events of replication stress. Therefore, we chose to overexpress c-MYC and H-RAS in U2OS and RPE-1 cells.

Concerning the overexpression system, two different approaches have been previously exploited in our laboratory[25]: the tetracycline-controlled Tet-Off gene expression (Tet-off) and the transient transduction using retroviral vectors. Although the Tet-off system allows timely-controlled and efficient transcription of the gene of interest, it also involves a multi-step cloning process that can be time consuming and laborious. For this reason, a faster and simpler transient transfection was applied in the first place to rapidly assess the feasibility of the approach. However, IF assay showed that, upon transient transfection of the vector carrying *CDC25A* gene used as control, only 30% of the cells were expressing the protein, compared to the stably transfected tetracycline-inducible expression that yielded ca. 70% of cells positive for CDC25A (Figure 7 **b-c**). Moreover, besides low efficiency, transient transfection does not permit a precise temporal activation of the gene.

Therefore, to obtain a fine control of the expression, we cloned the coding sequence of *c-MYC* and a constitutively active mutant of *H-RAS* (*H-RAS*^{V12}) in frame with the hormone-binding domain (HBD) of transcriptionally inactive mutant estrogen receptor (ER), referred to as ER^{TAM}. The modified receptor does not bind estrogens, but retains normal affinity for the synthetic ligand 4-hydroxy-tamoxifen (4-OHT). The fusion proteins are supposed to be expressed under the control of the retroviral 5' long terminal repeats (LTR), and to remain inactivated by complexing with heat shock protein 90 (HSP90) until 4-OHT treatment. Following administration of 4-OHT, the fusion protein is released from HSP90 inhibitory complex, allowing translocation from the

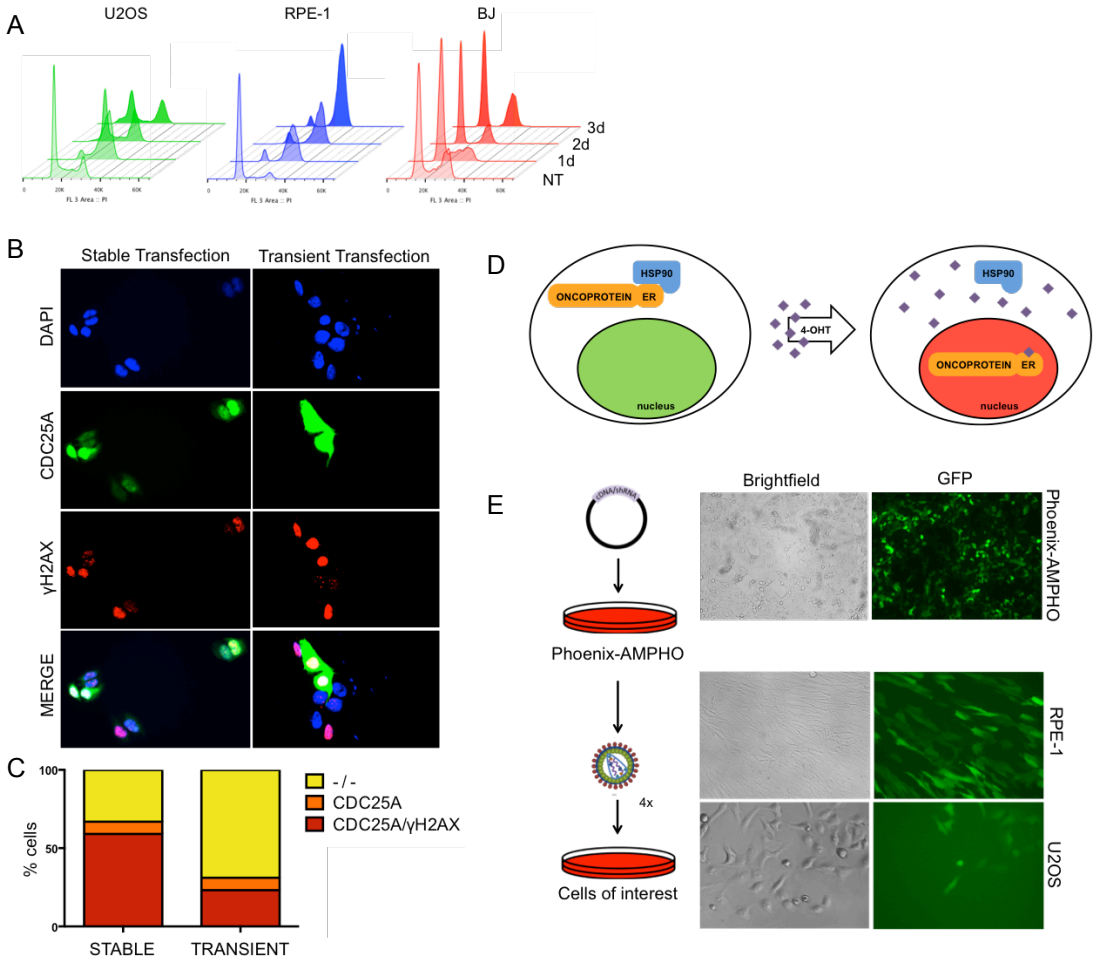

Figure 7 Selection of the cell line and gene overexpression technique. (a) FACS analysis of cell cycle progression in U2OS, RPE-1 and BJ cell lines treated with 25 nM of CPT for indicated time points. The DNA content was detected by propidium iodide staining. (b) Immunofluorescence (IF) staining of U2OS cells for CDC25A and the DNA damage marker γH2AX cells. The overexpression of CDC25A was induced by removing tetracycline from the media (Tet-off system) in case of stable transfection or by transiently transfecting the vector carrying CDC25A gene. (c) Quantification of double IF staining displayed in (b) in U2OS cells. A minimum of 130 cells was scored for each transfection system. (d) Schematic diagram of ER^{TAM}-Tamoxifen based temporal control of oncogene overexpression. (e) Schematic representation of retroviral packaging and transfection, left (see Method section for more details). Transfection of Phoenix-AMPHO cells and transduction of RPE-1 and U2OS cells was followed with GFP reporter gene, right. The pictures of Phoenix-AMPHO cells were taken 24h after the calcium phosphate mediated transfection and RPE-1 and U2OS 48h after the first round of viral infection.

cytoplasm to the nucleus and subsequent transcriptional activity[106] (Figure 7 **d**).

To achieve stable transgene integration we exploited a retroviral transduction. Here, the viruses are used as a vector to deliver the transgene within target cells. Antibiotic-treatment will subsequently allow selection of the transduced cells and the transgene integration it in the genome. Briefly, the retroviral plasmids carrying the fusion *c-MYC-*ER^{TAM} or *H-RAS-*ER^{TAM} were transfected in Phoenix amphotropic packaging cells, a 293T-based cell line that contains transgenes for the production of the viral capsid proteins gag, pol and env. Once the amphotropic

infectious particles are produced, the gene of interest is packaged within the viral genome. The viral particles can then be collected in large amounts and used to infect target cells. The activity of the viral integrase will stably integrate the gene in the cell and these will be selected with specific antibiotics. As an indirect readout for the efficiency of transfection and infection, we used a plasmidic vector encoding the reporter gene GFP (Figure 7 **e**). We observed a high infection efficiency of both target cell lines (40-50% in U2OS cells and ca. 80% in RPE-1 cells). In parallel, we were able to produce RPE-1 and U2OS cells carrying *c-MYC-ER^{TAM}* transgene, and RPE-1 (but not U2OS) cells with *H-RAS^{V12}-ER^{TAM}*. This was probably due to a lower infection efficiency of U2OS cells compared to RPE-1 (Figure 7 **e**).

3.1.2. Oncogenes overexpression and validation

Upon activation of c-MYC and H-RAS^{V12} by the ligand 4-OHT, the c-MYC-ER^{TAM} and H-RAS^{V12}-ER^{TAM} fusion protein should translocate from the cytosol to the nucleus. To investigate the efficiency and the precision of the temporal control of the translocation, we studied the subcellular localization of the tagged proteins at different time intervals after 4-OHT administration. We focused on RPE-1 cells and isolated the nuclear and cytosolic proteins (Figure 8 **a-b**). The levels of both cytoplasmic and nuclear c-MYC and H-RAS^{V12} significantly increased compared to parental cells and cells carrying the EV, which suggest a successful integration and overexpression of the genes. However, the nuclear levels of the proteins were high already at 0h of 4-OHT treatments. C-MYC levels in nuclear extract showed a slight increase upon longer exposure to 4-OHT (Figure 8 **a**), while there was no significant alteration of *H-RAS^{V12}* localization (Figure 8 **b**). This observation suggests a "leakiness" in the nuclear translocation of the two proteins. Nevertheless, the controls that we used to monitor cytoplasmic (GAPDH) and nuclear (RPA and TFIIH) proteins showed a cross-contamination between the two fractions, not allowing to a full extent the quantification of the nuclear translocation of c-MYC and H-RAS in the absence of 4-OHT. Improved fractionation of cytoplasmic versus nuclear proteins will be an important next step.

We also performed IF analysis, by staining with c-MYC and H-RAS specific antibodies and the DNA damage marker γH2AX, used as functional readout (Figure 8 **c-d**). Consistent with western blot data, IF detection of c-MYC was higher in transduced cells compared to parental or EV-transduced cells. As before, the cells displayed increased nuclear levels of c-MYC in the absence of 4-OHT suggesting a leaky overexpression and nuclear translocation of the protein. As seen by western blot, prolonged treatment with 4-OHT increased the number of cells positive for nuclear c-MYC. Unfortunately, we were not able to detect significant increase of H-RAS levels in RPE-1 cells carrying *H-RAS^{V12}-ER^{TAM}* construct, compared to control cells. An outlook to solve this problem will include testing different antibodies and/or sequencing of the plasmidic contruct, with

particular attention on the H-RAS coding sequence and the promoter driving its expression. Undesired mutations in these regions could in fact explain the absence of H-RAS expression. In addition, a new cloning strategy will be set up to produce an alternative overexpression construct for H-RAS.

Overall these results suggest that, particularly for c-MYC, we are able to efficiently overexpress the protein using retroviral transduction technique. The ER^{TAM} - 4-OHT system, however in our hands, did not allow a precise temporal control of the oncoprotein nuclear translocation.

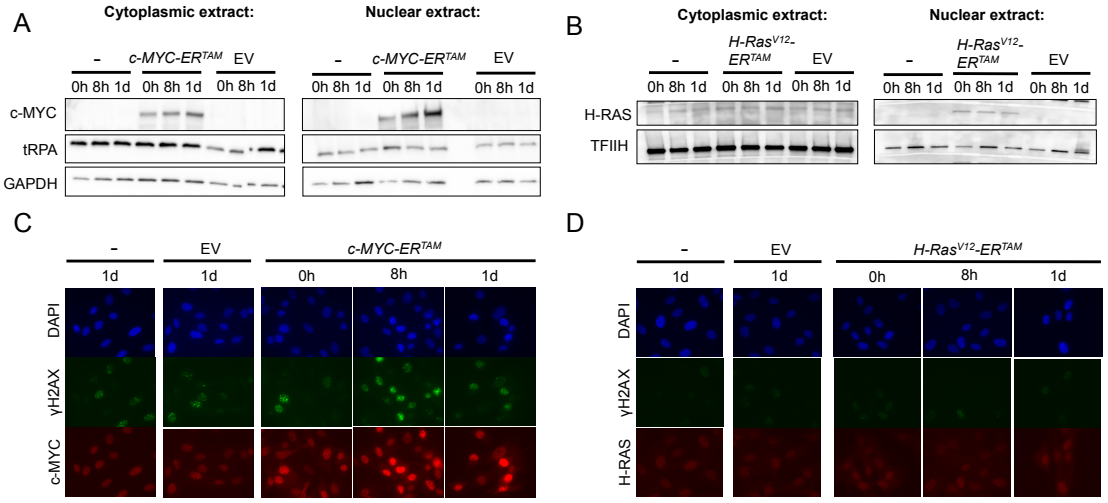

Figure 8 Expression kinetic of c-MYC-ER^{TAM} and H-RAS^{V12}-ER^{TAM} chimeric proteins in RPE-1 cells. (a) and (b) RPE-1 cells were transduced with vectors encoding c-MYC-ER and H-^{RASV12}-ER and treated with 4-OHT for indicated time points. Cytoplasmic and nuclear proteins from these cells were isolated and subjected to SDS-PAGE using specific antibodies against c-MYC and H-RAS. GAPDH, RPA and TFIIH were detected as fractionation controls. (c) and (d) The cells were treated as in (a) and (b) and analyzed by IF to determine the subcellular localization. γH2AX was used as functional readout.

3.1.3. Analysis of C-MYC-ER^{TAM} overexpression in RPE-1 cells

Encouraged by the increasing expression of c-MYC-ER^{TAM} in the nuclear extract upon prolonged time of 4-OHT (Figure 8 **a, c**), we aimed to perform a more sensitive quantification assay to evaluate the basal nuclear levels of the protein at 0h of 4-OHT. We established a FACS-based method to quantify chromatin bound c-MYC-ER^{TAM} and, performed a time course experiments upon 4-OHT treatment (Figure 9 **a**). FACS data clearly show a significant increase of c-MYC signal compared to the EV control, even in the absence of 4-OHT. The signal intensity remained unchanged upon prolonged 4-OHT treatments. This outcome was confirmed by analyzing the transcription levels of the known c-MYC target genes encoding eukaryotic translation initiation factor 4E (eIF4E) and nucleolin (NCL)[107] using real-time quantitative RT-PCR assay (Figure 9 **b**). The amount of the eIF4A and NCL transcript was significantly higher in unstimulated RPE-1-c-MYC-ER^{TAM} cells in comparison to EV-transduced cells. Collectively, these analyses confirmed

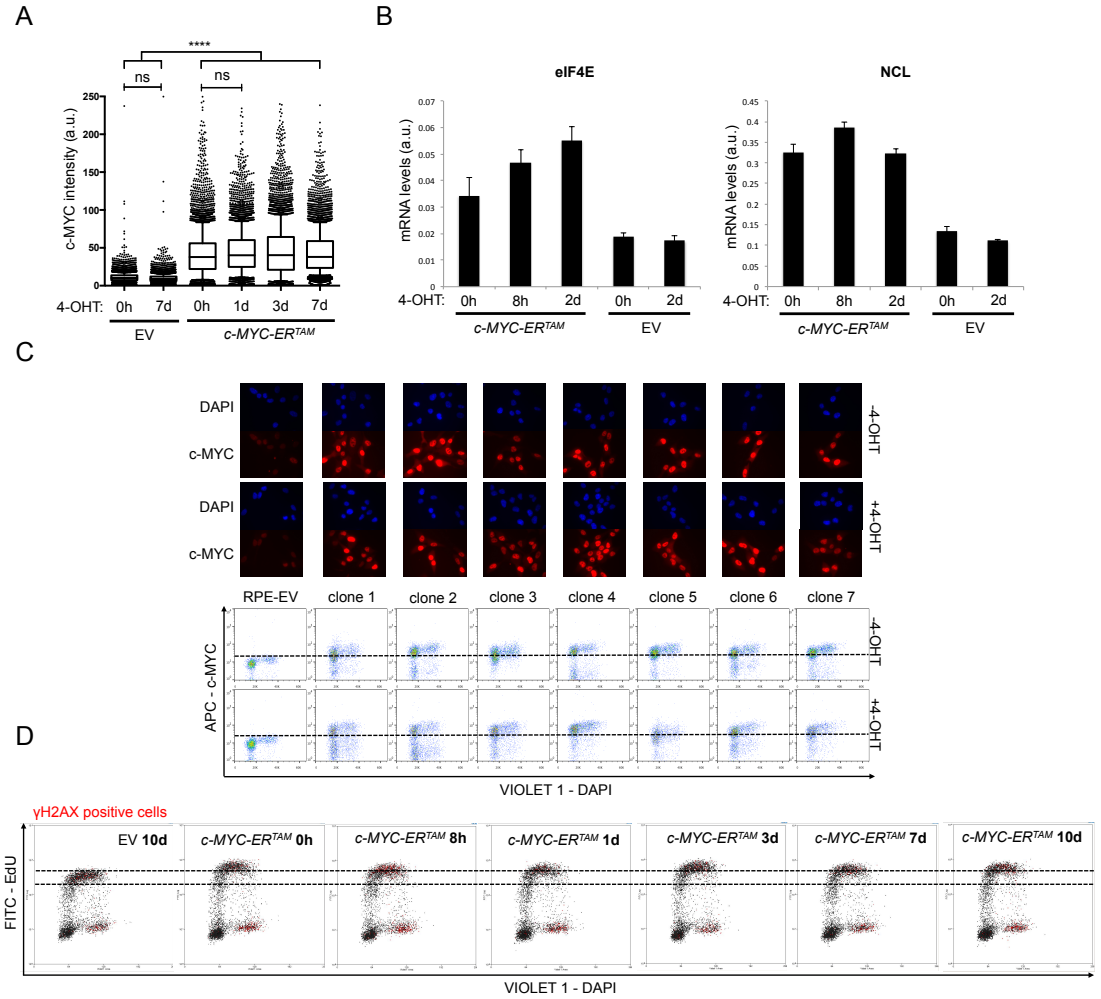

Figure 9 Analysis of C-MYC-ER^{TAM} overexpression in RPE-1 cells. (a) FACS-based quantification of c-MYC staining in RPE-1-c-MYC-ER^{TAM} cells and RPE-1-EV treated with 4-OHT for indicated time points. (b) RPE-1-c-MYC-ER^{TAM} and RPE-1-EV cells were treated with 4-OHT for indicated time points. Total RNAs were isolated and mRNA levels of eIF4A and NCL were analyzed by RT-PCR and normalized to actin expression. (c) IF staining and FACS-based analysis of RPE-1-c-MYC-ER^{TAM} selected single clones cells for c-MYC expression 24h after 4-OHT stimulation. Plots depict c-MYC signal intensity versus DAPI. (d) FACS analysis for DNA synthesis (EdU incorporation), DNA content (DAPI) and DDR activation (γH2AX) in RPE-1-EV and RPE-1-c-MYC-ER^{TAM} cells treated with 4-OHT for indicated time points. Plots depict EdU incorporation versus DAPI. γH2AX positive cells are depicted in red.

that ER^{TAM} - 4-OHT is not a suitable experimental system for precise temporal controls of the gene expression.

Because the IF analysis at time point 0h of 4-OHT showed a mixed population of cells expressing different levels of c-MYC, we diluted the bulk population and isolated single cell-derived clones to possibly select for the cells that did not show high basal levels of c-MYC expression (Figure 9 **c**). However, FACS analysis performed on each isolated clone showed elevated amount of c-MYC expression in the absence of the intracellular ligand 4-OHT.

Although we were not able to precisely control the expression of c-MYC, we sought that this system could allow us to obtain insights in c-MYC induced replication stress. We treated RPE-1 cells harboring *c-MYC-ER^{TAM}* by increasing time exposure of 4-OHT, and analyzed the rate of

DNA synthesis by measuring EdU incorporation and the activation of DDR via γH2AX staining (Figure 9 **d**). C-MYC overexpression induced a burst of DNA replication, as detected by higher EdU incorporation compared to EV-cells. Moreover, we could observe marked increase of γH2AX in cells approaching completion of DNA replication (late S phase): these cells likely accumulated more damage during replication. These are important observations, as they - in line with previous reports - suggest that c-MYC overexpression increases replication origin activity – or transiently accelerates replication forks - leading to subsequent replication stress and DDR activation[32].

3.1.4. BRCA2 depletion causes reduced DNA replication and G1 arrest

In another line of investigation, I focused my attention on the functions of BRCA2 during replication stress and investigated the consequences on replication dynamics upon its loss. Efficient downregulation of BRCA2 after more than 3d in U2OS cells (Figure 10 **a**) resulted in a marked reduction in replication fork speed, measured by DNA fiber spreading compared with control (siLuc) cells (Figure 10 **b**). Reduced fork progression rate was also observed by FACS analysis, where we monitored a reduced EdU incorporation upon BRCA2 loss. The under-replicated DNA in BRCA2-deficient cells resulted in phosphorylation of H2AX histone variant, indicative of DDR activation, after more than 3 cell cycles (Figure 10 **c**). The unresolved damage induced these cells to stall in G1 phase (5d - 7d). Interestingly, these observations have been recently reported in a recent publication from Maria Jasin lab: they showed that BRCA2 loss leads to replication stress that is transmitted to the next cell cycle through DNA under-replication, which causes mitotic abnormalities, 53BP1 nuclear bodies and G1 arrest[108]. This represents an independent validation of the experimental set-up tested in this study.

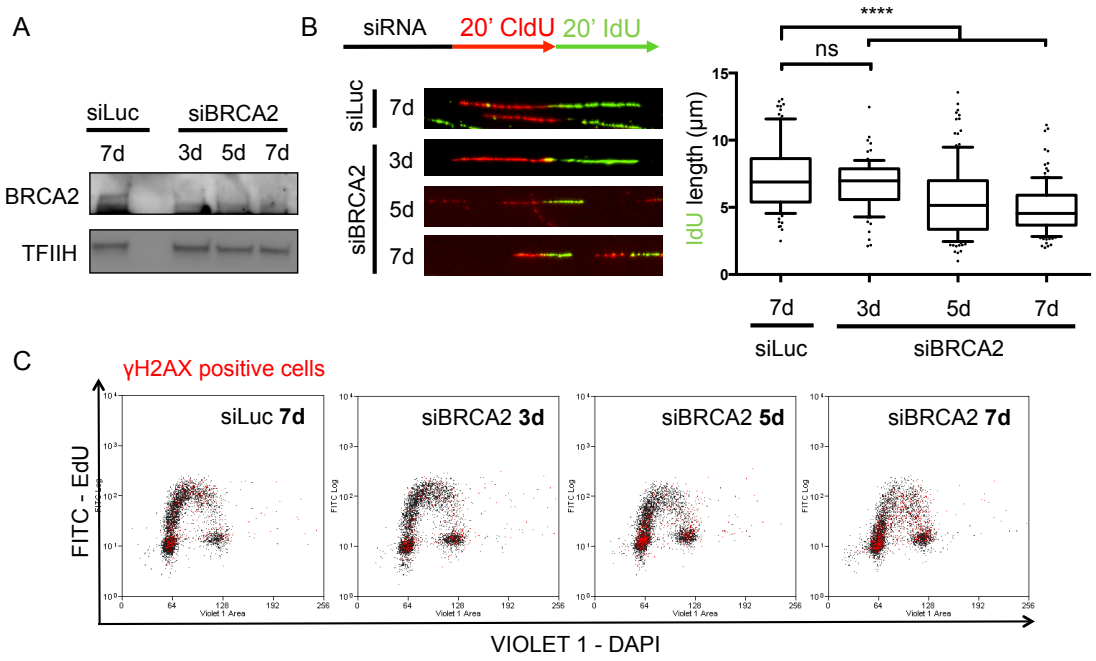

Figure 10 BRCA2 depletion causes reduced DNA replication rate and G1 arrest. (a) Western blot analysis of BRCA2 levels in mock-depleted (siLuc) and BRCA2-depleted (siBRCA2) U2OS, 3 days, 5 days and 7 days after siRNA transfection. TFIIH is used as loading control. (b) DNA fiber spreading of mock (siLuc) and BRCA2-depleted cells (siBRCA2). As shown in the scheme, CldU/IdU-containing tracts were immunostained in red and green for 20 min, respectively. Representative fibers are shown for each sample. The IdU replicate tracks are plotted. Horizontal lines indicate the median value. One hundred replication forks were analyzed for each condition. Statistical analysis: Mann-Whitney test; ns, not significant; ****, P< 0.0001. (c) FACS analysis for DNA synthesis (EdU incorporation), DNA content (DAPI) and DDR activation (γH2AX) in siLuc and siBRCA2 U2OS cells. Plots depict EdU incorporation versus DAPI. γH2AX positive cells are depicted in red.

3.1.5. BRCA2 suppresses re-replication in oncogene overexpressing cells

The results described above, provided the impetus to investigate BRCA2 function in oncogene-induced replication stress. As the construction of a suitable system to overexpress c-MYC and H-RAS was still in progress (see section 3.1.3), I exploited a series of reagents already present in the lab, allowing a finely-tuned tetracycline-dependent CYCE overexpression in U2OS. We downregulated *BRCA2* for 3 days in U2OS, and induced CYCE overexpression at different time points (Figure 11 **a**). We assessed the DNA replication dynamics by analyzing single DNA fibers as done in Figure 4 b, in combination with FACS analysis (Figure 11 **b,c**). In line with previous experiments[25], the control CYCE overexpression sample was associated with a significant replication fork slowdown assessed by DNA fibers. FACS analysis, however, displayed a high EdU incorporation, suggesting that while individual forks slowed down, the global replication rate appeared to be higher, likely because of increased origin firing. Moreover, DDR activation (i.e. γH2AX) upon prolonged CYCE overexpression was mainly present in cells accumulating in S/G2 or attempting re-replication at later time points (Figure 11 **c**). The observed replication stress was

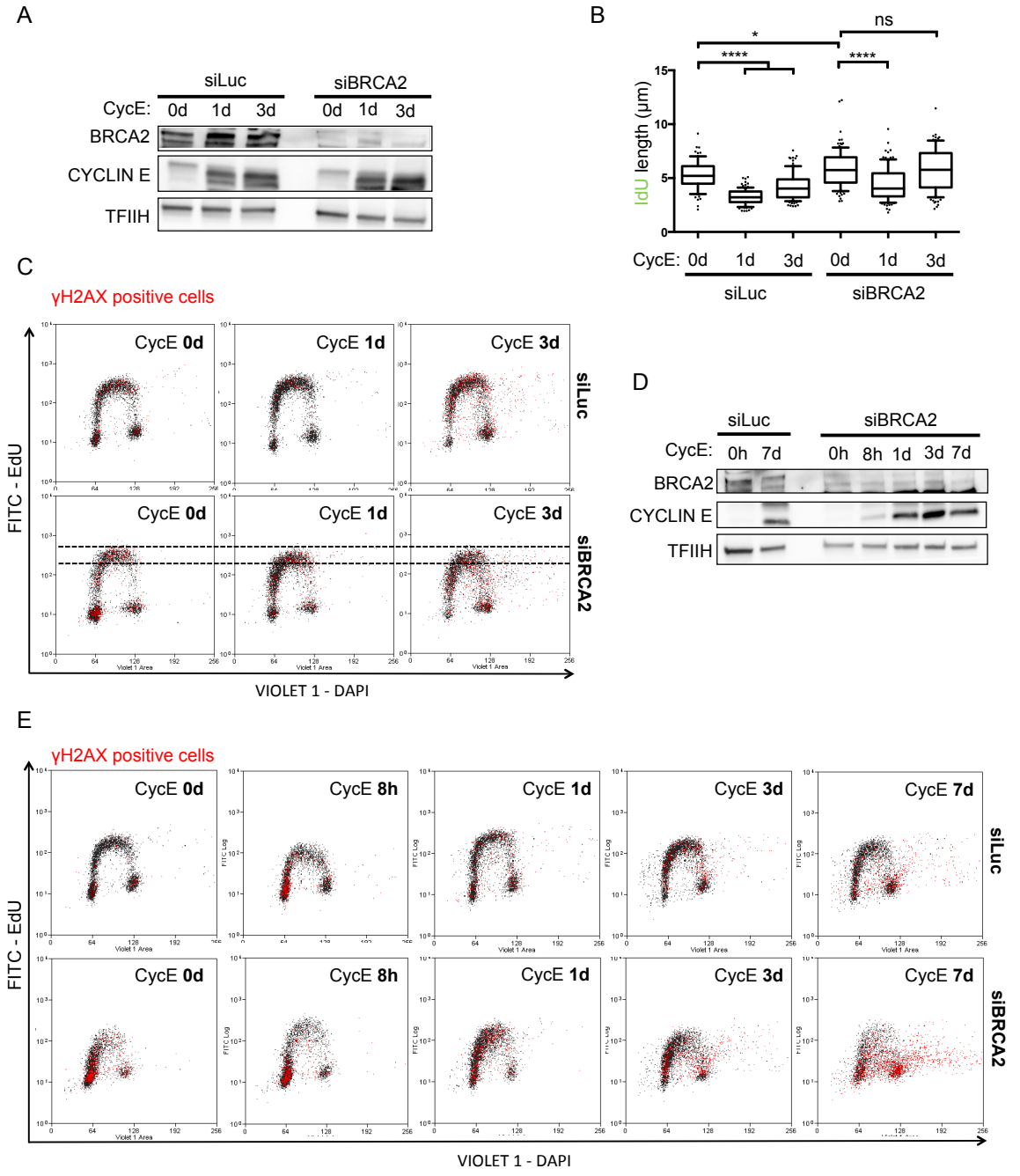

Figure 11 BRCA2 suppresses re-replicaton in oncogene overexpression cells. (a) and (c) Western blot analysis of BRCA2 and CYCE levels in mock-depleted (siLuc) and BRCA2-depleted (siBRCA2) U2OS cells overexpressing CYCE for indicated time points. TFIIH is used as loading control. (b) Analysis of DNA replication progression of samples from (a) by fiber spreading like in Figure 4 b. The IdU replicate tracks are plotted. Horizontal lines indicate the median value. One hundred replication forks were analyzed for each condition. Statistical analysis: Mann-Whitney test; ns, not significant; ****, P< 0.0001. (c) and (e) FACS analysis for DNA synthesis (EdU incorporation), DNA content (DAPI) and DDR activation (γH2AX) in siLuc and siBRCA2 U2OS cells overexpressing CYCE for 0 days, 8hours, 1 day, 3 days and 7days. Plots depict EdU incorporation versus DAPI. γH2AX positive cells are depicted in red.

DNA Fiber experiments showed faster fork progression after *BRCA2* downregulation, which is only marginally affected by CYCE overexpression (Figure 11 **b**). This is not in line with the observed decrease of global DNA synthesis rate as assessed by EdU incorporation after CYCE overexpression (Figure 11 **c**). We do not currently have a clear explanation for this discrepancy. Additional experiments will be performed to validate this observation. However, these preliminary results suggest that BRCA2 depletion induced lower rate of DNA replication, which is associated with re-replication and DDR activation.

Interestingly, when we downregulated *BRCA2* for longer time (7 days) while overexpressing CYCE, we observed that the cells initially stalled in G1, were then pushed toward the S phase (1 day) (Figure 11 **d, e**). Subsequently, they experienced major replication stress shown by compromised EdU incorporation (day 3), intermediate DNA content and extensive re-replication events (7d). Consistent with our results, it has been reported that DNA re-replication caused by deregulating origin firing, for example by CDT1 overexpression[109] or geminin inactivation[110], results in replication fork stalling and DSBs. Interestingly, HR-mediated repair is a primary mechanism to repair re-replication-induced DSBs[111]. Many models have been proposed to explain the formation and processing of DSBs at re-replicated DNA: (i) replication of gapped DNA templates that are accumulated during re-replication[26] (ii) head-to-tail collision of re-replication and replication forks[112]; (iii) stalling and collapse of re-replication forks[111]; (iv) re-replication forks might be processed by endonucleases activity[111]; (v) stalled re-replicated DNA could be resected by exonucleases[111]. However, the underlying mechanisms are still under investigation as they represent a new and interesting biological question.

Conclusive remarks

Our results suggest that ER^{TAM}-4-OHT system is not suitable to activate C-MYC and H-RAS activity in a precise controlled manner. A possible solution we set out to establish the same system that has been previously used for CYCE and CDC25A, namely tetracycline-controlled transcriptional activation (in place of the ER-mediated conditional protein translocation). The generation of the stable cell line with tetracycline-inducible *c-MYC* and *H-RAS* expression will be not described in this thesis as it is an unfinished ongoing effort in our laboratory.

While we generate the stable cell line with tetracycline-inducible *c-MYC* and *H-RAS* expression, we decided to study the BRCA2 function in fork remodeling and stability upon different source of replication stress, such as TOP1 inhibition (CPT) and nucleotide depletion (HU).

3.2 Replication fork reversal triggers fork degradation in BRCA2-defective cells

Manuscript accepted in Nature Communications

Bellow I attached the complete manuscript in which we investigate the role of BRCA2 in remodeling and stability of the replication forks. This work is currently in press in Nature Communications.

Replication fork reversal triggers

fork degradation in BRCA2-defective cells

Sofija Mijic[1], Ralph Zellweger[1], Nagaraja Chappidi[1], Matteo Berti[1], Kurt Jacobs[1], Karun Mutreja[1], Sebastian Ursich[1], Arnab Ray Chaudhuri[2,§], Andre Nussenzweig[2], Pavel Janscak[1] and Massimo Lopes[1]

1. Institute of Molecular Cancer Research, University of Zurich, 8057 Zurich, Switzerland
2. Laboratory of Genome Integrity, National Cancer Institute, National Institutes of Health, Bethesda, Maryland 20892, USA

§ Current address: Department of Molecular Genetics, Erasmus University Medical Center, 3000CA, Rotterdam, The Netherlands

* Corresponding Author: lopes@imcr.uzh.ch

Abstract

Besides its role in homologous recombination (HR), the tumor suppressor *BRCA2* protects stalled replication forks from nucleolytic degradation. Defective fork stability contributes to chemotherapeutic sensitivity of *BRCA2*-defective tumors by yet-elusive mechanisms. Using DNA fiber spreading and direct visualization of replication intermediates, we report that reversed replication forks are entry points for fork degradation in *BRCA2*-defective cells. Besides MRE11 and PTIP, we show that RAD52 promotes stalled fork degradation and chromosomal breakage in *BRCA2*-defective cells. Inactivation of these factors restores reversed fork frequency and chromosome integrity in *BRCA2*-defective cells. Conversely, impairing fork reversal prevents fork degradation, but increases chromosomal breakage, uncoupling fork protection and chromosome stability. We propose that BRCA2 is dispensable for RAD51-mediated fork reversal, but assembles stable RAD51 nucleofilaments on regressed arms, to protect them from degradation. Our data uncover the physio-pathological relevance of fork reversal and illuminate a complex interplay of HR factors in fork remodeling and stability.

Introduction

BRCA1 and *BRCA2* genes represent paradigmatic examples of tumour suppressors, linking genome instability and cancer susceptibility[1]. Although several nuclear and cytoplasmic functions have been described for these proteins, mutations predisposing to cancer predominantly affect their common function in HR. BRCA2 biochemical function in HR has been linked to the replacement of the main ssDNA-binding protein RPA with the central recombination factor RAD51, which channels extended ssDNA regions for strand exchange reactions[1,2]. The HR function of BRCA2 has been mostly studied in response to double-strand breaks (DSBs). As a result, both the cancer predisposition and the effectiveness of certain chemotherapeutic drugs associated with *BRCA2* deficiencies have long been linked to the DSB-repair defect[3]. However, recent work has uncovered a second, genetically separable function for BRCA2 in protecting stalled replication forks from extensive nucleolytic degradation[4]. This concept was later extended to several additional HR factors, as well as factors mutated in the cancer predisposition syndrome *Fanconi anemia* (FA)[5]. While controlled nucleolytic degradation of stalled replication forks likely plays a physiological role to tolerate replication stress, uncontrolled fork degradation upon HR/FA defects is detrimental for genome stability and affects cellular resistance to replication inhibitors[4,6-8]. Most recently, this uncontrolled fork degradation – as opposed to the classical DSB repair defect - was linked both to the lethality of *BRCA2*-defective embryonic stem cells and to the exquisite sensitivity of *BRCA*-defective cells to certain chemotherapeutic treatments, elucidating a novel crucial mechanism of therapy resistance of *BRCA*-defective tumours[9]. It is thus of clinical relevance to investigate the detailed molecular mechanisms mediating or limiting fork degradation in response to chemotherapeutic treatments.

Recent visualization of replication intermediates in human cells has revealed replication fork reversal – i.e. the conversion of replication forks into four way junctions by strand exchange reactions – as a global, evolutionary conserved cellular response to various conditions of replication stress, such as oncogene activation, chemotherapeutic treatments and replication of genomic sequences intrinsically prone to form secondary structures[10-13]. Reversed forks were also recently shown to protect genome integrity in unperturbed embryonic stem cells (ESCs),

which experience endogenous replication stress as a consequence of their accelerated cell cycle progression[14]. Fork reversal was shown to require the central recombinase RAD51[11], suggesting that classical HR factors mediate strand exchange reactions at replication forks. Furthermore, reversed forks can be restarted by RECQ1-dependent branch migration[15], but can also undergo controlled resection by DNA2/WRN[7]. The involvement of HR factors in reversed fork formation and processing suggests that fork reversal might be mechanistically linked to the extensive fork degradation observed in *BRCA2*-defective cells.

Here we show that replication fork reversal is required for fork degradation in BRCA2-defective cells, as regressed arms act as entry points for MRE11-dependent degradation. Furthermore, we clarify the differential contribution of RAD51 and RAD52 in different steps of fork remodelling and protection. Finally, we provide evidence that, albeit priming fork degradation, reversal of stalled forks is essential to prevent excessive chromosomal breakage in BRCA2-defective tumour cells.

Results

Unstable reversed forks and extended ssDNA upon BRCA2 defects

To assess replication fork architecture during fork degradation in *BRCA2*-defective cells, we visualized replication intermediates *in vivo* by an established electron microscopy (EM) method[16]. We treated untransformed human retinal pigmented epithelial (RPE-1) cells with hydroxyurea (HU) to deplete nucleotides and stall replication forks. As previously shown[11], the HU treatment led to significant accumulation (20%) of reversed replication forks, but their frequency was decreased 2-fold upon BRCA2 depletion by siRNA (Fig. 1a-b; Supplementary Table 1). MRE11 inhibition by mirin[17] had no significant effect on reversed fork frequency in untreated cells or in HU-treated wild type cells, but restored full fork reversal levels in BRCA2-depleted HU-treated cells (Fig. 1b; Supplementary Table 1). Thus, replication forks can be effectively reversed upon HU treatment also in the absence of BRCA2, but they are targeted by MRE11-dependent degradation. Although we did not detect a specific accumulation of ssDNA on regressed arms in HU-treated *BRCA2*-defective cells (Supplementary Fig. 1a), extended ssDNA stretches were observed upon *BRCA2* downregulation at standard three-way fork junctions and were suppressed by mirin treatment in HU-treated cells (Fig. 1c-d). Shorter HU treatments also led to reduced reversed fork frequency in BRCA2-defective cells, but did not reveal increased ssDNA at fork junctions or regressed arms (Supplementary Fig. 1b-c, Supplementary Table 2). Taken together, these data suggest that nucleolytic processing in HU-treated *BRCA2*-defective RPE-1 cells rapidly degrades regressed arms and, upon prolonged treatments, continues on newly synthesized DNA behind the fork. Whether or not transient accumulation and/or partial resection of reversed forks is visible by EM upon short genotoxic treatments in *BRCA2*-defective cells likely reflects different kinetics of fork reversal and processing in different cell lines[18]. These data highlight the different resolution and limitations of DNA fiber assays and EM visualization of fork remodeling and degradation, as recently discussed[19].

As PTIP depletion in mouse B cells was recently reported to suppress fork degradation in *BRCA2*-defective cells by limiting MRE11 recruitment at stalled forks[9], we identified conditions to downregulate *PTIP* by two different siRNAs in RPE-1 cells, preceding long-term effects on cell

cycle progression (Supplementary Fig. 2a-b)[20], and monitored fork degradation by DNA fibers. As reported[4,9], HU-treated *BRCA2*-defective cells displayed marked degradation of nascent DNA, also by a labeling scheme that excludes shortening of replicated tracts by fork breakage (Supplementary Fig. 2c-d). In these conditions, similarly to mirin, *PTIP* downregulation suppressed fork degradation (Supplementary Fig. 2c) and restored wild type levels of reversed forks and ssDNA in *BRCA2*-defective HU-treated cells (Supplementary Fig. 2e-f and Supplementary Table 3). Thus, reversed forks appear as "entry points" for extensive MRE11-dependent degradation of stalled forks in *BRCA2*-defective RPE-1 cells.

Chinese Hamster *BRCA2*-defective cells (V-C8), previously reported to undergo fork degradation upon HU treatment[4], also displayed reduced reversed fork levels and extended ssDNA stretches at forks (Fig. 2a, Supplementary Fig. 3a). Mirin treatment or complementation of these cells with WT BRCA2 restored high frequencies of reversed forks and short ssDNA stretches at forks. However, expression of the *BRCA2* phosphorylation mutant S3291A – which causes a defect in fork integrity, but allows HR-mediated DSB repair[4] – failed to complement either defect in V-C8 cells (Fig. 2a, Supplementary Table 4 and Supplementary Fig. 3a), further linking reversed fork instability and fork degradation upon *BRCA2* defects. Notably, reduced reversed fork frequency and extended ssDNA stretches at forks – both effectively suppressed by MRE11 inhibition - were also observed in BRCA2-depleted cells upon short treatments with low dose (25 nM) of CPT (Fig. 2b, Supplementary Table 5 and Supplementary Fig. 3b), which induces frequent fork reversal but does not completely arrest fork progression[11,21]. These data show that BRCA2 generally protects reversed forks from nucleolytic degradation also in conditions of mild replication interference, where fork degradation is difficult to monitor by DNA fiber assays.

Replication fork reversal is required for fork degradation

The role of BRCA2 in fork protection was previously linked to RAD51 chromatin loading[5,22]. However, RAD51 is also essential for the accumulation of reversed forks, which appear to be the substrate for degradation in *BRCA2*-defective cells (Figs. 1-2). To resolve this conundrum, we analyzed fork degradation upon effective *RAD51* downregulation. In contrast to *BRCA2*

defects[4,22], depletion of RAD51 by two different siRNA sequences in HU-treated cells did not lead to fork degradation and surprisingly suppressed fork degradation in BRCA2-depleted cells (Fig. 3a, Supplementary Fig. 4a). This data suggests that preventing fork reversal by *RAD51* inactivation prevents fork degradation in *BRCA2*-defective cells. Indeed, in our EM analysis, RAD51 depletion abolished HU-induced fork reversal also in the presence of mirin and prevented mirin-dependent restoration of reversed fork levels in *BRCA2*-defective cells (Fig. 3b and Supplementary Table 6). Notably, a different genetic perturbation that was recently shown to affect reversed fork formation *in vivo*[23] – i.e. depletion of the DNA translocase ZRANB3[24-26] – also completely suppressed fork degradation in *BRCA2*-defective cells (Fig. 3c). Reversed fork formation requires the helicase, but not the nuclease activity of ZRANB3[23,24,26]. Accordingly, we found that cells expressing at endogenous levels[23] helicase-defective – but not wild type or nuclease-defective – ZRANB3 are resistant to fork degradation upon *BRCA2* downregulation (Fig. 3d). Furthermore, PARP inhibition prior to HU treatment, which was previously reported to prevent efficient fork reversal[11], also suppressed fork degradation in BRCA2-depleted cells (Fig. 3e). Interestingly, this effect was not reported when the PARP inhibitor was added concomitantly with HU[27]. The latter conditions are likely to be initially permissive for HU-dependent reversed fork accumulation and thus prime fork degradation before PARP inhibition results in RECQ1-dependent reversed fork resolution[11,15]. Altogether, these results strongly support the notion that fork reversal triggers fork degradation in *BRCA2*-deficient cells. PARP inhibitor and cisplatin treatments were also recently used to link chemoresistance in *BRCA2*-defective cells with restored fork stability[9,28]. However, it should be noted that this outcome requires PARP inhibition or downregulation before *BRCA2* inactivation[9,28], under which conditions the efficiency of fork remodeling has not been directly tested.

Fork reversal does not require stable RAD51 nucleofilaments

In light of these data and previous reports[4], RAD51 seems to be essential both for BRCA2-independent reversed fork formation and for BRCA2-dependent protection of reversed forks from nucleolytic degradation. Thus, different genetic manipulations affecting *RAD51* function may have

diverse effects on each step of fork remodeling, likely explaining the different fork degradation phenotypes reportedly associated with *RAD51* defects[4,22]. A dominant *RAD51* mutant allele, found in FA patients, i.e. *RAD51-T131P*, was recently reported to destabilize RAD51 nucleofilaments, by constitutive activation of RAD51 ATPase activity, leading to ssDNA accumulation by nucleolytic processing of replicating DNA[8]. Upon HU treatment, these patient cells – similarly to *BRCA2*-deficient cells - displayed extensive fork degradation, which was suppressed by mirin treatment (Fig. 4a). EM analysis of *RAD51-T131P* cells revealed a marked reduction in reversed fork levels, compared to wild-type counterparts, which was also suppressed by MRE11 inhibition (Fig. 4b and Supplementary Table 7). Together with our previous results, these data strongly suggest that unstable RAD51 filaments in *RAD51-T131P* cells are still capable of driving fork reversal, but fail to protect reversed forks from nucleolytic degradation, uncoupling RAD51 functions in fork remodeling and stability.

RAD52 promotes stalled fork degradation via MRE11 recruitment

As RAD51-mediated fork reversal is BRCA2 independent, we next tested whether RAD52 - which was shown to play an essential role in the absence of BRCA2 and to assist HR mechanisms specifically upon replication stress[29-31] - could assist RAD51 in reversed fork formation and mediate fork degradation upon *BRCA2* deficiency. Besides its recently established role in mitotic DNA synthesis and upon breakage of persistently stalled forks[31,32], RAD52 is also stably recruited to chromatin in unperturbed S phase[32] and might thus participate in early events occurring at transiently stalled replication forks. Importantly, RAD52 depletion by two independent siRNA sequences - as well as treatment with a specific RAD52 inhibitor[32,33] – completely abolished fork degradation in *BRCA2*-deficient cells (Fig. 5a), in conditions that do not drastically affect cell cycle progression (Supplementary Fig. 4b). However, differently from RAD51 depletion, RAD52 depletion did not *per se* affect fork reversal, but rather restored normal reversed fork levels in HU-treated *BRCA2*-defective cells (Fig. 5b and Supplementary Table 8). These effects are highly reminiscent of those observed for MRE11 inhibition or PTIP depletion (Supplementary Fig. 2)[9] and suggest a key role for RAD52 in driving MRE11-dependent reversed fork processing. In line

with this interpretation, RAD52 inhibition significantly reduced recruitment of MRE11 to HU-stalled forks in BRCA2-defective cells, as monitored by iPOND (Fig. 5c). Furthermore, similarly to MRE11 inhibition and PTIP depletion[9], RAD52 depletion markedly suppressed HU-induced chromosomal breakage associated with *BRCA2* deficiency (Fig. 5d). Thus, RAD52 is required to prime MRE11-dependent stalled fork resection in *BRCA2*-defective cells. Whether the role of RAD52 in MRE11 recruitment and reversed fork resection reflects its strand exchange[34,35], single-strand annealing[36], inverse RNA/DNA strand exchange[37] or other yet uncharacterized biochemical activities will require further investigation.

Fork reversal prevents chromosome breakage upon fork stalling

Reversed forks were recently shown to protect against genome instability during accelerated proliferation in early embryogenesis[14]. We thus tested whether the reported rescue of viability of mouse *Brca2*-null embryonic stem cells (ESCs) by PTIP depletion[9] was also related to the protection of reversed forks from nucleolytic degradation. Upon transient downregulation of *Brca2* in unperturbed mouse embryonic stem cells (Supplementary Fig. 4c), we observed a decrease in the level of endogenous reversed forks, as compared to control cells. Notably, rescuing fork degradation by PTIP depletion restored normal frequencies of reversed forks in *Brca2*-null cells (Fig. 6a and Supplementary Table 9). These data further support a model where the essential role of key HR factors – e.g. RAD51 and BRCA2 - in early embryogenesis reflects their function in replication fork remodeling and protection[9,14].

Preventing MRE11-dependent degradation by mirin treatment, as well as *PTIP* or *RAD52* downregulation, suppressed the chromosomal breakage observed in HU-treated *BRCA2*-defective cells (Figs. 5d and 6b)[9]. However, preventing fork reversal – e.g. by *ZRANB3* inactivation - also suppressed nucleolytic degradation (Fig. 3c), but rather elevated chromosomal breakage in *BRCA2*-defective U2OS cells. Chromosomal breaks upon simultaneous inactivation of *ZRANB3* and *BRCA2* were not suppressed by mirin treatment or PTIP depletion, indicating that they are not directly associated with unscheduled fork degradation (Fig. 6b), but likely with defective HR-mediated repair of DSBs arising upon genotoxic stress in the absence of fork

reversal. Furthermore, PARP inhibition shortly before HU treatment – which is also preventing effective fork reversal[11] – increased chromosomal breakage in *BRCA2*-defective cells, but did not further increase chromosome instability in *ZRANB3-KO BRCA2*-defective cells, showing epistatic effects of these two means of fork reversal impairment (Fig. 6c). Altogether, these data strongly suggest that preventing fork degradation by abolishing fork reversal is detrimental for genome stability in *BRCA2*-defective cells, as it likely results in replication fork collapse. Thus fork reversal limits chromosomal breakage and genome instability at stalled forks, providing additional evidence for the physiological role of this global DNA transaction occurring upon replication stress[11,13]. These data also support a recent alternative model for the specific toxicity of PARP inhibition in *BRCA2*-defective tumors, where fork reversal suppression by PARP inhibitors[11,21] underlies the observed increase in fork breakage, requiring BRCA2 classical function in DSB repair[13].

Discussion

Taken together, our data reveal a complex interplay of different HR factors in forming and processing reversed forks. We propose that the same apparatus which mediates controlled resection of reversed forks - to allow their effective restart - may become deregulated in *BRCA2*-defective cells and mediate extensive degradation of reversed forks (Fig. 7). Importantly, we show that these processing events are primed by fork reversal and can potentially occur even upon genotoxic treatments that do not completely block replication fork progression (e.g. mild CPT treatments), which better reflect clinically relevant conditions of replication interference and are anyway strong inducers of fork reversal[21]. RAD51 is clearly involved both in the formation and in the protection of reversed forks. Therefore, the molecular consequences of specific *RAD51* mutations will likely depend on residual fork reversal and fork protection activities in each genetic background. Based on our data, stable RAD51 nucleofilaments are strictly required to protect regressed arms, but unstable filaments and/or inefficient loading of RAD51 on ssDNA - as in *BRCA2*-deficient or *RAD51-T131P* cells – would not impair strand exchange reactions at replication forks (i.e. fork reversal), probably because they do not imply extensive homology search at a distance. It is intriguing that *BRCA2* defects and this specific *RAD51* mutation are both associated with FA and it will be crucial to extend this molecular analysis to other FA mutations.

An intriguing implication of our work is the BRCA2-independent role of RAD51 in promoting fork reversal. This is in principle surprising, as RPA is known to rapidly bind ssDNA generated at forks and BRCA2 has been clearly implicated in replacing RPA with RAD51[38], in order to form a stable nucleofilament. However, previous reports have suggested BRCA2-independent RAD51 chromatin loading upon replication stress[9,39]. We envision several non-mutually exclusive scenarios to explain this intriguing observation: 1) besides BRCA2-mediated RAD51 loading at DNA ends, alternative mediators may have evolved to assist RPA-RAD51 exchange specifically in the context of ssDNA accumulating at a fork junction; 2) direct displacement of ssDNA-bound RPA by RAD51 at replication forks may be assisted by local exhaustion of free RPA[40] and/or reported direct interactions between RAD51 and the replicative helicase[41]; 3) as suggested by our

data on *RAD51-T131P* mutant cells, inefficient and partial replacement of RPA with short and unstable RAD51 filaments in the absence of BRCA2 may be sufficient to assist strand annealing at uncoupled forks and thus prime fork reversal, which is anyway assisted by other enzymatic activities[23]. Uncovering the specific regulation of RAD51 activity in fork remodeling will require extensive biochemical reconstitution and *in vivo* investigations on replication intermediates.

Another important implication of our data is that not all genetic conditions suppressing fork nucleolytic degradation in *BRCA2*-defective cells are expected to rescue genome stability and survival to genotoxic treatments, which is relevant for informed predictions on chemoresistance of *BRCA2*-defective tumors. Based on these data, we would expect that only genetic alterations still allowing reversed fork formation, but preventing their degradation would truly result in resistance to classical chemotherapeutic treatments (Fig. 7). However, due to the involvement of several factors – such as MRE11 and, here, RAD52 - in both fork degradation and restart of collapsed forks[31,42], a detectable decrease in chromosomal breakage due to limited fork resection may not *per se* predict better recovery and resistance to genotoxic treatments. Indeed, despite extensive resection, *BRCA2*-defective cells are able to restart stalled forks[4,9] and a significant proportion of the observed chromosomal breaks may in fact reflect fork restart pathways contributing to cell survival[18]. This intricate series of events likely explains why suppression of fork degradation is observed upon transient *RAD52* downregulation in *BRCA2*-defective cells, although inactivation of these genes is reportedly synthetically lethal[29] and RAD52 is actively explored as potential therapeutic target in *BRCA2*-defective tumors[43,44].

In light of our data and of the structural resemblance of regressed arms to DSBs, it is tempting to speculate that other classical DSB processing and repair factors may play relevant roles in replication fork remodeling, protection and restart, thereby determining sensitivity or resistance to current chemotherapeutic treatments.

Methods

Cells and cell culture

Human osteosarcoma U2OS cells, retinal pigment epithelium RPE-1 cells and VC-8 hamster cells, V-C8 cells complemented with human BACs (V-C8+*BRCA2* and V-C8+*BRCA S3291A*[4] were cultured in DMEM (41966-029, Life Technologies) supplemented with 10 % (v/v) FBS, 100 U ml^{-1} penicillin, and 100 µg ml^{-1} streptomycin at 37 °C and 6 % CO_2. Patient fibroblasts *RAD51-T131P* and BJ foreskin fibroblasts (ATCC) were grown in DMEM (41965-039, Life Technologies) supplemented with 15% (v/v) FBS, 100 U ml^{-1} penicillin, and 100 µg ml^{-1} streptomycin at 37 °C and 6 % CO_2[8]. PL2F2 mouse ESCs were maintained in DMEM with 15 % fetal bovine serum, 0.00072 % β-mercaptoethanol, 100 U ml^{-1} penicillin, 100 µg ml^{-1} streptomycin and 0.292 mg ml^{-1} L-glutamine at 37 °C and 5 % CO_2[9]. ESCs were cultured on feeder cells (MEFs inactivated with 10 mg ml^{-1} mitomycin C) for two passages, after they were transferred to feeder-free, gelatinized tissue culture dishes (0.1 % Gelatin from porcine skin, Sigma).

Transfections and treatments

For knockdown experiments, cells were transfected 20–48 h (as indicated below) prior to sample collection with the indicated siRNA using RNAiMax transfection reagent (Life Technologies) according to the manufacturer's instructions:

siLuc (40 nM; 5′-CGUACGCGGAAUACUUCGATT-3′);

siBRCA2 (48 h, 40 nM; 5'-UUGACUGAGGCUUGCUCAGUUTT-3');

siRAD51#1 (24 h, 40 nM; 5'-GACUGCCAGGAUAAAGCUUTT-3');

siRAD51#2 (24h, 40 nM; 5'-GUGCUGCAGCCUAAUGAGA-3');

siPTIP#1 (20 h, 40 nM; 5'-AAGGAAGAAGAGGAAGAGGAATT-3');

siPTIP#2 (20h, 40 nM; 5' UGUUUGCAAUUGCGGAUUAUU-3');

siRAD52#1 (24 h,10 nM, ON-TARGETplus Human RAD52 (5893), Dharmacon);

siRAD52#2 (48h, 10 nM, s11746 (4392420), Ambion).

Mouse ESCs were passaged in feeder-free conditions and plated in 50 % standard culture medium and 50 % Opti-MEM (Thermo Fisher Scientific) containing RNAiMax transfection reagent (Life Technologies) with the mix of following siRNAs at final concentration of 60 nM for 48 h:

siBrca2#1 (5'-UGUUAGGAGAUUCAUCUGGTT-3');

siBrca2#2 (5'-GGCCUAGUCUCAAGAACUCTT-3');

siBrca2#3 (5'-GGAAUUGUAAGGUAGGCUCTT-3').

BRCA2 conditional knockout cells with shRNAs against *Ptip* mRNA ESCs were provided by the lab of A. Nussenzweig[9].

The following reagents were used to treat the cells for the indicated time at the indicated final concentrations before collection: HU (H8627, Sigma-Aldrich) was prepared in double-distilled

H_2O to obtain a 100 mM (7.6 mg ml^{-1}) stock (freshly made); Mirin (M9948, Sigma-Aldrich) was dissolved in DMSO to yield a 50 mM stock, and aliquots were stored at −80 °C; CPT (C9911, Sigma-Aldrich) was dissolved in DMSO to yield a 20 mM (7 mg ml^{-1}) stock (freshly made); Nocodazole (M1404, Sigma-Aldrich) was prepared in DMSO at the final concentration of 1 mg ml^{-1}, aliquoted and stored at −80 °C. The Rad52 inhibitor (AICAR, A9978, Sigma-Aldrich) was dissolved in H_2O to a final concentration of 40 mM and stored at -20 °C. The PARP inhibitor Olaparib (AZD2281, Ku-0059436; S1060, Selleckchem) was prepared in DMSO to obtain the concentration of 20mM, aliquoted and stored at -20°C.

Western blotting

Cells were collected using trypsin, immediately lysed using SDS buffer (0.16 M Tris-HCl pH 6.8, 4 % SDS, 20 % glycerol, 100 mM DTT and 0.01 % bromophenol blue) and sonicated by Bioruptor (Diagenode) at 4 °C with the highest setting for 10 min (30 s on and 30 s off cycles). The lysates were incubated at 70 °C for 10 min and centrifuged at 13000 rpm for 7 min. Protein concentration in samples was measured using Nanodrop (A280). Equal amounts of protein (50–100 µg) were loaded on a NuPAGE-Novex 3–8 % Tris-Acetate or NuPAGE-Novex 10 % Bis-Tris gels (Life Technologies) and ran for 1 h, 180 V at room temperature. Proteins were blotted for 100 min (30 V, room temperature) on Amersham Protran 0.2 mm NC (GE Healthcare). Membranes were blocked in 5 % milk in 0.1 % TBST (1 × TBS supplemented with 0.1 % Tween 20) for at least 30 min and incubated in 2 % BSA with primary antibodies overnight at 4 °C. Membranes were probed for BRCA2 (1:500, Ab-1, OP 95, EMD Millipore); RAD51 (1:1000, H-92, sc-8349, Santa Cruz Biotechnology); RAD52 (1:1000, F-7, sc-365341, Santa Cruz Biotechnology); PTIP (1:500, ab214732, Abcam); ZRANB3 (1:1000, 23111-1-AP, ProteinTech); TFIIH (1:2000, S-19, sc-293, Santa Cruz Biotechnology). Secondary antibodies were added for 1 h at room temperature (in blocking solution). Membranes were washed three times with 0.1% TBST, 10 min each, after primary and secondary antibody incubations and detected with ECL detection reagent (GE healthcare). Uncropped blots for each western blot figure are provided in Supplementary Fig. 5.

Electron microscopy analysis

The procedure was performed as recently described[16], with minor modifications described below. Following the depletion of the protein of interest, asynchronous subconfluent cells were treated with 25 nM CPT for 1 h or 4 mM HU for 5 h. Where indicated, cells were pretreated with 50 mM Mirin for 1h. Cells were collected, resuspended in PBS and crosslinked with 4,5', 8-trimethylpsoralen (10 µg ml^{-1} final concentration), followed by irradiation pulses with UV 365 nm monochromatic light (UV Stratalinker 1800; Agilent Technologies). For DNA extraction, cells were lysed (1.28 M sucrose, 40 mM Tris-HCl [pH 7.5], 20 mM $MgCl_2$, and 4 % Triton X-100; Qiagen) and digested (800 mM guanidine–HCl, 30 mM Tris–HCl [pH 8.0], 30 mM EDTA [pH 8.0], 5 %

Tween-20, and 0.5 % Triton X-100) at 50 °C for 2 h in presence of 1 mg ml^{-1} proteinase K. The DNA was purified using chloroform/isoamylalcohol (24:1) and precipitated in 0.7 volume of isopropanol. Finally, the DNA was washed with 70 % EtOH and resuspended in 200 µl TE (Tris-EDTA) buffer. 100 U of restriction enzyme (PvuII high fidelity, New England Biolabs) were used to digest 12 µg of mammalian genomic DNA for 4-5 h. Replication intermediates enrichment was performed by QIAGEN Plasmid Mini Kit columns. The QIAGEN-tip 20 surface tension was reduced by applying 1 ml QBT buffer. The columns were washed and equilibrated with 10 mM Tris-HCl (pH 8.0), 1 M NaCl, followed by 10 mM Tris-HCl (pH 8.0), 300 mM NaCl, respectively. DNA was then loaded onto the columns. The columns were then washed with high NaCl solution (10 mM Tris-HCl [pH 8.0] and 900 mM NaCl) and eluted in caffeine solution (10 mM Tris-HCl [pH 8.0], 1 M NaCl, and 1.8 % [w/v] caffeine). To purify and concentrate the DNA an Amicon size-exclusion column was used. DNA was then resuspended in TE buffer. The Benzyldimethylalkylammonium chloride (BAC) method was used to spread the DNA on the water surface and then load it on carbon-coated 400-mesh copper grids. Subsequently, DNA was coated with platinum using a High Vacuum Evaporator MED 020 (BalTec). Microscopy was performed with a transmission electron microscope (Tecnai G2 Spirit; FEI; LaB6 filament; high tension ≤ 120 kV) and picture acquisition with a side mount charge-coupled device camera (2,600 × 4,000 pixels; Orius 1000; Gatan, Inc.). For each experimental condition at least 70 replication fork molecules were analyzed. DigitalMicrograph version 1.83.842 (Gatan, Inc.) and ImageJ (National Institutes of Health) were used to process and analyze the images.

DNA fibre analysis

Following the depletion of proteins of interest, cells were sequentially pulse-labelled with 30 µM CldU (c6891, Sigma-Aldrich) and 250 µM IdU (I0050000, European Pharmacopoeia) for 20 min and treated with hydroxyurea (4 mM) for 5 h. The cells were collected and resuspended in PBS at 2.5×10^5 cells ml^{-1}. The labeled cells were diluted 1:5 (v/v) with unlabeled cells, and 2.5 µl of cells were mixed with 7.5 µl of lysis buffer (200 mM Tris-HCl, pH 7.5, 50 mM EDTA, and 0.5 % [w/v] SDS) on a glass slide. After 9 min, the slides were tilted at 15–45°, and the resulting DNA spreads were air dried, fixed in 3:1 methanol/acetic acid overnight at 4 °C. The fibers were denatured with 2.5 M HCl for 1 h, washed with PBS and blocked with 0.2 % Tween 20 in 1 % BSA/PBS for 40 min. The newly replicated CldU and IdU tracks were labeled (for 2.5 h in the dark, at RT) with anti-BrdU antibodies recognizing CldU (1:500, ab6326; Abcam) and IdU (1:100, B44, 347580; BD), followed by 1 h incubation with secondary antibodies at RT in the dark: anti–mouse Alexa Fluor 488 (1:300, A11001, Invitrogen) and anti–rat Cy3 (1:150, 712-166-153, Jackson ImmunoResearch Laboratories, Inc.). Fibers were visualized (IX81; Olympus; objective lenses: LC Plan Fluor 60×, 1.42 NA oil Olympus BX60 microscope) and analyzed using ImageJ

software. The Mann–Whitney test was applied for statistical analysis using Prism (GraphPad Software).

Isolation of proteins on nascent DNA or iPOND

iPOND was performed essentially as described[45]. At least 1.0 x 10^8 of HEK293T cells were used per sample. BRCA2 depletion was performed 2 days before EdU labelling. The RAD52 inhibitor (AICAR, 40 μM) was optionally added 2 h before 10 μM EdU labeling (15 min), followed by 5 h 4 mM HU treatment (HU) or by 2 h 10 μM thymidine chase (Thy-chase). Cells were cross-linked with 1% formaldehyde for 12 min at room temperature, quenched with 0.125 M glycine and collected by scraping. The cells were washed with PBS three times and permeabilized with 0.25% Triton X-100/ PBS at room temperature for 30 min. Before the click reaction, samples were washed once in 0.5% BSA/PBS and once in PBS.

For the conjugation of EdU with biotin azide (Vanderbilt University, Chemical Synthesis Core), cells were incubated with click reaction buffer (10 mM sodium-L-ascorbate, 10 μM biotin azide and 2 mM CuSO4) for 2 h at room temperature. Following the click reaction, cells were washed once in 0.5% BSA/PBS and once in PBS. Cells were then resuspended in lysis buffer (50 mM Tris-HCl, pH 8.0, and 1% SDS) supplemented with protease inhibitors (Roche), and chromatin was solubilized by sonication in a Bioruptor (Diagenode) at 4 °C for 20 min (20 sec pulse/40 sec pause). After centrifugation at 16,100 g for 10 min, clarified supernatants were collected and diluted 1:1 (v/v) with PBS containing proteinase inhibitor. To capture biotin-tagged nascent DNA, each sample was incubated at 4 °C o/n in the dark with streptavidin-agarose beads (Novagen, D00148073). 200 μL of bead slurry was used per 1x10^8 cells. After binding, beads were washed with lysis buffer, followed by one time wash with 1 M NaCl and two times with lysis buffer. Captured proteins were eluted by boiling beads in 2 × SDS Laemmli Sample Buffer (0.4 g SDS, 2 ml 100% Glycerol, 1.25 mL 1 M Tris pH 6.8, and 0.01 g Bromophenol blue in 8 mL H2O) for 25 min at 95 °C. Proteins were resolved by electrophoresis using Mini-PROTEAN TGXTM gels (BioRad) and detected by western blotting with the indicated antibodies: MRE11 (1:2000, NB100-142, Novusbio); PCNA (1:1000, PC10, sc-56) and H3 (1:2000, Ab1791, Abcam).

Analysis of chromosome spreads

After the transfection with specific siRNAs, cells were treated with 4 mM HU for 5 h. The genotoxic agent was removed by washing 3 times with 1× PBS and the cells were then released into fresh medium containing 200 ng ml^{-1} nocodazole for 16 h. Cells were harvested and swollen with 75 mM KCl for 20 min at 37 °C. Swollen mitotic cells were collected and fixed with methanol:acetic acid (3:1). The fixing step was repeated 2 times. Cells were then dropped onto pre-hydrated glass slides and air-dried overnight. The following day, slides were mounted with Vectashield medium containing DAPI. Images were acquired with a microscope (model DMRB;

Leica) equipped with a camera (model DFC360 FX; Leica) and visible chromatid breaks/ gaps were counted.

Flow cytometry

For flow cytometric analysis of EdU/DAPI, cells were labelled for 30 min with 10 μM EdU, harvested and fixed for 15 min with 4 % formaldehyde/PBS. Cells were washed with 1 % BSA/PBS, pH 7.4 and permeabilized with 0.5% saponin/1 % PBS. Incorporated EdU was labelled according to the manufacturer's instructions (#C-10425; Life Technologies). DNA was stained with 1 μg ml^{-1} DAPI. Samples were measured on a Cyan ADP and ATTUNE NXT flow cytometer (Beckman Coulter) and analyzed by the FlowJo software.

Quantitative RT-PCR

Total RNA was isolated from cells using the Oligotex mRNA Mini Kit (Qiagen). 500 ng of RNA was used for cDNA synthesis using Transcriptor First Strand cDNA Synthesis Kit (Roche). Quantitative real-time SYBR-Green-based PCR reactions were performed in triplicate and monitored with the Light Cycler 480 (Roche) system. The following primer pairs were used to determine BRCA2 mRNA levels: forward 5'-CACCTCTGGAGCGGACTTATT-3'; reverse 5'-GCTTTGTTGCAGCGTGTCTT-3'.

The housekeeping gene GAPDH, used as a control, was amplified with the following primers: forward 5'-GACATTGTTGCCATCAACGACC-3'; reverse 5'-CCCGTTGATGACCAGCTTCC-3'.

Data availability

The authors declare that all relevant data supporting the findings of this study are available within the article and its Supplementary Information files, or from the corresponding author upon reasonable request.

ACKNOWLEDGEMENTS

We thank the Center for Microscopy and Image Analysis of the University of Zurich for technical assistance with electron microscopy. We are grateful to B. Conti, A. Smogorzewska and M. Jasin for sharing useful reagents and to all members of the Lopes group for useful discussions. This work was supported by the SNF grant 31003A_169959, the ERC Consolidator Grant 617102 and the Swiss Cancer League grant KFS-3967-08-2016 to M.L. and by the SNF grant 31003A_166451 to P.J. A.R.C. was supported by Human Frontier Science Fellowship (LT000393/2013), by the Center of Cancer Research and US Department of Defense (BCRP DOD Idea Expansion Award BC133858 and BCRP Break -through Award BC151331) to A.N.

AUTHOR CONTRIBUTIONS

S.M. performed and analyzed all EM, DNA fibers, iPOND, western blot and FACS experiments in RPE-1, U2OS and V-C8 Chinese Hamster cells, with extensive technical assistance of R.Z., S.U. and K.M.. N.C. performed all metaphase spread analyses, supervised by P.J.. M.B. assisted with iPOND and with EM experiments on BJ and RAD51-T131P fibroblasts. K. J. helped performing key experiments with mouse ESCs. A.R.C. and A.N. provided crucial reagents ahead of publication and assisted with experimental design and manuscript finalization. M.L. designed and supervised the project and wrote the manuscript.

COMPETING FINANCIAL INTERESTS

The authors declare no competing financial interests.

REFERENCES

1. Roy, R., Chun, J. & Powell, S. N. BRCA1 and BRCA2: different roles in a common pathway of genome protection. *Nat Rev Cancer* **12,** 68–78 (2012).
2. Thorslund, T. *et al.* The breast cancer tumor suppressor BRCA2 promotes the specific targeting of RAD51 to single-stranded DNA. *Nat Struct Mol Biol* **17,** 1263–1265 (2010).
3. Lord, C. J. & Ashworth, A. Mechanisms of resistance to therapies targeting BRCA-mutant cancers. *Nat. Med.* **19,** 1381–1388 (2013).
4. Schlacher, K. *et al.* Double-strand break repair-independent role for BRCA2 in blocking stalled replication fork degradation by MRE11. *Cell* **145,** 529–542 (2011).
5. Schlacher, K., Wu, H. & Jasin, M. A distinct replication fork protection pathway connects Fanconi anemia tumor suppressors to RAD51-BRCA1/2. *Cancer Cell* **22,** 106–116 (2012).
6. Berti, M. & Vindigni, A. Replication stress: getting back on track. *Nat Struct Mol Biol* **23,** 103–109 (2016).
7. Thangavel, S. *et al.* DNA2 drives processing and restart of reversed replication forks in human cells. *J Cell Biol* **208,** 545–562 (2015).
8. Wang, A. T. *et al.* A Dominant Mutation in Human RAD51 Reveals Its Function in DNA Interstrand Crosslink Repair Independent of Homologous Recombination. *Mol Cell* **59,** 478–490 (2015).
9. Ray Chaudhuri, A. *et al.* Replication fork protection confers chemoresistance in BRCA-deficient cells. *Nature* **535,** 382–387 (2016).
10. Neelsen, K. J., Zanini, I. M. Y., Herrador, R. & Lopes, M. Oncogenes induce genotoxic stress by mitotic processing of unusual replication intermediates. *J Cell Biol* **200,** 699–708 (2013).
11. Zellweger, R. *et al.* Rad51-mediated replication fork reversal is a global response to genotoxic treatments in human cells. *J Cell Biol* **208,** 563–579 (2015).
12. Follonier, C., Oehler, J., Herrador, R. & Lopes, M. Friedreich's ataxia-associated GAA repeats induce replication-fork reversal and unusual molecular junctions. *Nat Struct Mol Biol* (2013). doi:10.1038/nsmb.2520
13. Neelsen, K. J. & Lopes, M. Replication fork reversal in eukaryotes: from dead end to dynamic response. *Nat Rev Mol Cell Biol* **16,** 207–220 (2015).
14. Ahuja, A. K. *et al.* A short G1 phase imposes constitutive replication stress and fork remodelling in mouse embryonic stem cells. *Nature Communications* **7,** 10660 (2016).
15. Berti, M. *et al.* Human RECQ1 promotes restart of replication forks reversed by

DNA topoisomerase I inhibition. *Nat Struct Mol Biol* **20,** 347–354 (2013).

16. Zellweger, R. & Lopes, M. in *Genome Instability: Methods and Protocols* (eds. Muzi-Falconi, M. & Brown, G.) **Methods in Molecular Biology, v.1672,** (Springer Science+Business Media LLC 2017, 2017).
17. Dupré, A. *et al.* A forward chemical genetic screen reveals an inhibitor of the Mre11-Rad50-Nbs1 complex. *Nat. Chem. Biol.* **4,** 119–125 (2008).
18. Lemacon, D. *et al.* MRE11 and EXO1 nucleases degrade reversed forks and lead to MUS81-dependent fork
rescue in BRCA2-deficient cells. *accompanying manuscript*
19. Vindigni, A. & Lopes, M. Combining electron microscopy with single molecule DNA fiber approaches to study DNA replication dynamics. *Biophys. Chem.* **225,** 3–9 (2017).
20. Wang, X., Takenaka, K. & Takeda, S. PTIP promotes DNA double-strand break repair through homologous recombination. *Genes Cells* **15,** 243–254 (2010).
21. Ray Chaudhuri, A. *et al.* Topoisomerase I poisoning results in PARP-mediated replication fork reversal. *Nat Struct Mol Biol* **19,** 417–423 (2012).
22. Leuzzi, G., Marabitti, V., Pichierri, P. & Franchitto, A. WRNIP1 protects stalled forks from degradation and promotes fork restart after replication stress. *Embo J* **35,** 1437–1451 (2016).
23. Vujanovic, M. *et al.* Replication fork slowing and reversal upon genotoxic stress require PCNA polyubiquitination and ZRANB3 DNA translocase activity. *Molecular Cell, accepted for publication*
24. Ciccia, A. *et al.* Polyubiquitinated PCNA recruits the ZRANB3 translocase to maintain genomic integrity after replication stress. *Mol Cell* **47,** 396–409 (2012).
25. Yuan, J., Ghosal, G. & Chen, J. The HARP-like Domain-Containing Protein AH2/ZRANB3 Binds to PCNA and Participates in Cellular Response to Replication Stress. *Mol Cell* **47,** 410–421 (2012).
26. Weston, R., Peeters, H. & Ahel, D. ZRANB3 is a structure-specific ATP-dependent endonuclease involved in replication stress response. *Genes Dev* **26,** 1558–1572 (2012).
27. Ying, S., Hamdy, F. C. & Helleday, T. Mre11-dependent degradation of stalled DNA replication forks is prevented by BRCA2 and PARP1. *Cancer Res.* **72,** 2814–2821 (2012).
28. Ding, X. *et al.* Synthetic viability by BRCA2 and PARP1/ARTD1 deficiencies. *Nature Communications* **7,** (2016).
29. Feng, Z. *et al.* Rad52 inactivation is synthetically lethal with BRCA2 deficiency. *Proc Natl Acad Sci U S A* **108,** 686–691 (2011).

30. Wray, J., Liu, J., Nickoloff, J. A. & Shen, Z. Distinct RAD51 associations with RAD52 and BCCIP in response to DNA damage and replication stress. *Cancer Res.* **68,** 2699–2707 (2008).
31. Sotiriou, S. K. *et al.* Mammalian RAD52 Functions in Break-Induced Replication Repair of Collapsed DNA Replication Forks. *Mol Cell* **64,** 1127–1134 (2016).
32. Bhowmick, R., Minocherhomji, S. & Hickson, I. D. RAD52 Facilitates Mitotic DNA Synthesis Following Replication Stress. *Mol Cell* **64,** 1117–1126 (2016).
33. Sullivan, K. *et al.* Identification of a Small Molecule Inhibitor of RAD52 by Structure-Based Selection. *PLoS One* **11,** e0147230 (2016).
34. Kumar, J. K. & Gupta, R. C. Strand exchange activity of human recombination protein Rad52. *Proc Natl Acad Sci U S A* **101,** 9562–9567 (2004).
35. Bi, B., Rybalchenko, N., Golub, E. I. & Radding, C. M. Human and yeast Rad52 proteins promote DNA strand exchange. *Proc Natl Acad Sci U S A* **101,** 9568–9572 (2004).
36. Rothenberg, E., Grimme, J. M., Spies, M. & Ha, T. Human Rad52-mediated homology search and annealing occurs by continuous interactions between overlapping nucleoprotein complexes. *Proc Natl Acad Sci U S A* **105,** 20274–20279 (2008).
37. Mazina, O. M., Keskin, H., Hanamshet, K., Storici, F. & Mazin, A. V. Rad52 Inverse Strand Exchange Drives RNA-Templated DNA Double-Strand Break Repair. *Mol Cell* (2017). doi:10.1016/j.molcel.2017.05.019
38. Jensen, R. B., Carreira, A. & Kowalczykowski, S. C. Purified human BRCA2 stimulates RAD51-mediated recombination. *Nature* **467,** 678–683 (2010).
39. Tarsounas, M., Davies, D. & West, S. C. BRCA2-dependent and independent formation of RAD51 nuclear foci. *Oncogene* **22,** 1115–1123 (2003).
40. Ma, C. J., Gibb, B., Kwon, Y., Sung, P. & Greene, E. C. Protein dynamics of human RPA and RAD51 on ssDNA during assembly and disassembly of the RAD51 filament. *Nucleic Acids Res* **45,** 749–761 (2017).
41. Bailis, J. M., Luche, D. D., Hunter, T. & Forsburg, S. L. Minichromosome maintenance proteins interact with checkpoint and recombination proteins to promote s-phase genome stability. *Mol Cell Biol* **28,** 1724–1738 (2008).
42. Hashimoto, Y., Puddu, F. & Costanzo, V. RAD51- and MRE11-dependent reassembly of uncoupled CMG helicase complex at collapsed replication forks. *Nat Struct Mol Biol* **19,** 17–24 (2011).
43. Huang, F. *et al.* Targeting BRCA1- and BRCA2-deficient cells with RAD52 small molecule inhibitors. *Nucleic Acids Res* **44,** 4189–4199 (2016).
44. Hengel, S. R. *et al.* Small-molecule inhibitors identify the RAD52-ssDNA interaction

as critical for recovery from replication stress and for survival of BRCA2 deficient cells. *Elife* **5,** (2016).

45. Sirbu, B. M., Couch, F. B. & Cortez, D. Monitoring the spatiotemporal dynamics of proteins at replication forks and in assembled chromatin using isolation of proteins on nascent DNA. *Nat Protoc* **7,** 594–605 (2012).

Figure Legends

Figure 1. Stalled replication forks can reverse in the absence of BRCA2, but are targeted by nucleolytic degradation. (a, c) Electron micrographs of representative replication forks from RPE-1 cells: parental (P) and daughter (D) duplexes. (a) The black arrow indicates the regressed arm (R); the four-way junction at the reversed fork is magnified in the inset. (c) The white arrow points to a ssDNA region at the fork. Scale bar, 200 nm (= 460 bp), 40 nm (= 92 bp) in the inset. (b) Left panel: frequency of reversed replication forks isolated from mock-depleted (siLuc) and BRCA2-depleted (si*BRCA2*) RPE-1 cells upon optional 5 h treatment with 4 mM HU; where indicated 50 mM mirin was added 1h before HU treatment (6 h total treatment). The number of replication intermediates analyzed is indicated in parentheses. The graph depicts mean and standard deviations from three independent EM experiments, blinded to the investigator. The results of the individual biological replicates are in Supplementary Table 1. Right panel: western blot analysis of BRCA2 levels in siLuc and siBRCA2 RPE-1 cells, 48 h after transfection. TFIIH, loading control. (d) Graphical distribution of ssDNA length at the junction (white arrow in Fig. 1c) in siLuc and siBRCA2 RPE-1 cells optionally treated with 4mM of HU for 5 h and 50 mM of mirin for 6 h. Only molecules with detectable ssDNA stretches are included in the analysis. The lines show the median length of ssDNA regions at the fork in the specific set of analyzed molecules. Statistical analysis: Mann-Whitney test; ns, not significant; **, P< 0.01; ***, P< 0.001; ****, P< 0.0001. The number of analyzed molecules is in brackets.

Figure 2. BRCA2 maintains reversed fork stability in different cell lines and upon different genotoxic treatments. (**a**) Top: schematic representation of BRCA2 protein. Green boxes: RAD51-binding BRC repeats; Black box: DBD, DNA binding domain; C-ter, yellow bar: RAD51-biding c-terminal region. Blue arrows indicate truncations in V-C8 cells; the S3291A mutation is marked in red. Bottom: frequency of reversed replication forks isolated from VC-8 cells and V-C8 cells stably expressing full-length BRCA2 or BRCA2 containing the S3291A mutation, treated as in Fig. 1 (4 mM HU for 5 h; 50 mM mirin for 6 h). The number of analyzed molecules is indicated in brackets. Results of two independent EM experiments are in Supplementary Table 4. Right: western blot analysis of BRCA2 levels in V-C8 and complemented cells. TFIIH, loading control. (**b**) EM-based analysis of reversed replication forks isolated from siLuc and siBRCA2 (48 h) RPE-1 cells treated with 25 nM CPT for 1h; where indicated 50 mM mirin was added 1h before CPT treatment (2h total treatment). In brackets the total number of analyzed molecules. Results of two independent EM experiments are in Supplementary Table 5.

Figure 3. Impairing replication fork reversal prevents fork degradation in BRCA2-defective cells. (**a**) RPE-1 cells were transfected with siRNA before CldU (red) and IdU (green) labeling (siBRCA2, 48 h; siRAD51, 24 h), followed by treatment with 4 mM HU for 5 h. Left panel: levels of indicated proteins, assessed by western blot. TFIIH, loading control. Middle panel: a representative set of DNA fibers from each condition is shown. Right panel: IdU/CIdU tract length ratio is plotted. Horizontal lines and the numbers indicate the median value. Whiskers indicate the 10-90 percentiles. At least one hundred replication forks were analyzed for each condition. Statistical analysis: Mann-Whitney test; ns, not significant; ****, P< 0.0001. See also Supplementary Fig. 4a. (**b**) Frequency of reversed replication forks isolated from siLuc, siBRCA2 (48 h) and siRAD51 (24 h) RPE-1 cells treated as in Fig. 1 (4 mM HU for 5 h; 50 mM mirin for 6 h). In brackets the total number of analyzed molecules. Results of two independent EM experiments are in Supplementary Table 6. (**c**) The indicated U2OS-based cell lines were transfected with siRNA before CldU (red) and IdU (green) labeling (siBRCA2, 48 h; siRAD51, 24 h), followed by treatment with 4 mM HU for 5 h and DNA fibre spreading. Left panel: levels of indicated proteins, assessed by western blot. TFIIH, loading control. Right panel: IdU/CIdU tract length ratio is plotted. Track length analysis and statistics as in Fig. 3a. (**d**) Stable derivatives of *ZRANB3-KO* U2OS cells, expressing wild type (WT), helicase-dead (HD) or nuclease-dead (ND) ZRANB3 at endogenous levels were transfected with siRNA for BRCA2 48h before CldU (red) and IdU (green) labeling, followed by treatment with 4 mM HU for 5 h. Track length analysis and statistics as in Fig. 3a. (**e**) U2OS cells were transfected with the indicated siRNAs 48h before CldU (red) and IdU (green) labeling, followed by treatment with 4 mM HU for 5 h. The PARP inhibitor olaparib (10 mM) was optionally added 2h before CldU addition. Track length analysis and statistics as in Fig. 3a.

Figure 4. Stable RAD51 nucleofilaments are required not to form, but rather to protect reversed forks from nucleolytic degradation. (**a**) Control (BJ) or RAD51-T131P fibroblasts were labeled with CldU (red) and IdU (green), followed by treatment with 4 mM HU for 5 h and 50 mM mirin for 6 h, as indicated. A set of representative DNA fibers from each condition is shown. Ratios of IdU versus CldU tracts are plotted. Track length analysis and statistics as in Fig. 3a. (**b**) EM-based assessment of the frequency of reversed replication forks isolated from BJ and T131P treated as indicated (4 mM HU for 5 h; 50 mM mirin for 6 h). In brackets the total number of analyzed molecules. Results of two independent EM experiments are in Supplementary Table 7.

Figure 5. RAD52 promotes stalled fork degradation in BRCA2-defective cells (**a**) U2OS cells were transfected with siRNA before labeling (siBRCA2, 48 h; siRAD52, 24 h) with CldU (red) and IdU (green), followed by treatment with 4 mM HU for 5 h. The RAD52 inhibitor (AICAR 40

mM) was optionally added 2h before CldU labelling. Left: levels of indicated proteins, assessed by western blot. TFIIH, loading control. Middle panel: a representative set of DNA fibers from each condition is shown. Right: ratios of IdU versus CldU tracts are plotted. Track length analysis and statistics as in Fig. 3a. (**b**) EM-based assessment of the frequency of reversed replication forks isolated from U2OS cells transfected with control and siRNA against BRCA2 (48 h) and/or RAD52 (24 h). Cells were treated with 4 mM HU for 5 h and 50 mM mirin for 6 h, as indicated. In brackets, the total number of analyzed molecules. Results of two independent EM experiments are in Supplementary Table 8. (**c**) HEK293T cells were transfected by the indicated siRNAs 48 h before the EdU-labelling for 15 min and then treated with HU 4 mM for 5 h. AICAR 40 mM (RAD52 inhibitor) was optionally added 2 h before EdU labelling and retained throughout the experiment. Proteins associated with nascent DNA were isolated by iPOND (see Methods) and detected with the indicated antibodies. For the thymidine chase experiment (Thy-chase) 10 mM thymidine was added for 2 h directly after the EdU labelling. In the control experiment (no EdU), the click reaction is performed using DMSO instead of biotin azide. The graph represents average and standard deviations (error bars) of quantified of MRE11 capture signals from three independent experiments. (**d**) Chromosomal breakage quantification after HU and mirin treatment (4 mM HU for 5 h; 50 mM mirin for 6 h) of U2OS cells after depletion of BRCA2 (48 h) and/or RAD52 (24 h). One hundred cells in pro-metaphase were analyzed. Similar results were obtained in two biological replicates.

Figure 6. Fork reversal impairment suppresses fork degradation, but increases chromosomal breakage in BRCA2-defective cells. (**a**) Frequency of reversed replication forks isolated from unperturbed mouse ESCs – transfected with siLuc or siBrca2 (48 h) - and from $Brca2^{-/-}$ shPtip ESCs. In brackets the total number of analyzed molecules. Results of two independent EM experiments are in Supplementary Table 9. (**b**) Representative count of chromatid breaks upon 5 h treatment with HU 4 mM in control and ZRANB3 knockout (KO) U2OS cells; where indicated, 50 mM mirin was added 1h before HU treatment (6h total treatment), and siRNA transfection was performed 48 h (BRCA2) or 20 h (PTIP) before HU treatment. The number of chromatid breaks per chromosome spread was plotted. At least 150 chromosome spreads were analyzed. Error bars represent SEM. A representative DAPI stained chromosome spread is shown. Inset 1 and 2 show intact chromosomes while 3 and 4 display chromosomal breaks. (**c**) Chromosomal breakage quantification of HU treated (4 mM HU, 5 h) U2OS after optional depletion of BRCA2 (48 h) and/or PARP inhibition (Olaparib 10mM, added 2h before HU). At least 180 cells in pro-metaphase were analyzed. The number of chromatid breaks per chromosome spread was plotted. Error bars represent SEM. Similar results were obtained in three biological replicates.

Figure 7. Model for the role of different HR factors in stalled fork remodeling and protection. With the help of ZRANB3 and PARP activity, RAD51 promotes efficient reversal of stalled replication forks independently of BRCA2. Upon initial resection of reversed forks, RAD51 is efficiently loaded by BRCA2 on regressed arms to limit MRE11/PTIP/RAD52-dependent nucleolytic degradation and promote efficient fork restart. In BRCA2-defective cells, deregulated MRE11-dependent degradation of reversed forks leads to ssDNA accumulation and chromosomal breaks. Limiting reversed fork degradation restores fork integrity and prevents chromosomal breakage. Preventing fork reversal also restores fork integrity in BRCA2-defective cells - by reduced availability of degradation substrates – but leads to increased chromosomal breakage, and is thus detrimental for genome stability.

Figure 1

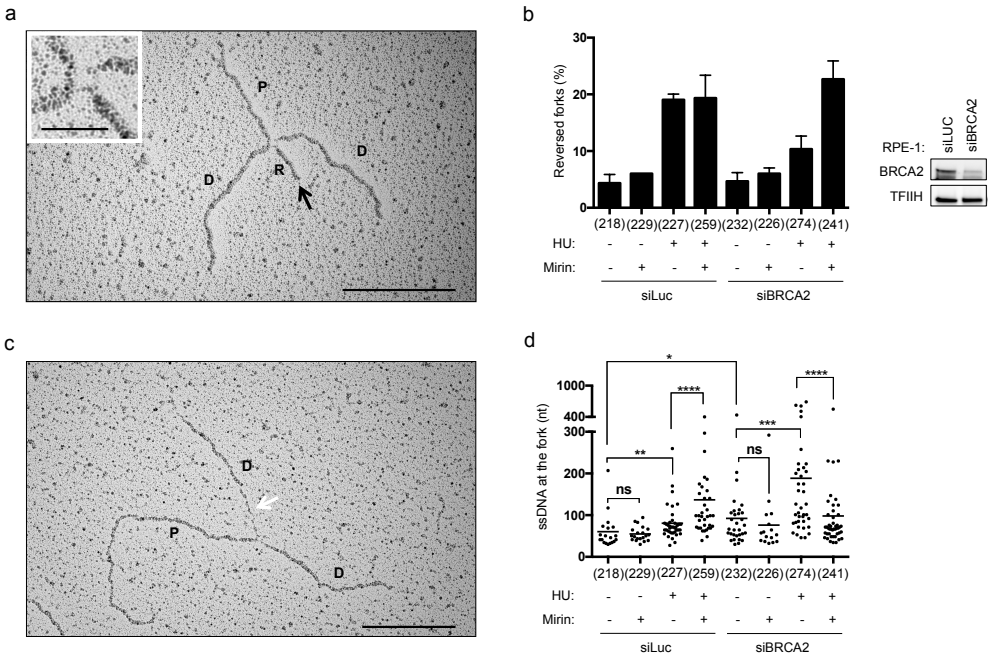

Figure 2

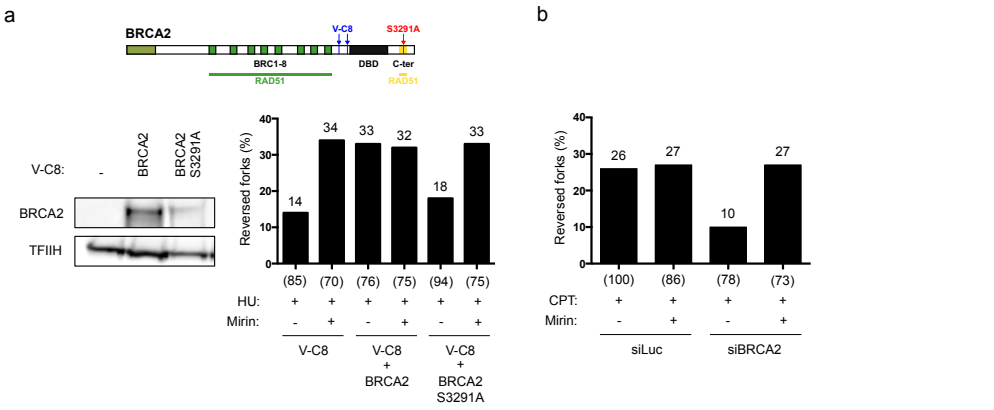

Figure 3

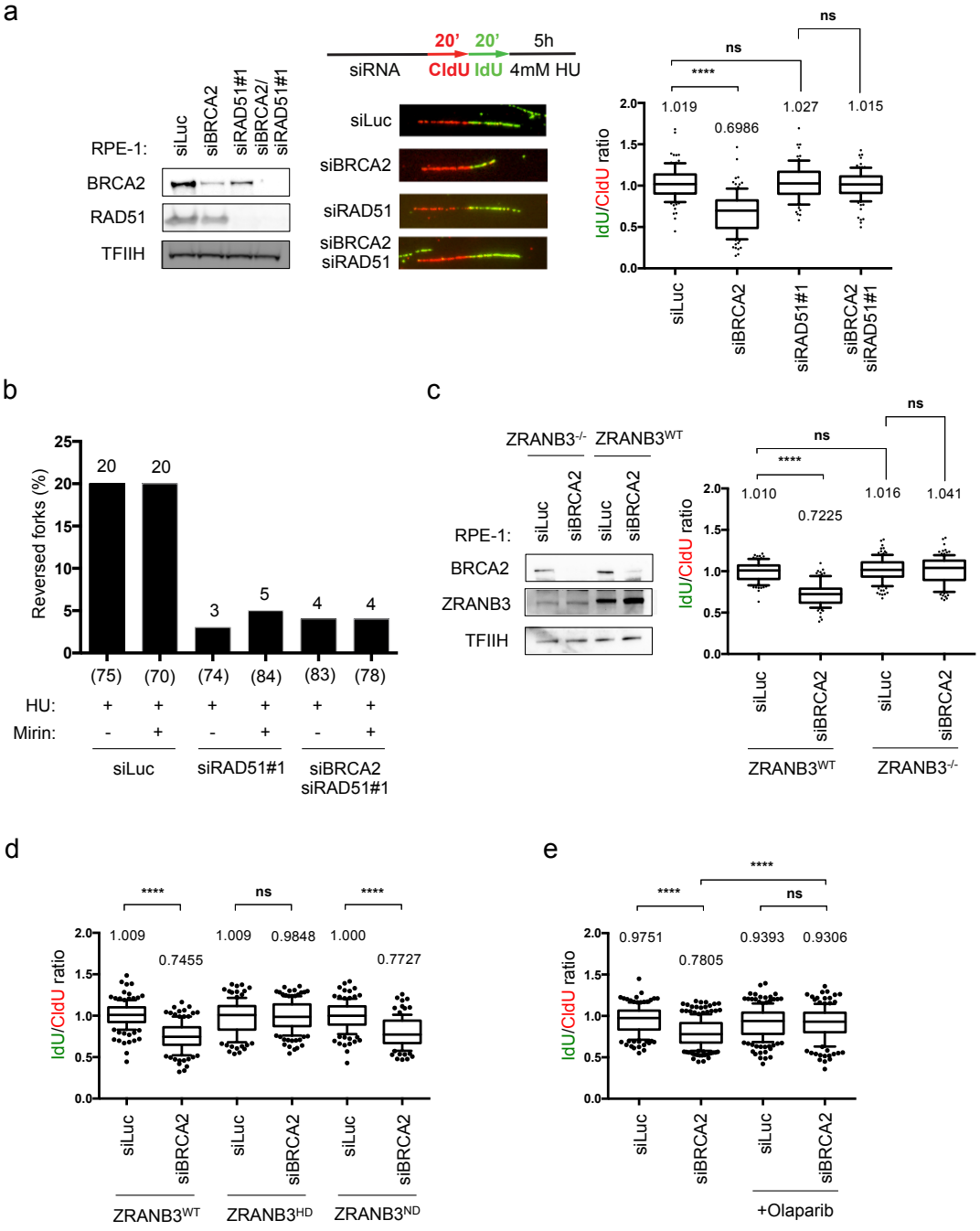
a
RPE-1:
siLuc
siBRCA2
siRAD51#1
siBRCA2/ siRAD51#1
BRCA2
RAD51
TFIIH
siRNA
20'
CldU
20'
IdU
5h
4mM HU
siLuc
siBRCA2
siRAD51
siBRCA2 siRAD51
IdU/CldU ratio
ns
****
1.019
0.6986
1.027
1.015
b
Reversed forks (%)
20
20
3
5
4
4
(75)
(70)
(74)
(84)
(83)
(78)
HU:
Mirin:
siLuc
siRAD51#1
siBRCA2 siRAD51#1
c
ZRANB3-/-
ZRANB3WT
RPE-1:
BRCA2
ZRANB3
TFIIH
1.010
0.7225
1.016
1.041
ZRANB3WT
ZRANB3-/-
d
1.009
0.7455
1.009
0.9848
1.000
0.7727
ZRANB3WT
ZRANB3HD
ZRANB3ND
e
0.9751
0.7805
0.9393
0.9306
+Olaparib

Figure 4

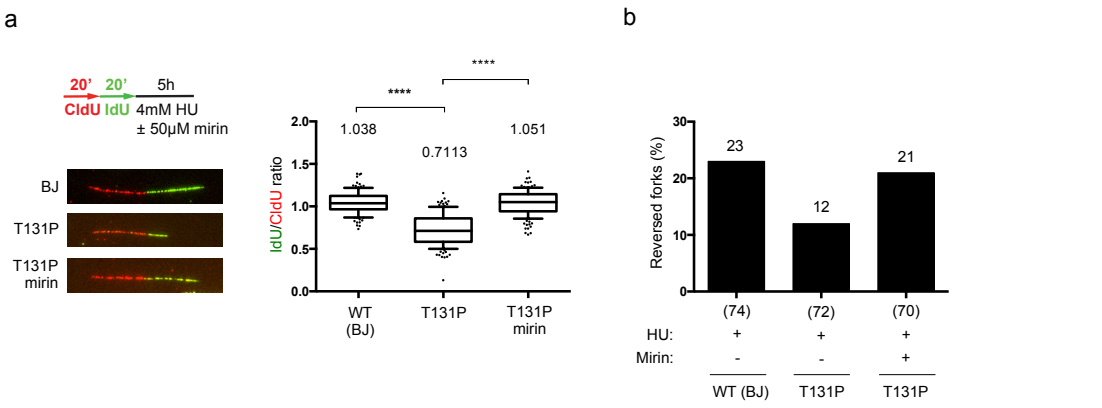

Figure 5

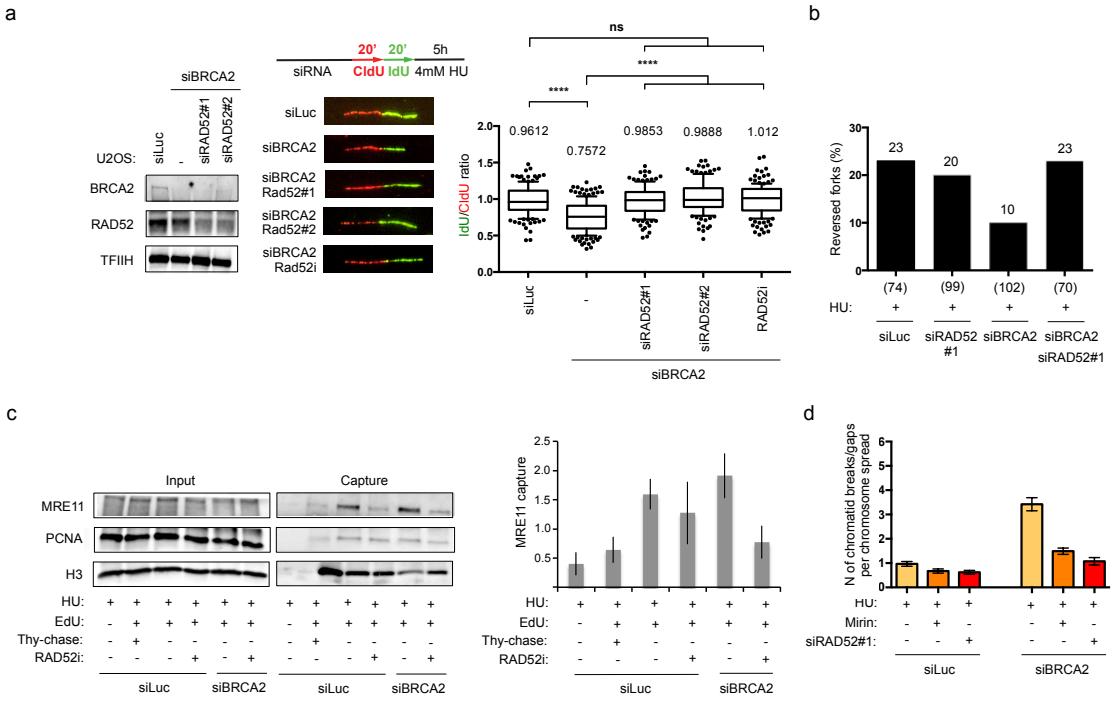

Figure 6

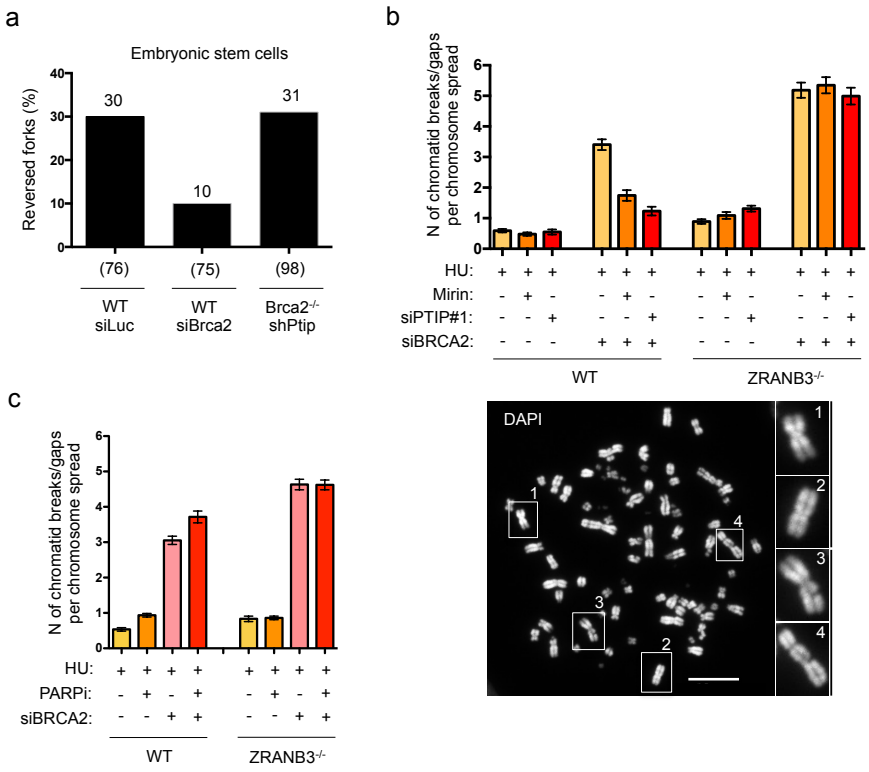

Figure 7

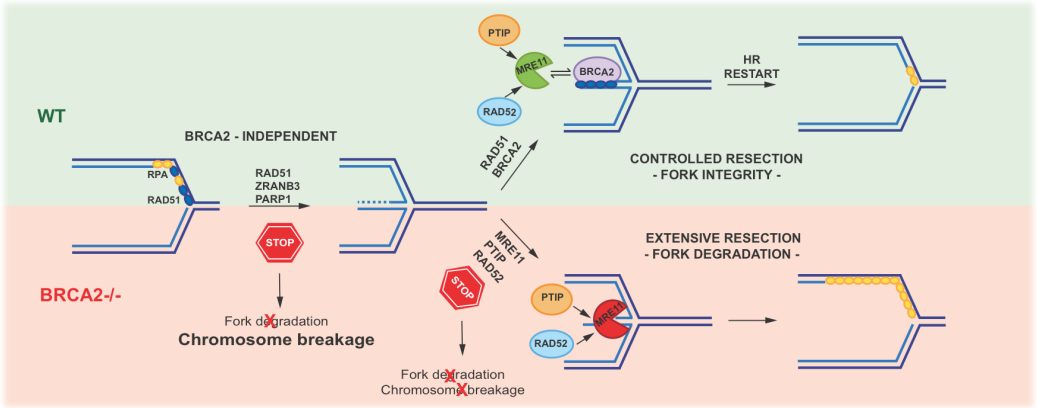

Replication fork reversal triggers fork degradation in BRCA2-defective cells

Sofija Mijic, Ralph Zellweger, Nagaraja Chappidi, Matteo Berti, Kurt Jacobs, Karun Mutreja, Sebastian Ursich, Arnab Ray Chaudhuri, Andre Nussenzweig, Pavel Janscak and Massimo Lopes

Supplementary information

9 Supplementary Tables

5 Supplementary Figures

RPE-1	siLuc				siBRCA2			
5h HU	-	-	+	+	-	-	+	+
mirin	-	+	-	+	-	+	-	+
% RF Exp #1	**6 (70)**	**6 (87)**	**19 (84)**	**20 (102)**	**5 (76)**	**5 (76)**	**9 (110)**	**25 (74)**
% RF Exp #2	**3 (71)**	**6 (70)**	**20 (71)**	**23 (84)**	**3 (71)**	**6 (76)**	**9 (78)**	**24 (89)**
% RF Exp #3	**4 (77)**	**6 (72)**	**18 (72)**	**15 (73)**	**6 (87)**	**7 (74)**	**13 (86)**	**19 (78)**

Supplementary Table 1. Electron microscopy data for Figure 1b. Percentage of observed reversed forks (% RF) in three independent EM experiments for samples in Figure 1b. Number of analyzed molecules is indicated in brackets.

RPE-1	siLuc	siBrca2
30min HU	-	-
% RF Exp #1	**16 (88)**	**11 (71)**
% RF Exp #2	**16 (83)**	**11 (76)**

Supplementary Table 2. Electron microscopy data for Supplementary Figure 1b. Percentage of observed reversed forks (% RF) in two independent EM experiments for samples in Supplementary Figure 1b. Number of analyzed molecules is indicated in brackets.

RPE-1	siLuc	siPTIP	siBRCA2	siBRCA2 siPTIP
HU	+	+	+	+
mirin	-	-	-	-
% RF Exp #1	**19 (84)**	**20 (81)**	**9 (110)**	**22 (95)**
% RF Exp #2	**20 (71)**	**23 (78)**	**9 (78)**	**21 (77)**

Supplementary Table 3. Electron microscopy data for Supplementary Figure 2e. Percentage of observed reversed forks (% RF) in two independent EM experiments for samples in Supplementary Figure 2e. Number of analyzed molecules is indicated in brackets.

VC-8	VC-8		+BRCA2		+S3291A	
HU	+	+	+	+	+	+
mirin	-	+	-	+	-	+
% RF Exp #1	**14** **(85)**	**34** **(70)**	**33** **(76)**	**32** **(75)**	**18** **(94)**	**33** **(75)**
% RF Exp #2	**14** **(80)**	**30** **(92)**	**31** **(84)**	**34** **(74)**	**19** **(100)**	**34** **(82)**

Supplementary Table 4. Electron microscopy data for Figure 2a. Percentage of observed reversed forks (% RF) in two independent EM experiments for samples in Figure 2a. Number of analyzed molecules is indicated in brackets.

RPE-1	siLuc		siBRCA2	
CPT	+	+	+	+
mirin	-	+	-	+
% RF Exp #1	**26** **(100)**	**27** **(86)**	**10** **(78)**	**27** **(73)**
% RF Exp #2	**30** **(75)**	**29** **(89)**	**10** **(84)**	**26** **(76)**

Supplementary Table 5. Electron microscopy data for Figure 2b. Percentage of observed reversed forks (% RF) in two independent EM experiments for samples in Figure 2b. Number of analyzed molecules is indicated in brackets.

RPE-1	siLuc		siRAD51		siBRCA2 siRAD51	
HU	+	+	+	+	+	+
mirin	-	+	-	+	-	+
% RF Exp #1	**20 (75)**	**20 (70)**	**3 (74)**	**5 (84)**	**4 (83)**	**4 (78)**
% RF Exp #2	**23 (83)**	**21 (78)**	**6 (80)**	**6 (74)**	**5 (71)**	**4 (83)**

Supplementary Table 6. Electron microscopy data for Figure 3b. Percentage of observed reversed forks (% RF) in two independent EM experiments for samples in Figure 3b. Number of analyzed molecules is indicated in brackets**.**

BJ/T131P	BJ	T131P	
HU	+	+	+
mirin	-	-	+
% RF Exp #1	**23 (74)**	**12 (72)**	**21 (70)**
% RF Exp #2	**25 (72)**	**11 (73)**	**19 (82)**

Supplementary Table 7. Electron microscopy data for Figure 4b. Percentage of observed reversed forks (% RF) in two independent EM experiments for samples in Figure 4b. Number of analyzed molecules is indicated in brackets.

U2OS	siLuc	siRAD52	siBRCA2	siBRCA2 siRAD52
HU	+	+	+	+
% RF Exp #1	**23** **(74)**	**20** **(99)**	**10** **(102)**	**23** **(70)**
% RF Exp #2	**24** **(83)**	**22** **(70)**	**10** **(70)**	**21** **(70)**

Supplementary Table 8. Electron microscopy data for Figure 5b. Percentage of observed reversed forks (% RF) in two independent EM experiments for samples in Figure 5b. Number of analyzed molecules is indicated in brackets.

mESC	siLuc	siBrca2	Brca2$^{-/-}$ shPtip
HU	-	-	-
% RF Exp #1	**30** **(76)**	**10** **(75)**	**31** **(98)**
% RF Exp #2	**30** **(84)**	**11** **(71)**	**38** **(86)**

Supplementary Table 9. Electron microscopy data for Figure 6a. Percentage of observed reversed forks (% RF) in two independent EM experiments for samples in Figure 6a. Number of analyzed molecules is indicated in brackets.

Supplementary figures

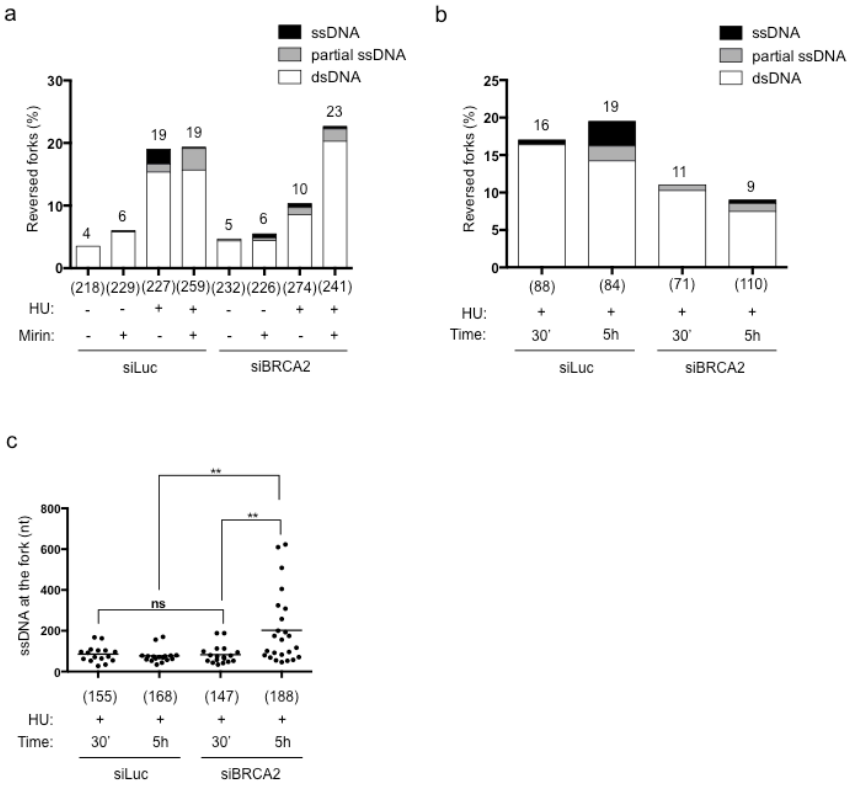

Supplementary Figure 1. ssDNA detection at stalled and reversed replication forks in BRCA2-defective cells. (a) Distribution of the reversed forks scored in Fig. 1b among different categories, based on the presence of detectable ssDNA stretches on the regressed arm. "dsDNA" represents reversed forks where no ssDNA is detected, while "ssDNA" represents regressed arms that are entirely single-stranded. **(b)** Frequency of reversed forks scored in siLuc and siBRCA2 RPE-1 treated with 4mM of HU for the indicated time. Different reversed fork categories are represented, as in panel (a). The total frequency of reversed forks is indicated above the bars. The total number of replication intermediates analyzed is indicated in parentheses. Results of two independent EM experiments are in Supplementary Table 2. **(c)** Graphical distribution of ssDNA length at the junction for the samples in (b). Only molecules with detectable ssDNA stretches are included in the analysis. The lines show the median length of ssDNA regions at the fork in the specific set of analyzed molecules. Statistical analysis: Mann-Whitney test; ns, not significant; **, P< 0.01. The number of analyzed molecules is in brackets.

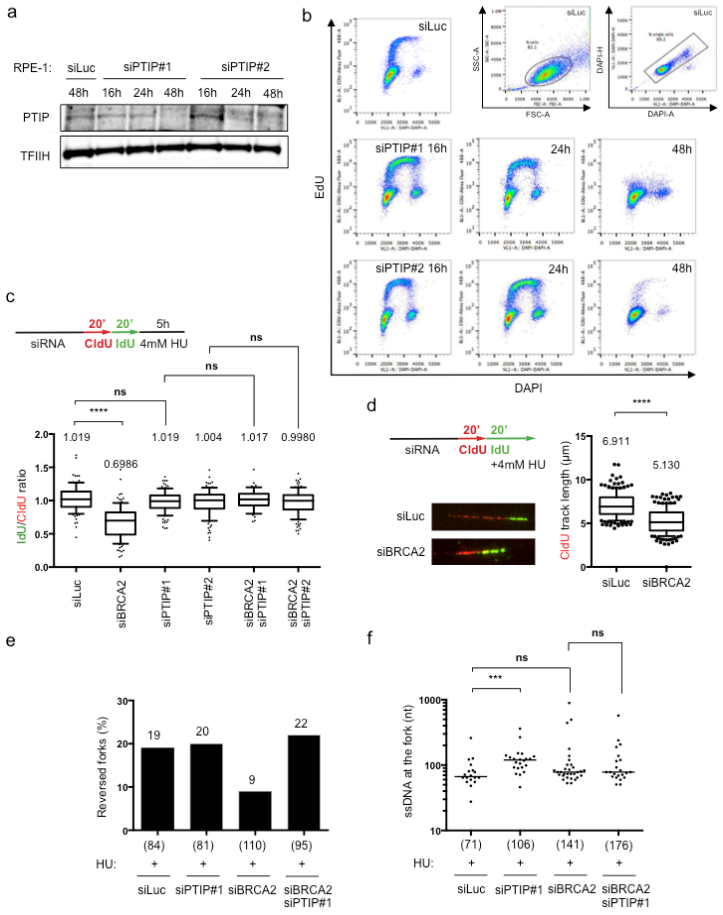

Supplementary Figure 2. PTIP depletion suppresses reversed fork processing in HU-treated BRCA2-defective RPE-1 cells (**a**) Western blot analysis of PTIP levels and (**b**) FACS analysis for DNA synthesis (EdU incorporation) and DNA content (DAPI) in mock-depleted and PTIP-depleted RPE-1 cells 16h, 24h and 48h after siRNA transfection. Top right: gating strategy to identify intact cells (SSC/FSC) and exclude doublets (DAPI-A/DAPI-H). Overall, roughly 80% of the 20'000 analyzed cells is scored for EdU/DAPI analysis in each samples. At 48 h, PTIP depleted cells undergo cell cycle arrest in G1 phase, while no such effect is observed shortly after protein depletion. (**c**) RPE-1 cells were transfected with siRNA before CldU (red) and IdU (green) labeling (siBRCA2, 48 h; siPTIP, 20 h), followed by treatment with 4 mM HU for 5 h, as indicated in the scheme. IdU/CIdU ratio is plotted. Horizontal lines and the numbers indicate the median value. Whiskers indicate the 10-90 percentiles. At least one hundred replication forks were analyzed for each condition. Statistical analysis: Mann-Whitney test; ns, not significant; ****, P< 0.0001. (**d**) Schematic of the alternative labeling protocol for single-molecule DNA fiber tract analysis and representative images of control and BRCA2-defective U2OS cells. U2OS cells were transfected with siRNA before CldU labeling (red) and IdU labeling (green) concomitantly with 4mM HU treatment as indicated. Size distribution of IdU tract length is plotted. Horizontal lines and the numbers indicate the median value. Whiskers indicate the 10-90 percentiles. At least one hundred replication forks were analyzed for each condition. Statistical analysis: Mann-Whitney test; ns, not significant; ****, P< 0.0001. (**e**) Frequency of reversed replication forks isolated from siLuc, siBRCA2 (48 h) and siPTIP#1 (20 h) RPE-1 cells upon 5 h treatment with 4 mM HU. The number of replication intermediates analyzed is indicated in parentheses. Results of two independent EM experiments are in Supplementary Table 3. (**f**) Graphical distribution of ssDNA length at the junction in siBRCA2 (48 h) and/or siPTIP#1 (20 h) RPE-1 cells treated with 4 mM of HU for 5 h. Only molecules with detectable ssDNA stretches are included in the analysis. The lines show the median length of ssDNA regions at the fork in the specific set of analyzed molecules. Statistical analysis: Mann-Whitney test; ns, not significant; ***, P< 0.001. The number of analyzed molecules is in brackets.

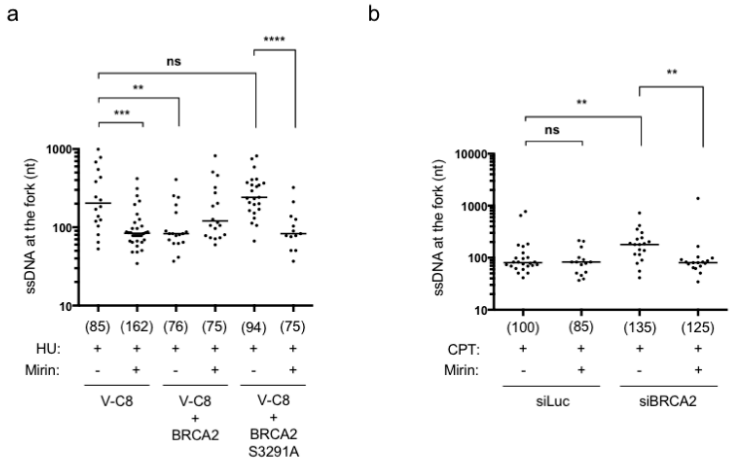

Supplementary Figure 3. ssDNA accumulation upon BRCA2 defects in HU-treated V-C8 cells and CPT-treated U2OS cells (**a**) Graphical distribution of ssDNA length at the junction found in VC-8 cells and V-C8 cells stably expressing a full-length or mutated variant of BRCA2 (S3291A) treated with 4mM of HU for 5 h and 50 μM of mirin for 6 h. (**b**) Graphical distribution of ssDNA length at the junction in siLuc and siBRCA2 (48 h) RPE-1 cells treated with 25 nM of CPT for 1 h and 50 μM of mirin for 2 h. For both panels, only the molecules with detectable ssDNA stretches are included in the analysis. The lines show the median length of ssDNA regions at the fork. Statistical analysis: Mann-Whitney test; ns, not significant; **, $P \leq 0.01$; ***, $P \leq 0.001$; ****, $P \leq 0.0001$.

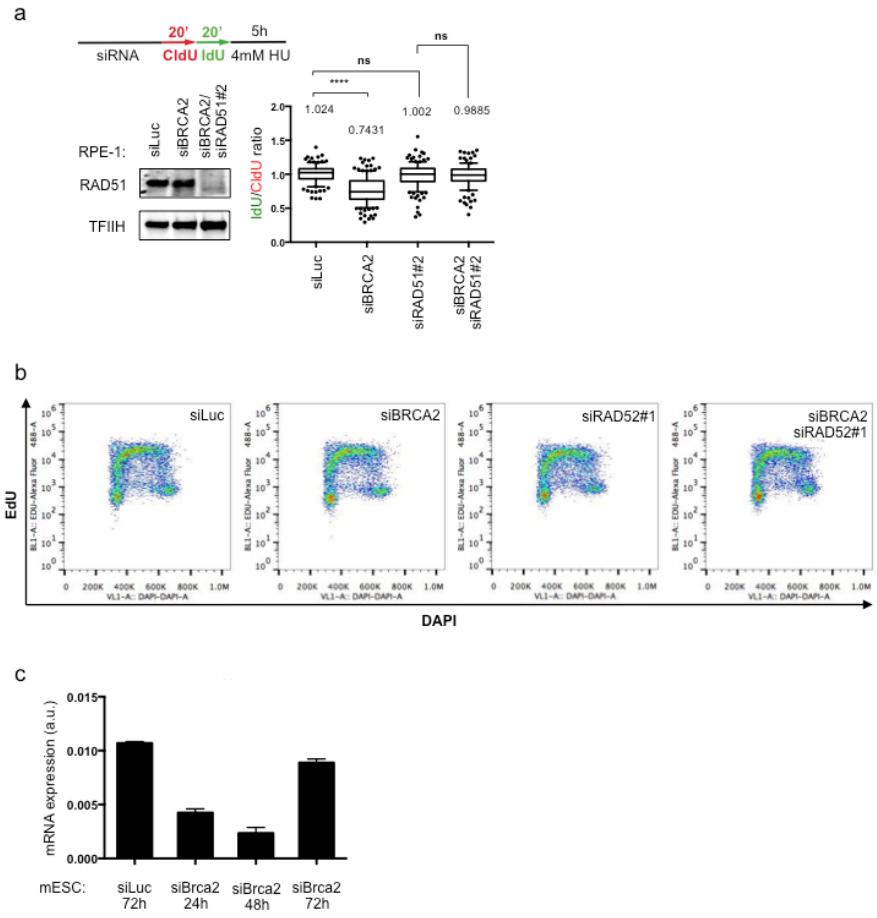

Supplementary Figure 4. Control experiments for the effects of RAD51 and RAD52 downregulations in RPE-1 cells and for BRCA2 downregulation in ESCs. (**a**) RPE-1 cells were transfected with the indicated siRNAs before CldU (red) and IdU (green) labeling, followed by treatment with 4 mM HU for 5 h. Left: levels of indicated proteins, assessed by western blot. TFIIH, loading control. Right panel: IdU/CIdU tract length ratio is plotted. Track length analysis and statistics as in Fig. 3d. (**b**) FACS analysis for DNA synthesis (EdU incorporation) and DNA content (DAPI) in U2OS cells after transfection with siRNA targeting BRCA2 (48h) and/or RAD52 (24h). No obvious defect in cell cycle progression is induced by downregulation of these proteins in the experimental conditions of Fig. 5a-b. (**c**) Time course for *Brca2* mRNA abundance measured by quantitative RT-PCR in mouse embryonic stem cells transfected with siLuc or siBrca2. The increase of *Brca2* mRNA at 72h is most likely due to selective elimination of ESCs effectively depleted of Brca2 and overgrowth of cells that were not transfected by the siRNA.

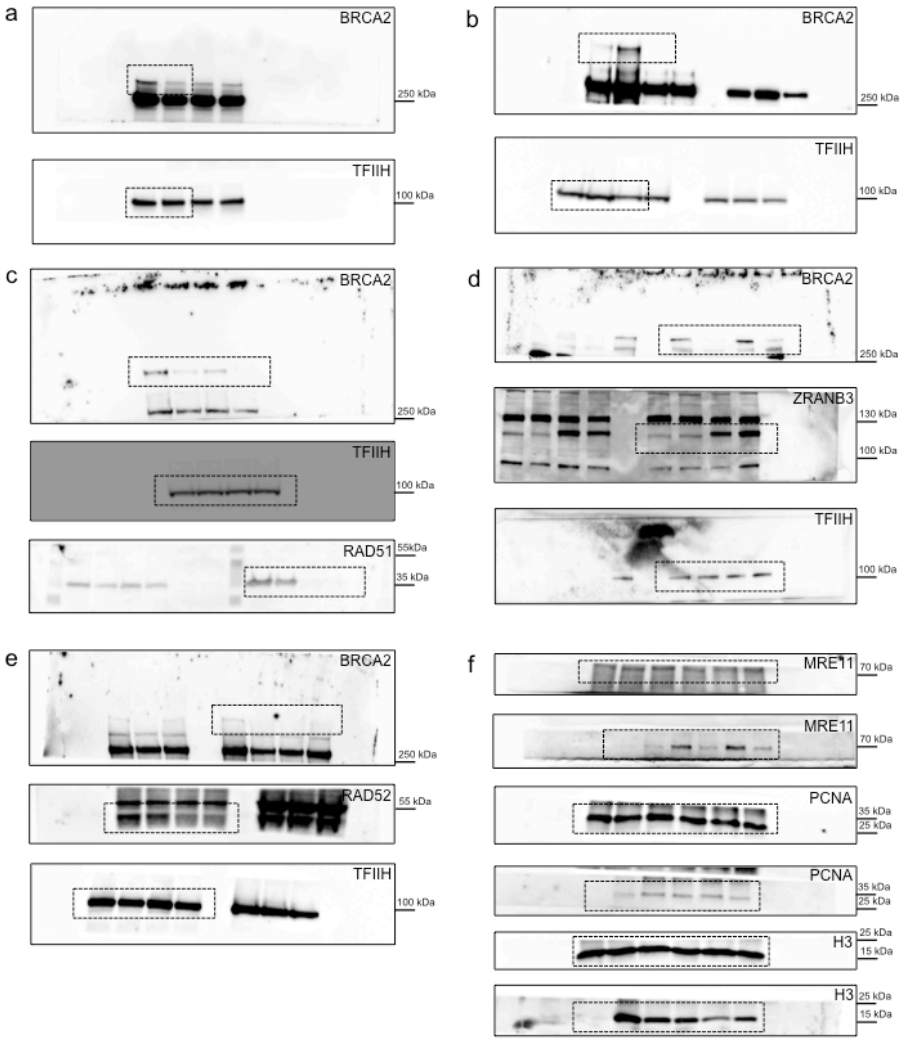

Supplementary Figure 5. Uncropped western blots. (**a**) Figure 1b, (**b**) Figure 2a, (**c**) Figure 3a, (**d**) Figure 3c, (**e**) Figure 5a, (**f**) Figure 5c.

3.3 Personal contribution in other projects

3.3.1 Deregulated origin licensing leads to chromosomal breaks by rereplication of a gapped DNA template

I started my PhD training in the lab of Massimo Lopes working on an advanced project whose aim was to unravel new mechanistic insights of DNA rereplication, a notorious causative factor of genome instability. We showed that origin firing deregulation by EMI1 depletion leads to rapid origin reactivation and checkpoint-blind ssDNA gaps. These gaps persist in the template and are converted to DSBs due to uncontrolled reactivation of replication origins.

My contribution consisted in performing the experiments shown in the following figures: FACS analysis in Fig 1, Fig 2, Fig S1, Fig S2, Fig S3; Western blot in Fig 1, Fig 2, Fig S1, Fig S4; Fibers analysis Fig 3.

In addition to allow me to become a contributing author to the final publication, this initial period was fundamental for introducing me in the use of the majority of the techniques I exploited in the other studies presented in this thesis.

Deregulated origin licensing leads to chromosomal breaks by rereplication of a gapped DNA template

Kai J. Neelsen,[1,3,4] Isabella M.Y. Zanini,[1,3,5] Sofija Mijic,[1] Raquel Herrador,[1] Ralph Zellweger,[1] Arnab Ray Chaudhuri,[1,6] Kevin D. Creavin,[2] J. Julian Blow,[2] and Massimo Lopes[1,7]

[1]Institute of Molecular Cancer Research, University of Zurich, CH-8057 Zurich, Switzerland; [2]Centre for Gene Regulation and Expression, University of Dundee, Dundee DD1 5EH, United Kingdom

Deregulated origin licensing and rereplication promote genome instability and tumorigenesis by largely elusive mechanisms. Investigating the consequences of *Early mitotic inhibitor 1* (Emi1) depletion in human cells, previously associated with rereplication, we show by DNA fiber labeling that origin reactivation occurs rapidly, well before accumulation of cells with >4N DNA, and is associated with checkpoint-blind ssDNA gaps and replication fork reversal. Massive RPA chromatin loading, formation of small chromosomal fragments, and checkpoint activation occur only later, once cells complete bulk DNA replication. We propose that deregulated origin firing leads to undetected discontinuities on newly replicated DNA, which ultimately cause breakage of rereplicating forks.

Supplemental material is available for this article.

Received July 12, 2013; revised version accepted October 30, 2013.

The activation of DNA replication origins is a tightly regulated mechanism, entailing two main steps: (1) "origin licensing," restricted to late mitosis and early G1, when essential replication initiation proteins (ORC1, Cdc6, Cdt1, and Mcm2–7) are sequentially loaded on origin DNA sequences, forming the "prereplicative complex" (preRC), and (2) "origin firing," occurring throughout S phase, when additional proteins are recruited to the preRC and start unwinding and DNA synthesis (Arias and Walter 2007). As relicensing and thus rereplication are detrimental to genome stability, several cyclin-dependent kinase (CDK)-dependent and -independent mechanisms have evolved to coordinate these steps with cell cycle progression (Blow and Dutta 2005; Arias and Walter 2007).

Although several preRC components are targets of regulation, the major mechanism by which metazoans prevent origin licensing during S phase is inactivation of Cdt1 by ubiquitin-mediated degradation or binding to its inhibitor Geminin. Cdt1 proteolysis is tightly linked to the cell cycle, as ubiquitylation requires CDK-dependent phosphorylation (Li et al. 2003; Sugimoto et al. 2004; Nishitani et al. 2006). Moreover, CUL4/DDB1-mediated ubiquitylation of Cdt1 occurs in S phase or in response to DNA damage (Arias and Walter 2006; Nishitani et al. 2006; Senga et al. 2006). Geminin exerts its inhibitory function on Cdt1 in S, G2, and early M phase and is inactivated in late M phase by anaphase-promoting complex (APC/C)-dependent polyubiquitylation, leading to reactivation of origin licensing (McGarry and Kirschner 1998; Wohlschlegel et al. 2000; Tada et al. 2001; Li and Blow 2004). Accordingly, Geminin depletion induces rereplication and activation of the DNA damage response (DDR) (Melixetian et al. 2004; Zhu et al. 2004).

By direct control of Geminin and indirect control of Cdt1 proteolysis via regulation of CycA–CDK activity, APC/C plays a pivotal role coordinating origin licensing with cell cycle progression (Hook et al. 2007). APC/C activity is inhibited by *Early mitotic inhibitor 1* (Emi1) (Wang and Kirschner 2013), which thereby stabilizes APC/C substrates like Geminin and Cyclin A (Di Fiore and Pines 2007). Thus, inactivation of Emi1 leads to degradation of both inhibitors of Cdt1 activity, resulting in massive rereplication and DDR activation (Machida and Dutta 2007).

As many origin licensing genes are overexpressed in cancer cells and several oncogenes are known to affect origin licensing, it is suspected that deregulated licensing contributes to genome instability and tumorigenesis (Hook et al. 2007; Blow and Gillespie 2008). However, our understanding of how rereplication challenges genome stability is very limited. Studies with *Xenopus laevis* egg extracts provided the first insight into the effects of rereplication. Addition of recombinant Cdt1 to G2-arrested egg extracts was shown to trigger DNA breaks, proposed to arise from head-to-tail collision of rereplicating forks (Davidson et al. 2006). However, little information is available on the mechanisms leading to DNA damage and DDR activation in rereplicating human cells.

We combined cell/molecular biology and in vivo single-molecule approaches to investigate how deregulated origin licensing by Emi1 depletion affects replicating chromosomes. We show that cells experience mild DNA replication stress and ssDNA accumulation during the first replication round upon licensing deregulation, which may act as precursor for DNA breaks, when rereplicating forks approach ssDNA gaps on the template. Extending the analysis to other experimental systems of deregulated

[*Keywords*: DNA replication; genome integrity; origin licensing; rereplication; tumorigenesis]
[3]**These authors contributed equally to this work.**
Present addresses: [4]The Novo Nordisk Foundation Center for Protein Research, Blegdamsvej 3, 2200 Copenhagen, Denmark; [5]ETH Zurich, Institute of Biochemistry, Schafmattstrasse 18, 8093 Zurich, Switzerland; [6]Laboratory for Genome Integrity, National Institutes of Health, 10 Center Drive, Bethesda, MD 20892, USA.
[7]**Corresponding author**
E-mail lopes@imcr.uzh.ch
Article is online at http://www.genesdev.org/cgi/doi/10.1101/gad.226373.113.

licensing (Geminin depletion and Cdt1 addition in *X. laevis* extracts), we propose a new model for rereplication-induced chromosomal breakage, which may contribute to cancer-relevant genome rearrangements.

Results and Discussion

Emi1 depletion affects DNA synthesis prior to accumulation of >4N DNA, chromosomal breakage, and checkpoint activation

To gain mechanistic insight into how deregulated origin licensing affects the replication process, leading to DNA breaks and DDR activation, we depleted Emi1 in U2OS cells, a condition previously associated with rereplication and DNA damage (Machida and Dutta 2007). Using flow cytometry, we monitored cell cycle progression (DNA content), DNA synthesis (EdU incorporation), and DDR activation (phosphorylation of H2AX [γH2AX]) (Supplemental Fig. S1) after Emi1 depletion. Sixteen hours to 24 h after siEmi1 transfection, we noticed accumulation of cells in S phase and a reduced incorporation rate in mid–late S phase (Fig. 1A). In synchronized cells, the impact of deregulated origin licensing on DNA synthesis was detected from the onset of the first S phase (Supplemental Fig. S2). At these time points, γH2AX was only detected in cells close to having completed a first round of bulk DNA replication (Fig. 1A,B). Later (32–40 h), γH2AX and a markedly reduced rate of DNA synthesis were detected in cells displaying >4N DNA, a commonly used readout for rereplication (Fig. 1A,C). Only at 32–40 h did cells accumulate detectable levels of double-strand breaks (DSB) and display activation of ATM and ATR pathways (phosphorylation of KAP1/RPA2-S4/S8 and CHK1/RPA2-S33, respectively), as expected for DSB-induced DDR (Fig. 1D,E). A relevant fraction of chromosomal fragments induced by Emi1 depletion is significantly smaller (20–100 kb) than camptothecin-induced DSB (0.5–2 Mb) (Fig. 1E; Supplemental Fig. S1B; Hanada et al. 2007), suggesting that rereplication-induced DSBs are clustered. DNA breakage at 32–40 h was also confirmed by colocalization of γH2AX and 53BP1, particularly evident in cells with "giant nuclei," a sign of extensive rereplication (Supplemental Fig. S1C–E; Zhu et al. 2004). Altogether, these data indicate that mild replication stress during the first S phase after Emi1 depletion precedes cell cycle arrest, DNA breakage, and DDR activation, which are coupled to overt rereplication (DNA content >4N). Similar observations were made in untransformed human epithelial cells (RPE-1) (Supplemental Fig. S3), showing that the stepwise impact on DNA replication and genome stability is a general consequence of Emi1 depletion.

Progressive RPA accumulation on chromatin precedes rereplication-associated DNA damage

To further characterize DNA replication stress early after Emi1 depletion, we monitored chromatin loading of the human ssDNA-binding protein (RPA) (Forment et al. 2012). Limited amounts of ssDNA are present during DNA replication, leading to RPA chromatin loading in S phase (Fig. 2A; Supplemental Fig. S4A; Forment et al. 2012). While this signal is rapidly lost as control cells complete S phase, Emi1 depletion leads to progressive accumulation of RPA on chromatin and unusually high

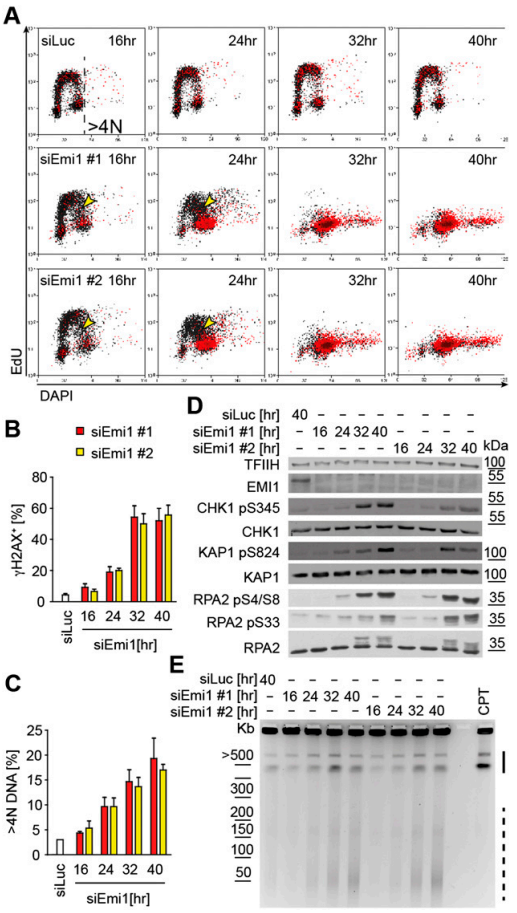

Figure 1. Emi1 depletion causes DNA replication stress in S phase and DDR activation and DNA breakage in cells with ≥4 DNA. (*A*) FACS analysis of DNA synthesis (EdU), DNA content (DAPI), and DDR activation (γH2AX) after mock (siLUC) or Emi1 depletion in U2OS cells using two different siRNAs. γH2AX$^+$ cells are in red (see also Supplemental Fig. S1A). Yellow arrowheads indicate cells with compromised DNA synthesis. γH2AX$^+$ cells (*B*) and cells with >4N DNA (*C*) after mock (siLUC) or Emi1 depletion quantified by FACS. Mean + SEM; $n = 3$. (*D*) ATR (pCHK1), ATM (pKAP1) activation, RPA phosphorylation (RPA2 pS4/S8 and pS33), and total DDR proteins (CHK1, KAP1, and RPA2) assessed by Western blot upon Emi1 depletion. (TFIIH) Loading control. (*E*) DNA breakage after mock (siLUC) or Emi1 depletion monitored by pulse-field gel electrophoresis. The solid and dashed lines indicate large (0.5- to 2-Mb) and smaller (20- to 100-kb) chromosomal fragments, respectively. The molecular size markers are based on data in Supplemental Figure S1B. Four-hour treatment with 1 μM camptothecin (CPT) served as a positive control for DSB.

RPA levels in mid–late S-phase cells (Fig. 2A). RPA foci colocalized with γH2AX foci at late time points (32–40 h) (Supplemental Fig. S4A), presumably marking processing of the detected DSBs (Fig. 1E; Supplemental Fig. S1C,D). However, in both U2OS and RPE-1 cells, some RPA accumulation was already observed at earlier time points

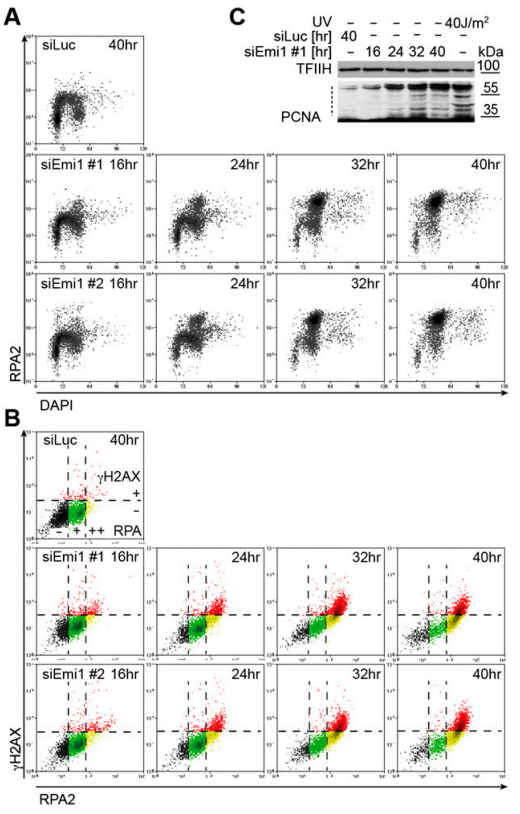

Figure 2. siEmi1-induced deregulation of origin licensing promotes RPA chromatin binding and ubiquitylation of PCNA from the first S phase. (*A*) FACS analysis of chromatin-bound RPA and DNA content (DAPI) after mock (siLuc) or Emi1 depletion in U2OS cells. (*B*) γH2AX/RPA levels in samples in *A*. Black, green, and yellow regions identify RPA negative cells (–), cells with S-phase RPA levels (+), and cells with elevated RPA (++), respectively. The red region identifies γH2AX^{+} cells. See Supplemental Figure S4B for Emi1 levels. (*C*) Analysis of PCNA ubiquitylation in mock-transfected cells (siLuc) and at the indicated time points after Emi1 depletion (siEmi1 #1). The dotted line indicates ubiquitylated PCNA. UV-irradiated cells served as positive control. (TFIIH) Loading control.

(16–24 h), when it was largely uncoupled from DDR activation, extensive rereplication (measured by flow cytometry), and DNA breaks (Figs. 1, 2A; Supplemental Fig. S3D). Furthermore, even at later time points (≥24 h) after Emi1 depletion, when γH2AX is clearly detectable in the population, our FACS experiments identified a cell population with unusually high RPA content in the absence of γH2AX (Fig. 2B, yellow dots, RPA^{++} γH2AX^{-}). These data suggest that Emi1 depletion progressively induces ssDNA accumulation, which goes undetected by the DDR and precedes rereplication-associated DNA breaks. Importantly, PCNA ubiquitylation, a sensitive marker of replication-associated ssDNA gaps (for review, see Chen et al. 2011), was detectable within 24 h (Fig. 2C) and thus earlier than other DDR markers (Fig. 1D).

Emi1 depletion does not detectably impair fork progression but induces refiring of clustered origins before accumulation of >4N DNA content

We next monitored the effect of Emi1 depletion on fork progression by DNA fiber spreading (Jackson and Pombo 1998). Ongoing forks were identified by a red–green pattern (Supplemental Fig. S5A). Fork progression appeared unaffected by Emi1 depletion when we used a 10-min labeling time (Fig. 3A). However, in Emi1-depleted cells, tract length increased more markedly than in control cells with longer labeling times (Fig. 3A; Supplemental Fig. S5C,D). This suggests that Emi1 depletion does not affect progression of individual forks but that deregulated activation of clustered replication origins leads to more frequent fork fusion and thus longer tracts. We then adapted the labeling protocol to detect DNA rereplication events, modifying a published protocol (Dorn et al. 2009). A 120-min CldU pulse followed by a 30-min IdU pulse allowed us to follow fork progression and reactivation of replication origins in previously replicated tracts (Supplemental Fig. S5A). "Rerep-

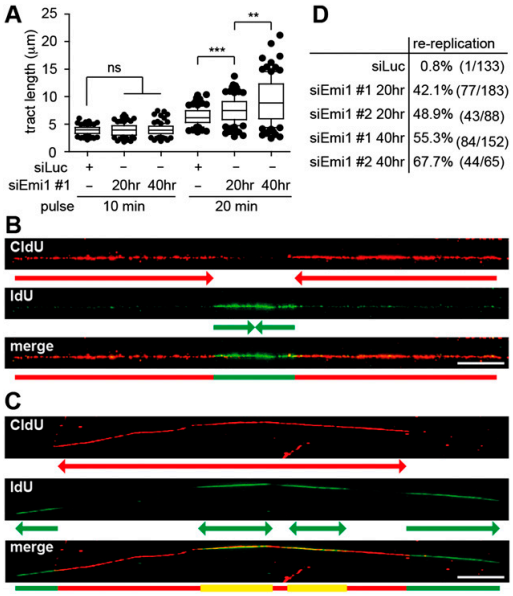

Figure 3. Rereplication is detectable by a DNA fiber-spreading assay before completion of bulk DNA synthesis. (*A*) Length of newly replicated tracts (IdU; green) in mock-depleted U2OS cells (siLuc) and after Emi1 depletion (siEmi1 #1), using 10-min or 20-min labeling pulses. (*B*,*C*) Representative DNA tracts labeled with CldU for 2 h and IdU for 30 min to identify termination and rereplication events. (*B*) A replication "termination" event. (*C*) Two "rereplication" events in close proximity. (*D*) Quantification of rereplication/termination events as shown in *B* and *C* after mock (siLuc) or Emi1 depletion. The percentage indicated represents the fraction of rereplication events in the total population of "red–green–red" tracts analyzed. (Whiskers) 10–90 percentile; (***) $P < 0.0001$; (**) $P < 0.005$; (ns) not significant, Mann-Whitney test; $n = 100$ in *A*. Bar, 10 μm. See Supplemental Figure S5, A and B, for Emi1 levels and labeling protocols to study fork progression (*A*) and rereplication events (*B*,*C*).

lication" events during the second labeling should appear as green signals embedded in a longer red tract. A similar pattern is expected for physiological fork fusion events during the second label ("termination"), but rereplication events can be distinguished by the substantial overlap of red and green signals (Fig. 3B,C). As expected, in control cells, virtually all green signals identified within red tracts displayed a termination pattern ("red–green–red") (Fig. 3B,D). In contrast, Emi1-depleted cells showed rereplication events ("red–yellow–red"), often coupled to further progression of the first set of forks during the second labeling period (Fig. 3C, note the distal green tracts). Surprisingly, these "rereplication" events were almost as frequent as "termination" events already 20 h after siRNA transfection (Fig. 3D). At 40 h, when rereplication has led to >4N DNA content (Fig. 1A,C), rereplication events were more frequent than fork fusions and were occasionally clustered on the same DNA fiber (Fig. 3C,D). These data demonstrate that origin reactivation can be detected by DNA fiber spreading before it is detectable by flow cytometry and that refiring of clustered origins occurs already during a first round of replication with deregulated origin licensing.

Deregulation of origin licensing induces ssDNA gaps on replicated duplexes, which can be template for rereplication

To gain additional insight into the molecular consequences of deregulated origin licensing, we investigated in vivo replication fork structure by electron microscopy (EM) (Neelsen et al. 2014). Already 20 h after siRNA transfection, several marks of replication stress were detectable (Fig. 4). Small (<1-kb) replication bubbles were overrepresented upon Emi1 depletion (9%–10% compared with 1%–2% in control U2OS cells), suggesting that deregulated firing is accompanied by reduced fork progression from the origin. These replicated tracts would be too small for detection in DNA fiber assays, which may explain why the reduced EdU incorporation after Emi1 depletion (Fig. 1A) is not accompanied by detectable reduction in fork progression (Fig. 3A). As implied by RPA chromatin loading and PCNA ubiquitylation (Fig. 2A,C), 11% of forks exposed ssDNA gaps 20 h after siEmi1 transfection compared with 1% of forks in control cells (Fig. 4A,B; Supplemental Fig. S6A). Furthermore, ~13% of the replication forks had undergone reversal (Supplemental Fig. S6B,C). The latter two features closely resemble the effects of oncogene activation (Neelsen et al. 2013) and thus most likely reflect the licensing defects common to these genetic conditions (Hook et al. 2007; Blow and Gillespie 2008) and their consequences in terms of nucleotide depletion (Bester et al. 2011) and/or interference with transcription (Jones et al. 2013). Although ssDNA sensors (e.g., RPA chromatin loading and PCNA ubiquitylation) (Fig. 2A,C) detected these changes in the architecture of replication intermediates, they are "checkpoint-blind" (i.e., not associated per se with DDR activation) (Fig. 1A,D), as already shown for CycE overexpression (Neelsen et al. 2013). The proportion of forks displaying ssDNA gaps increases from 11% to 37% between 20 and 40 h, when rereplication and DSB become detectable by flow cytometry and PFGE, respectively (Figs. 1A,C,E, 4B). Intriguingly, a significant proportion of the observed ssDNA gaps were located on template DNA ahead of the replication forks (Fig. 4B,C; Supplemental Fig. S6D). At 40 h, when all cells completed a first round of replication and the relative proportion of rereplicating forks in our EM samples is expected to increase, 20% of the ssDNA gaps (n = 6 of 22) were detected on template DNA ahead of the replication forks (Fig. 4B).

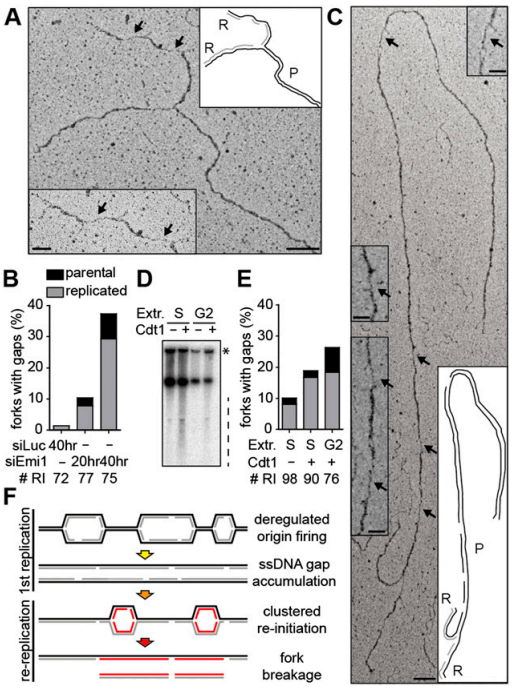

Figure 4. Emi1 depletion leads to ssDNA gaps on the replicated duplex, which persist as a template for rereplicating forks. (*A*,*C*) Electron micrographs of representative replication forks from U2OS cells 40 h after transfection with siEmi1. Black arrows indicate ssDNA gaps. The *insets* show magnified ssDNA gaps and schemes of fork structure, indicating parental (P) and replicated (R) duplexes. Gaps are on a replicated duplex in *A* and on the parental duplex in *C*. Black and gray lines describe parental and newly synthesized DNA strands in the replicated duplexes, respectively. Bars: 100 nm (250 base pairs [bp]); *inset*, 50 nm. (*B*) Frequency of replication forks with ssDNA gaps in mock-depleted cells (siLuc) and after Emi1 depletion (siEmi1 #1). #RI is the number of analyzed replication intermediates. (*D*) Sperm nuclei replication assays in *Xenopus* interphase extracts. For S-phase experiments, extracts were optionally supplemented with 10 ng/μL Cdt1 at the time of sperm and [α-^{32}P]dATP addition and incubated for 60 min. For G2 experiments, Cdt1 was optionally added with [α-^{32}P]dATP 90 min after sperm addition and incubated for a further 60 min. After incubation, DNA was isolated, separated by neutral agarose gel electrophoresis, and autoradiographed. The dashed line indicates sperm DNA fragmentation. The asterisk indicates branched replicating DNA molecules retained in the well. (*E*) Frequency of replication forks with ssDNA gaps recovered after sperm nuclei incubation in S-phase or G2-phase extracts (see *D*), with optional addition of Cdt1. # RI is the number of analyzed replication intermediates. (*F*) Model for the formation of chromosomal breaks upon deregulation of origin licensing by Emi1 depletion. Excessive firing of clustered origins leads to replication stress during the first S phase and accumulation of ssDNA gaps. Uncontrolled reactivation of replication origins in this context triggers chromosomal breakage by replication of a discontinuous template.

These data strongly suggest that gaps accumulating during the first round of replication after Emi1 depletion persist and present a damaged template for new replication rounds.

To further test this hypothesis, we analyzed by EM a different experimental system associated with rereplication and DNA breakage; i.e., addition of Cdt1 to replication sperm nuclei in *X. laevis* egg extracts (Davidson et al. 2006). In line with published results, addition of Cdt1 (Ferenbach et al. 2005) induced [α-^{32}P]dATP incorporation in G2 extracts, particularly visible on branched DNA molecules retained in the well (Fig. 4D; Supplemental Fig. S6E). Moreover, rereplication was associated with DNA breakage when Cdt1 was added to S-phase and G2 extracts (Fig. 4D). The analysis of replication intermediates confirmed an accumulation of ssDNA gaps upon Cdt1 addition, particularly marked in G2 extracts (Fig. 4E) where multiple rounds of rereplication have been reported (Davidson et al. 2006). Similar to Emi1 depletion, ssDNA gaps were also observed ahead of the replication forks, showing that rereplication was impaired by template discontinuities (Fig. 4E).

A new model for chromosomal breakage associated with deregulated origin licensing and rereplication

Our data strongly suggest that deregulated origin firing rapidly induces ssDNA gaps during DNA replication and that these persist in the template, where they cause stalling and eventually breakage of rereplicating forks (Fig. 4F). Rereplicating forks could break by simply impacting ssDNA gaps on the template ("runoff"). Alternatively, they could stall upstream of the gap and later be resolved into DSBs by slow "runoff," nucleolytic processing, or head-to-tail collision with forks generated in following rounds of rereplication. In support of transient stalling and remodeling, small replication bubbles accumulated upon Emi1 depletion, indicative of early fork stalling from reactivated origins. Moreover, the frequency of reversed forks remained high 40 h after Emi1 depletion, when rereplicating forks are overrepresented in our EM samples (Fig. 3D; Supplemental Fig. S6C). Fork reversal was associated with fork slowing during replication of a nicked template, thereby protecting forks from breakage (Ray Chaudhuri et al. 2012). Thus, rereplicating forks could transiently arrest and reverse at ssDNA gaps before eventually undergoing breakage.

A prediction of our model is that the genotoxicity of rereplication correlates with the extent of origin firing deregulation in the previous replication round, as this creates the template discontinuities for rereplication. We tested this hypothesis by comparing the described effects for Emi1 depletion with Geminin depletion, a genetic condition associated with mild overreplication (Melixetian et al. 2004; Zhu et al. 2004), in which CDK-dependent Cdt1 inactivation partially restrains deregulated origin firing (Hook et al. 2007; Machida and Dutta 2007). In line with a recent study (Klotz-Noack et al. 2012), Geminin-depleted cells showed unperturbed EdU incorporation and progression in the first S phase, indicating marginal replication stress (Supplemental Fig. S7A). Accordingly, Geminin-depleted cells undergoing overt rereplication (>4N DNA content) displayed γH2AX only after completion of the first S phase and transition into a mitotic state (H3 phosphorylation) (Supplemental Fig. S7B). In line with our model, rereplication induced by Geminin depletion is associated with higher EdU incorporation and less DNA damage than Emi1 depletion, indicated by reduced γH2AX in cells with >4N DNA content (40 h) (Supplemental Fig. S7A,C). Intriguingly, if deregulation of origin licensing is induced after S-phase completion, DNA breakage requires at least two rounds of rereplication, as observed with Cdt1 addition to sperm nuclei in G2-arrested *X. laevis* extracts (Davidson et al. 2006), reinforcing the conclusions of this study. In this view, fork breakage during rereplication would not require head-to-tail fork collision (Davidson et al. 2006) but would rather occur as forks approach ssDNA gaps in close proximity to the origin, resulting in the observed release of small DNA fragments (Figs. 1E, 4F; Davidson et al. 2006). Accordingly, even in experimental conditions where rereplicating forks should represent a substantial fraction of total replication intermediates (siEmi1 40 h, Cdt1 addition in G2 extracts), we could never identify by EM a replicating and a rereplicating fork on the same DNA fragment.

The molecular mechanisms characterized here under conditions of severe rereplication could also be relevant for milder deregulation of origin licensing, associated with genome evolution and tumorigenesis (Hook et al. 2007; Green et al. 2010). As mild oncogene-induced replication stress can go undetected by cell cycle checkpoints (Fig. 1D; Neelsen et al. 2013), reactivation of specific replication origins in the presence of unrepaired ssDNA gaps may compromise chromosome integrity. Intriguingly, complex rearrangements in tumors have been recently associated with replication errors and copy number changes (Liu et al. 2011), which could result from breakage and repair of overreplicating chromosomes by mechanisms similar to those described here.

Materials and methods

Cell culture and transfections

U2OS and hTERT RPE-1 retinal pigmented epithelial cells were grown in DMEM + 10% FCS. Cells were transfected with the indicated siRNAs using RNAiMAX (Invitrogen) according to the manufacturer's instructions: siLuc (10 nM; 5′-GGUACGCGGAAUACUUCGAdTdT-3′), siEmi1 #1 (10 nM; 5′-GAUUGUGAUCUCUUAUUAAdTdT-3′), siEmi1 #2 (10 nM; 5′-GAGAAUUUCGGUGACAGUCUAdTdT-3′), and siGeminin (20 nM; 5′- UGCCAACUCUGGAAUCAAAdTdT-3′).

Methods

Flow cytometry was essentially performed as described previously for γH2AX/EdU/DAPI in Neelsen et al. (2013) and for γH2AX/RPA/DAPI in Forment et al. (2012). DNA fiber spreadings were performed according to Ray Chaudhuri et al. (2012) with the modifications outlined in the text. Pulse-field gel electrophoresis, immunofluorescence, and sample preparation for EM have been described in Neelsen et al. (2013, 2014). Protocols for Cdt1 purification, replication assays in *X. laevis* egg extracts, and isolation of genomic DNA for electron microscopic analysis can be found in the Supplemental Material. Detailed protocols for all other methods and a list of antibodies are included in the Supplemental Material.

Acknowledgments

We are grateful to all members of the Lopes laboratory for helpful discussions. We thank the Center for Microscopy and Image Analysis of the University of Zurich for technical assistance with the EM experiments, and D. Hühn, A. Sartori, S. Bregenhorn, and J. Jiricny (Institute of Molecular Cancer Research, Zurich) for sharing reagents and technical assistance. This work was supported by the Swiss National Science

Foundation (grants PP0033-114922 and PP00P3_135292), Krebsliga Zurich, Stiftung zur Krebsbekämpfung, Research Priority Program on Systems Biology of the University of Zurich, and Wellcome Trust (grant WT097945). K.C. was supported by a Biotechnology and Biological Sciences Research Council/Doctoral Training Account studentship.

References

Arias EE, Walter JC. 2006. PCNA functions as a molecular platform to trigger Cdt1 destruction and prevent re-replication. *Nat Cell Biol* **8:** 84–90.

Arias EE, Walter JC. 2007. Strength in numbers: Preventing rereplication via multiple mechanisms in eukaryotic cells. *Genes Dev* **21:** 497–518.

Bester AC, Roniger M, Oren YS, Im MM, Sarni D, Chaoat M, Bensimon A, Zamir G, Shewach DS, Kerem B. 2011. Nucleotide deficiency promotes genomic instability in early stages of cancer development. *Cell* **145:** 435–446.

Blow JJ, Dutta A. 2005. Preventing re-replication of chromosomal DNA. *Nat Rev Mol Cell Biol* **6:** 476–486.

Blow JJ, Gillespie PJ. 2008. Replication licensing and cancer—a fatal entanglement? *Nat Rev Cancer* **8:** 799–806.

Chen J, Bozza W, Zhuang Z. 2011. Ubiquitination of PCNA and its essential role in eukaryotic translesion synthesis. *Cell Biochem Biophys* **60:** 47–60.

Davidson IF, Li A, Blow JJ. 2006. Deregulated replication licensing causes DNA fragmentation consistent with head-to-tail fork collision. *Mol Cell* **24:** 433–443.

Di Fiore B, Pines J. 2007. Emi1 is needed to couple DNA replication with mitosis but does not regulate activation of the mitotic APC/C. *J Cell Biol* **177:** 425–437.

Dorn ES, Chastain PD II, Hall JR, Cook JG. 2009. Analysis of re-replication from deregulated origin licensing by DNA fiber spreading. *Nucleic Acids Res* **37:** 60–69.

Ferenbach A, Li A, Brito-Martins M, Blow JJ. 2005. Functional domains of the *Xenopus* replication licensing factor Cdt1. *Nucleic Acids Res* **33:** 316–324.

Forment JV, Walker RV, Jackson SP. 2012. A high-throughput, flow cytometry-based method to quantify DNA-end resection in mammalian cells. *Cytometry A* **81:** 922–928.

Green BM, Finn KJ, Li JJ. 2010. Loss of DNA replication control is a potent inducer of gene amplification. *Science* **329:** 943–946.

Hanada K, Budzowska M, Davies SL, van Drunen E, Onizawa H, Beverloo HB, Maas A, Essers J, Hickson ID, Kanaar R. 2007. The structure-specific endonuclease Mus81 contributes to replication restart by generating double-strand DNA breaks. *Nat Struct Mol Biol* **14:** 1096–1104.

Hook SS, Lin JJ, Dutta A. 2007. Mechanisms to control rereplication and implications for cancer. *Curr Opin Cell Biol* **19:** 663–671.

Jackson DA, Pombo A. 1998. Replicon clusters are stable units of chromosome structure: Evidence that nuclear organization contributes to the efficient activation and propagation of S phase in human cells. *J Cell Biol* **140:** 1285–1295.

Jones RM, Mortusewicz O, Afzal I, Lorvellec M, Garcia P, Helleday T, Petermann E. 2013. Increased replication initiation and conflicts with transcription underlie Cyclin E-induced replication stress. *Oncogene* **32:** 3744–3753.

Klotz-Noack K, McIntosh D, Schurch N, Pratt N, Blow JJ. 2012. Re-replication induced by geminin depletion occurs from G2 and is enhanced by checkpoint activation. *J Cell Sci* **125:** 2436–2445.

Li A, Blow JJ. 2004. Non-proteolytic inactivation of geminin requires CDK-dependent ubiquitination. *Nat Cell Biol* **6:** 260–267.

Li X, Zhao Q, Liao R, Sun P, Wu X. 2003. The SCF(Skp2) ubiquitin ligase complex interacts with the human replication licensing factor Cdt1 and regulates Cdt1 degradation. *J Biol Chem* **278:** 30854–30858.

Liu P, Erez A, Nagamani SC, Dhar SU, Kolodziejska KE, Dharmadhikari AV, Cooper ML, Wiszniewska J, Zhang F, Withers MA, et al. 2011. Chromosome catastrophes involve replication mechanisms generating complex genomic rearrangements. *Cell* **146:** 889–903.

Machida YJ, Dutta A. 2007. The APC/C inhibitor, Emi1, is essential for prevention of rereplication. *Genes Dev* **21:** 184–194.

McGarry TJ, Kirschner MW. 1998. Geminin, an inhibitor of DNA replication, is degraded during mitosis. *Cell* **93:** 1043–1053.

Melixetian M, Ballabeni A, Masiero L, Gasparini P, Zamponi R, Bartek J, Lukas J, Helin K. 2004. Loss of Geminin induces rereplication in the presence of functional p53. *J Cell Biol* **165:** 473–482.

Neelsen KJ, Zanini IM, Herrador R, Lopes M. 2013. Oncogenes induce genotoxic stress by mitotic processing of unusual replication intermediates. *J Cell Biol* **200:** 699–708.

Neelsen KJ, Chaudhuri AR, Follonier C, Herrador R, Lopes M. 2014. Visualization and interpretation of eukaryotic DNA replication intermediates in vivo by electron microscopy. *Methods Mol Biol* **1094:** 177–208.

Nishitani H, Sugimoto N, Roukos V, Nakanishi Y, Saijo M, Obuse C, Tsurimoto T, Nakayama KI, Nakayama K, Fujita M, et al. 2006. Two E3 ubiquitin ligases, SCF–Skp2 and DDB1–Cul4, target human Cdt1 for proteolysis. *EMBO J* **25:** 1126–1136.

Ray Chaudhuri A, Hashimoto Y, Herrador R, Neelsen KJ, Fachinetti D, Bermejo R, Cocito A, Costanzo V, Lopes M. 2012. Topoisomerase I poisoning results in PARP-mediated replication fork reversal. *Nat Struct Mol Biol* **19:** 417–423.

Senga T, Sivaprasad U, Zhu W, Park JH, Arias EE, Walter JC, Dutta A. 2006. PCNA is a cofactor for Cdt1 degradation by CUL4/DDB1-mediated N-terminal ubiquitination. *J Biol Chem* **281:** 6246–6252.

Sugimoto N, Tatsumi Y, Tsurumi T, Matsukage A, Kiyono T, Nishitani H, Fujita M. 2004. Cdt1 phosphorylation by cyclin A-dependent kinases negatively regulates its function without affecting geminin binding. *J Biol Chem* **279:** 19691–19697.

Tada S, Li A, Maiorano D, Mechali M, Blow JJ. 2001. Repression of origin assembly in metaphase depends on inhibition of RLF-B/Cdt1 by geminin. *Nat Cell Biol* **3:** 107–113.

Wang W, Kirschner MW. 2013. Emi1 preferentially inhibits ubiquitin chain elongation by the anaphase-promoting complex. *Nat Cell Biol* **15:** 797–806.

Wohlschlegel JA, Dwyer BT, Dhar SK, Cvetic C, Walter JC, Dutta A. 2000. Inhibition of eukaryotic DNA replication by geminin binding to Cdt1. *Science* **290:** 2309–2312.

Zhu W, Chen Y, Dutta A. 2004. Rereplication by depletion of geminin is seen regardless of p53 status and activates a G2/M checkpoint. *Mol Cell Biol* **24:** 7140–7150.

Deregulated origin licensing leads to chromosomal breaks by re-replication of a gapped DNA template

Kai J. Neelsen, Isabella M. Y. Zanini, Sofija Mijic, Raquel Herrador, Ralph Zellweger, Arnab Ray Chaudhuri, Kevin D. Creavin, J. Julian Blow and Massimo Lopes

Supplemental Material

Supplemental Methods

Flow cytometry

Flow cytometric analysis for γH2AX/EdU/DAPI and H3-pS10/EdU/DAPI was carried out as described previously. Briefly, cells were labeled with EdU, harvested and fixed for 10 min with 4% formaldehyde/PBS. Cells were washed with 1% BSA/PBS pH 7.4, permeabilized with 0.5% saponin/1% BSA/PBS and stained with anti-γH2AX antibody (Millipore, # 05-636) or anti-H3-pS10 (Millipore, # 06-570), followed by incubation with a suitable secondary antibody. Incorporated EdU was labeled according to the manufacturer's instructions (Invitrogen, # C35002). For flow cytometric analysis for γH2AX/RPA/DAPI, non-chromatin bound proteins were pre-extracted with 0.2% Triton X-100/PBS for 10 minutes on ice, fixed as above and stained with antibodies against γH2AX (Cell Signaling, #9718) and RPA (Calbiochem, NA19L) and suitable secondary antibodies. In both assays, DNA was stained with 1 μg/ml DAPI, samples were measured on a Cyan ADP flow cytometer (Beckman Coulter) and analyzed with Summit software v4.3.

Pulse field gel electrophoresis, single cell microscopy and antibodies

Pulse-field gel electrophoresis and was performed as reported previously. Briefly, cells were embedded in a 0.8% agarose plug (2.5×10^5 cells/plug), digested in lysis

buffer (100 mM EDTA, 1% (w/v) sodium lauryl sarcosyne, 0.2% (w/v) sodium deoxycholate, 1 mg/ml proteinase K) at 37 °C for 48 h and washed in 10 mM TrisHCl pH8.0, 100 mM EDTA. Electrophoresis was performed at 14 °C in 0.9% (w/v) Pulse Field Certified Agarose (BioRad) containing Tris-borate/EDTA buffer in a BioRad CHEF DR III apparatus (9 h, 120°, 5.5 V/cm, 30 – 18 s switch time, 6 h, 117°, 4.5 V/cm, 18 – 9 s switch time, 6 h, 112°, 4 V/cm, 9 – 5 s switch time). Lambda Ladder (Biorad, #170-3635) was run as size standard. The gel was stained with ethidium bromide and imaged on an Alpha Innotech Imager. For single cell immunostaining, cells were pre-extracted with 0.5% Triton X-100/PBS for 5 minutes on ice, stained with indicated antibodies and mounted with Vectashield (Vector Laboratories). Images were acquired on a Leica CLSM SP2 microscope (Leica Microsystems) equipped with a HCX PL APO CS 63x objective. The following antibodies were used: γH2AX (Millipore, # 05-636), 53BP1 (Santa Cruz, sc-22760), CHK1 pS345 (Cell Signaling, #2348), CHK1 (Santa Cruz, sc-8408), EMI1 (Invitrogen, 38-5000), Geminin (Santa Cruz, sc-13015), KAP1-pS824 (Bethyl, A300-767A), KAP1 (Bethyl, A300-274A), PCNA (PC10, Santa Cruz, sc-56), RPA2 (Calbiochem NA19L), RPA2 (RPA32)-pS4/S8 (Bethyl, A300-245A), RPA2 (RPA32)-pS33 (Bethyl, A300-246A), TFIIH (Santa Cruz, sc-293). Secondary antibodies were Alexa Fluor-conjugates (Alexa Fluor-488, -594 and -647, Invitrogen).

Chromatin enrichment

For detection of ubiquitylated PCNA, cells were washed with ice-cold PBS and pre-extraction buffer containing 25 mM Hepes 7.4, 50 mM NaCl, 1 mM EDTA, 3 mM $MgCl_2$, 300 mM sucrose and 0.5% Triton X-100. Cells were then incubated in fresh pre-extraction buffer for 10 min on ice, washed with cold pre-extraction buffer and

PBS and collected by scraping in Laemmli buffer. Samples were boiled, sonicated and analysed by SDS-PAGE. PCNA protein was detected using Thermo Scientific SuperSignal West Femto Chemiluminescent Substrate.

DNA fiber spreadings

Cells were sequentially pulse labeled with 30 μM IdU and 250 μM CldU for the indicated times and harvested. Cells were then lysed and DNA fibers stretched onto glass slides, as described. Briefly, the fibers were denatured with 2.5 M HCl for 1 h, washed with PBS and blocked with 0.2% Tween 20 in 2% BSA/PBS. CldU and IdU tracks were revealed with anti-BrdU antibodies recognizing CldU (Abcam, ab6326) and IdU (BD, 347580), respectively, and appropriate secondary antibodies. Images were acquired with an Olympus IX81 microscope, CellR software (Olympus) and an Orca camera (Hamamatsu). Statistical analysis was carried out using GraphPad Prism.

Electron microscopic analysis of genomic DNA

In vivo psoralen cross-linking, isolation of total genomic DNA, enrichment of the replication intermediates and their EM visualization were carried out as described. Briefly, cells were harvested, genomic DNA was crosslinked by two rounds of incubation in 10 μM 4,5',8-Trimethylpsoralen and two minutes of irradiation with 366 nm UV light. Cells were lysed, genomic DNA was isolated from the nuclei by proteinase K digestion and phenol-chloroform extraction. Purified DNA was digested with PvuII and replication intermediates were enriched on a BND cellulose column. EM samples were prepared by spreading the DNA on carbon-coated grids and visualized by platinum rotary-shadowing. Images were acquired on a FEI Tecnai G2 Spirit microscope and analysed with ImageJ.

Cell synchronisation

For synchronization, 50% confluent U2OS cells were treated with 2 mM thymidine for 24 h, washed three times with PBS buffer and released into fresh media for 3 h. This was followed by nocodazole treatment for 12 h (75 ng/ml). The cells were again washed three times with PBS and incubated in fresh media for siRNA transfection. At the indicated times, samples were taken and processed for western blots and FACS analysis.

Cdt1 purification

His-Cdt1 was purified as described (Ferenbach et al. 2005). Briefly, His-tagged Cdt1 was expressed in *E. coli*, and solubilized from inclusion in 8 M urea and purified on Ni-NTA agarose beads. Urea was removed from protein eluate by dialysis in THED 200 (0.03% Triton, 20 mM HEPES, pH 8, 20% ethylene glycol, 1 mM DTT and 200 mM KCl).

X. laevis interphase egg extract preparation, replication assays and extraction of genomic DNA

X. laevis eggs were dejelled in buffer (20 mM Tris, pH 8.5, 110 mM NaCl, 5 mM DTT) for 5 min, washed with ¼ Marc's modified Ringer (MMR) (5 ×MMR: 100 mM HEPES, pH 7.5, 2 M NaCl, 10 mM KCl, 5 mM $MgSO_4$, 10 mM $CaCl_2$, 0.5 mM EDTA) and activated with 1 μg/ml calcium ionophore A23187 in MMR for 5 min. The activated eggs were washed with ¼ MMR and then washed three times with ice-cold S-buffer (50 mM HEPES–KOH, pH 7.5, 0.25 M sucrose, 50 mM KCl, 2.5 mM $MgCl_2$, 2 mM β-mercaptoethanol, 15 μg/ml leupeptin). The eggs were packed by

spinning and then crushed at 20000 *g* for 15 min. The cytoplasmic fraction between lipid cap and pellet was collected, supplemented with cytochalasin B (40 μg/ml final concentration) and centrifuged at 220000 *g* for 15 min to remove residual debris. The cytosolic and membrane fractions were collected and supplemented with 30 mM creatine phosphate and 150 mg/ml creatine phosphokinase. Extracts were snap-frozen with 3% glycerol in aliquots of 20 μl. For titration experiments (Supplemental Fig. S6E) demembranated sperm nuclei (4,000 /μl) were incubated in 20 μl of egg extract for 90 min at 23°C. At this time point, 0, 2.5 or 10 ng/μl $Cdt1^{243-620}$ was added to the extracts and incubated for another 90 min in the presence of [α-^{32}P]dATP at 23°C. The extracts were then diluted with 20 volumes of EB buffer (50 mM HEPES-KOH, pH 7.5, 100 mM KCl, 2.5 mM $MgCl_2$) containing 0.2% (v/v) Triton X-100 to stop replication. DNA was digested with 1 mg/ml proteinase K for 2 hours and the DNA was extracted with phenol/chloroform and electrophoresed on 0.8% agarose gel. For EM sample preparation, demembranated sperm nuclei (4,000 /μl) were incubated in 300 μl of egg extract for 60 min (with or without $Cdt1^{243-620}$) for studying re-replication in 1st S-phase or 150 min (addition of $Cdt1^{243-620}$ after 90 min) to study Re-replication in G2. The extracts were diluted with 1 ml of EB buffer, layered onto 1ml of EB buffer plus 30% (w/v) sucrose and centrifuged at 3000 *g* for 10 min at 4 °C. The pellets were resuspended in 300 μl of EB buffer, transferred to a 96-well plate (100 μl/well), and crosslinked with four cycles of incubation with 10 μg/ml 10 4,5□,8-Trimethylpsoralen (TMP) for 5 min on ice in the dark followed by irradiation with 366 nm light for 3 min. Genomic DNA was purified by proteinase K and RNase A treatment, phenol-chloroform extraction and isopropanol precipitation. The purified DNA (20 μg) was digested with NdeI endonuclease, and the replication intermediates were enriched on a BND cellulose column before processing for EM.

Supplemental Figures

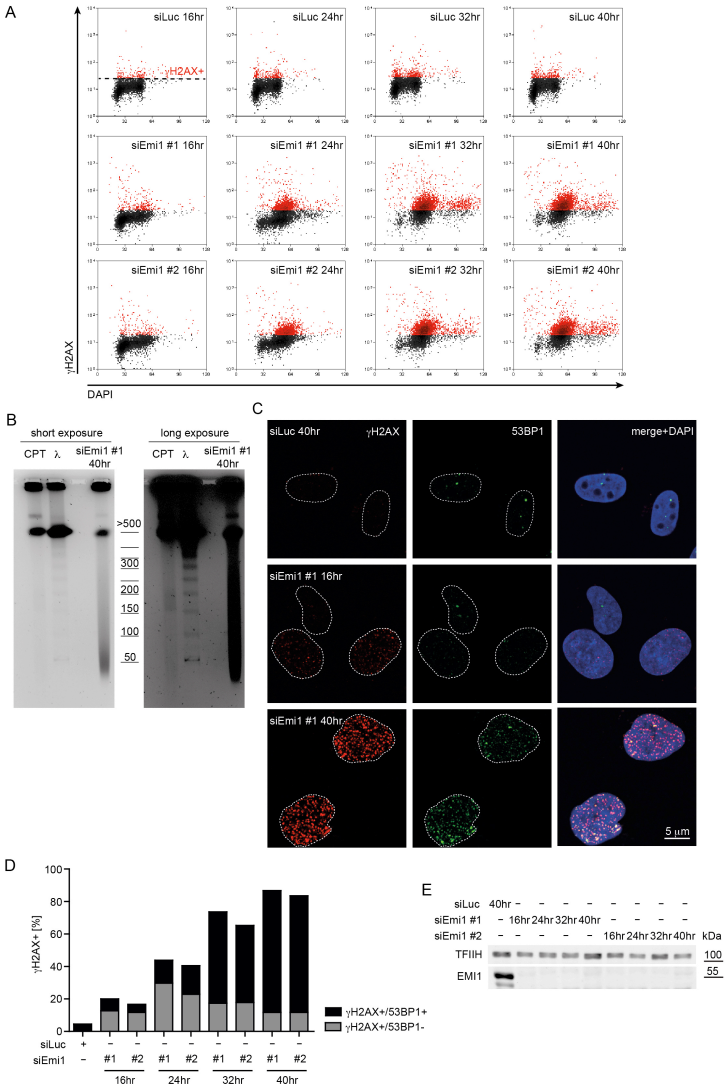

Supplemental Figure S1. Activation of the DNA damage response in Emi1-depleted cells upon completion of bulk DNA replication. (A) γH2AX levels in samples in Fig. 1A. Dashed line indicates threshold for γH2AX positivity, determined by single cell immunofluorescence staining (Neelsen et al. 2013). (B) Lambda Ladder (Biorad, #170-3635) was run along with a positive control for chromosomal breakage (CPT 1mM, 4 h) and with one of the samples from Fig. 1E, in identical electrophoretic conditions as in Fig. 1E, to determine the range of molecular size of the chromosomal fragments observed. A shorter and a longer exposure are shown. (C) Single cell immunofluorescence staining for γH2AX and 53BP1 in samples as in (A). Scale bar: 5 μm. (D) Quantification of γH2AX+/53BP1- (grey) and γH2AX+/53BP1+ (black) cells after mock- (siLuc) or Emi1 depletion. Cells with >3 53BP1 foci and >5 γH2AX foci were scored as positive. (E) Emi1 levels in samples in (C). TFIIH as loading control, molecular weight in kDa of nearest protein size marker is indicated.

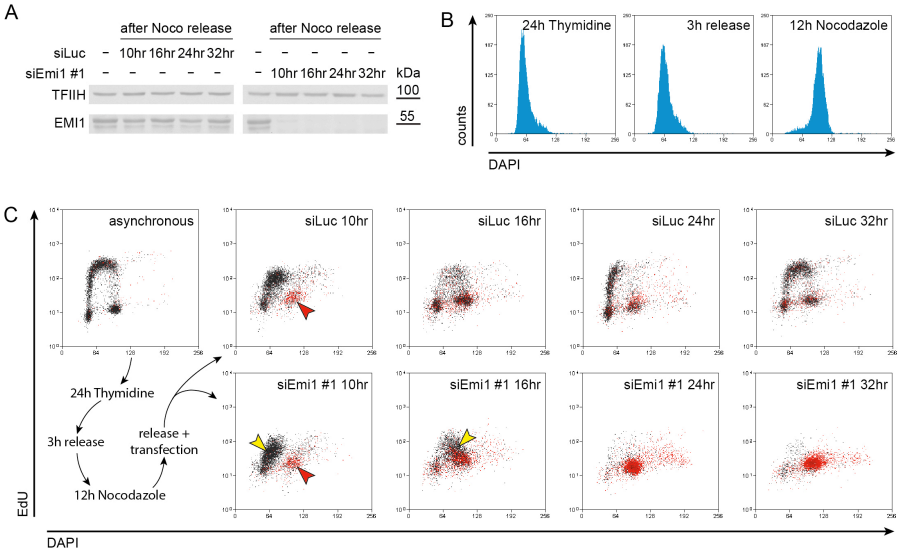

Supplemental Figure S2. Emi1-depletion in U2OS synchronised cells. (A) Emi1 levels in samples in (B, C). TFIIH as loading control, molecular weight in kDa of nearest protein size marker is indicated. (B) FACS analysis of DNA content (DAPI) of cells at indicated stages of the synchronisation procedure outlined in (C). (C) FACS analysis of DNA synthesis (EdU), DNA content (DAPI) and DDR activation (γH2AX) after mock- (siLuc) or Emi1 depletion at the indicated time points in synchronised U2OS cells. γH2AX-positive cells in red. The yellow and red arrowheads indicate cells with compromised DNA synthesis, and cells arrested after Nocodazole treatment with elevated levels of γH2AX, respectively. The presence of this subpopulation of cells that do not recover from Nocodazole arrest and display active DDR (red arrowheads) is a side-effect of the synchronization procedure coupled with siRNA transfection and impairs the assessment of DDR activation specifically induced by Emi1 depletion.

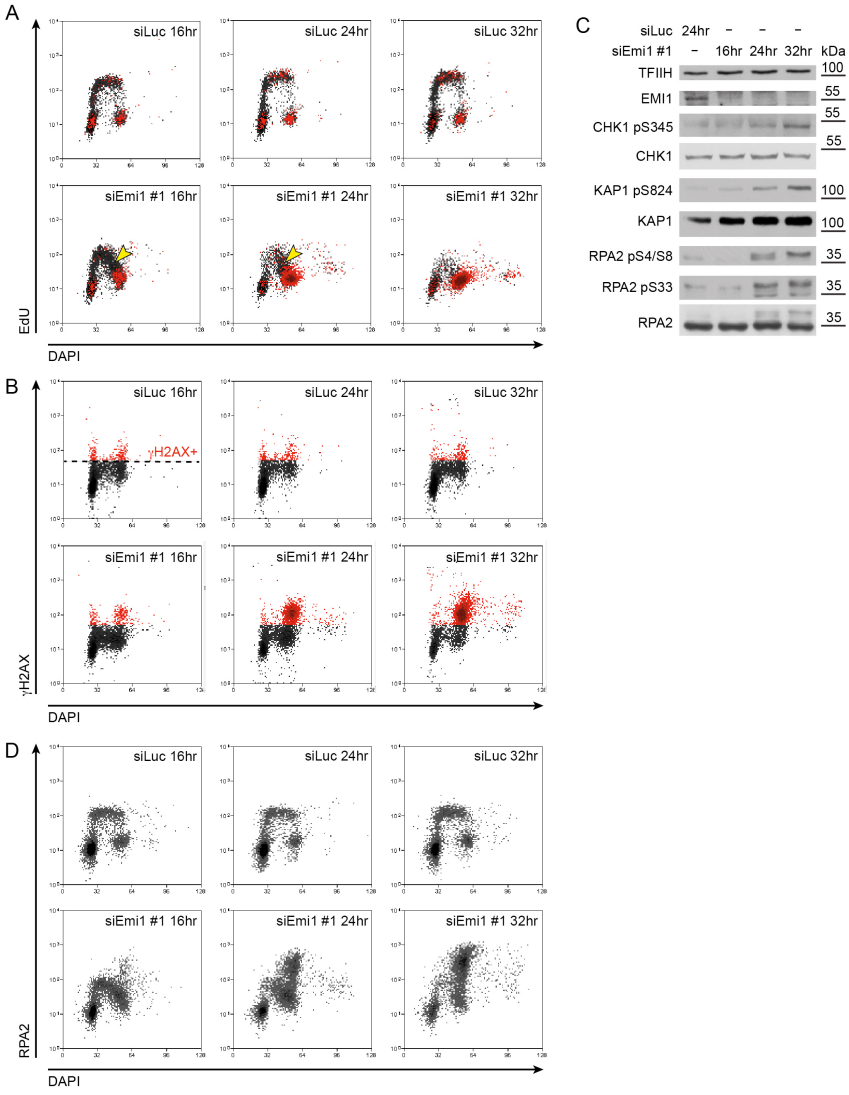

Supplemental Figure S3. Emi1-depletion in untransformed RPE-1 cells induces checkpoint activation and promotes RPA chromatin binding. (A) FACS analysis of DNA synthesis (EdU), DNA content (DAPI) and DDR activation (γH2AX) after mock- (siLuc) or Emi1 depletion at the indicated time points in RPE cells. γH2AX-positive cells in red. The yellow arrowheads indicate cells with compromised DNA synthesis in mid-late S-phase. (B) γH2AX levels in samples in (A). Dashed line indicates threshold for γH2AX positivity. (C) ATR- (pCHK1) and ATM- (pKAP1) activation, and RPA phosphorylation (RPA2 pS4/S8 and pS33) and total DDR proteins (CHK1, KAP1, RPA2) assessed by western blot upon Emi1-depletion. TFIIH as loading control. Molecular weight in kDa of nearest protein size marker is indicated. (D) FACS analysis of chromatin-bound RPA and DNA content (DAPI) after mock- (siLuc) or Emi1 depletion in RPE cells.

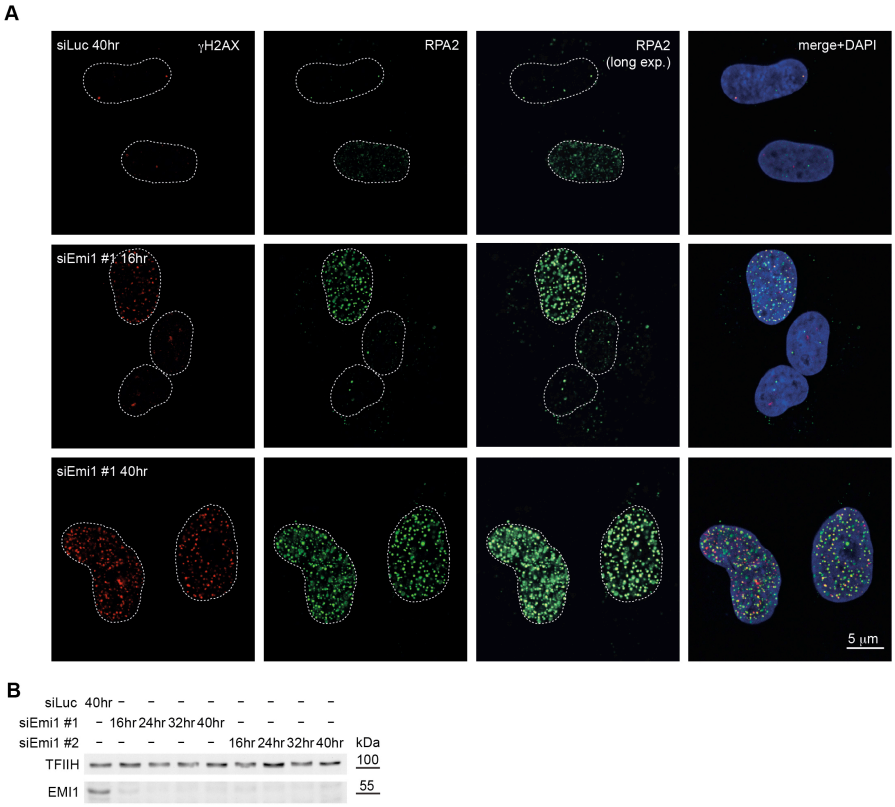

Supplemental Figure S4. Accumulation of chromatin-bound RPA in Emi1-depleted U2OS cells. (A) Single cell immunofluorescence staining for γH2AX and RPA2 in samples from Fig. 2A and B. The long exposure allows detection of physiological chromatin-bound RPA levels in S phase unperturbed cells. (B) Emi1 levels in samples in Fig. 2A, B and Supplemental Fig. 4A.

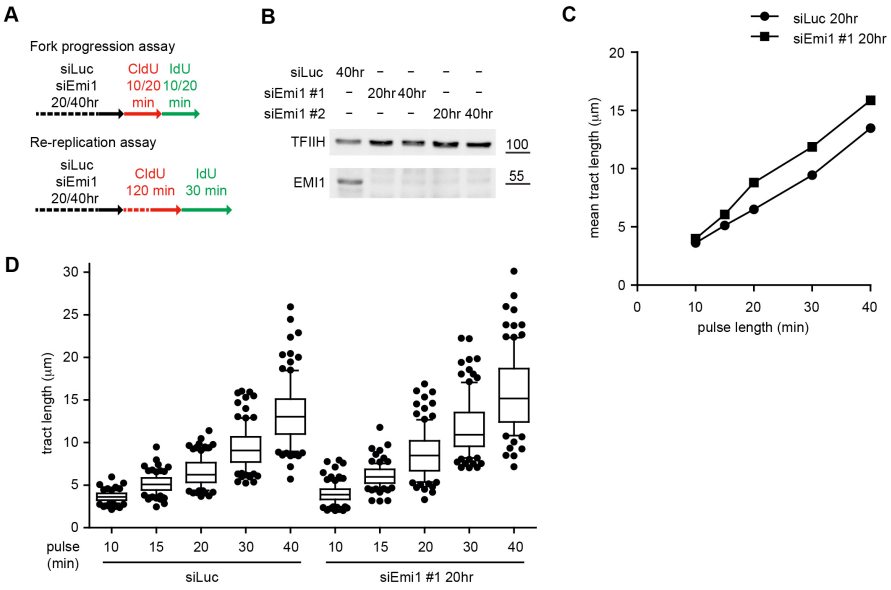

Supplemental Figure S5. Depletion of Emi1 promotes frequent fork fusion, but does not detectably interfere with the progression of individual replication forks. (A) Labelling protocols for assessment of replication fork progression (top, Fig. 3A and Supplemental Fig. S5C, D) and detection of re-replication events (bottom, Fig. 3B–D) by DNA fiber spreading. (B) Emi1 levels in samples in Fig. 3 and Supplemental Fig. S5C, D. (C) Mean length of newly replicated DNA tracts after indicated labelling pulses in mock-depleted cells (siLuc, circles) and 20 h after Emi1 depletion (siEmi1 #1, squares). (D) Length of newly replicated tracts in mock-depleted cells (siLuc) and 20 h after Emi1 depletion (siEmi1 #1) after indicated labelling pulses as shown in (A). Whiskers: 10-90 percentile, n = 100.

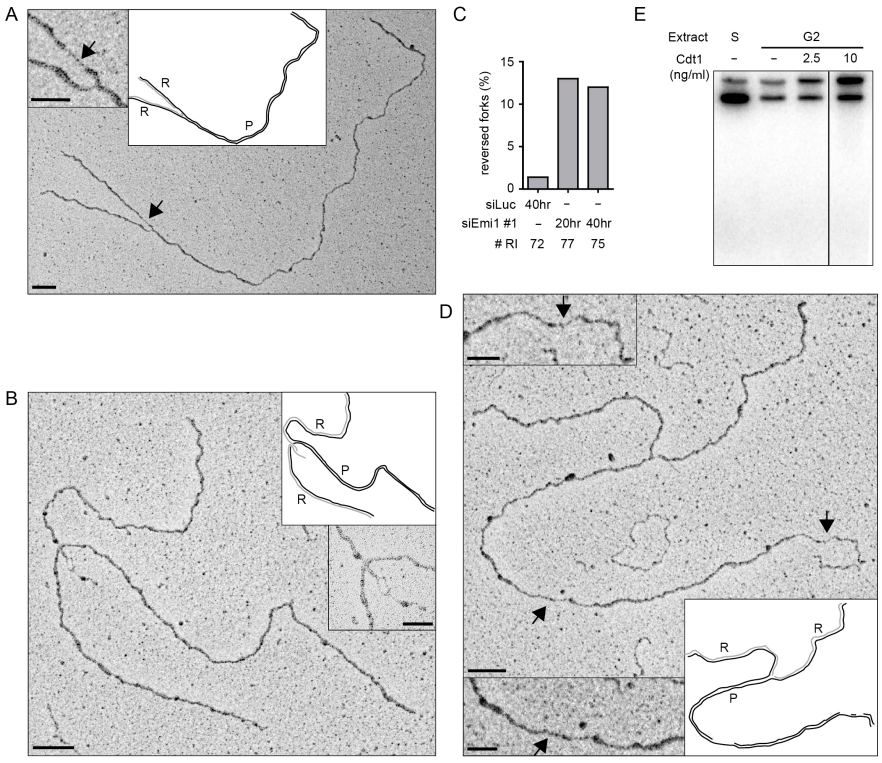

Supplemental Figure S6. Emi1-depletion leads to replication fork reversal. (A, D) Electron micrographs of representative replication forks from U2OS cells, 40 h after transfection with siEmi1. Black arrows indicate ssDNA gaps. Insets show magnified ssDNA gaps and schemes of fork structure, indicating parental (P) and replicated (R) duplexes. Gaps are in (A) on a replicated duplex and in (D) on the parental duplex. (B) Electron micrograph of a representative reversed replication fork from U2OS cells, 40 h after transfection with siEmi1. Insets show magnified junction and fork structure. In (A, B, D) black and grey lines describe parental and newly synthesized DNA strands in the replicated duplexes, respectively. Scale bar: 100nm (= 250bp), 50nm in inset. (C) Frequency of reversed replication forks in mock-depleted cells (siLuc) and at the indicated time points after Emi1 depletion (siEmi1 #1). # RI is the number of analysed replication intermediates. (E) Sperm nuclei re-replication assay in Xenopus interphase extracts in G2. The indicated concentrations of Cdt1 were added along with [α^{32}P]dATP 90 min after sperm addition (G2) and incubated for further 90 min. After incubation, DNA was isolated, separated by neutral agarose gel electrophoresis, and autoradiographed. As control, [α^{32}P]dATP was added along with the sperm, and DNA was isolated after 60 min (S). The grey line indicates a cropped lane in the gel.

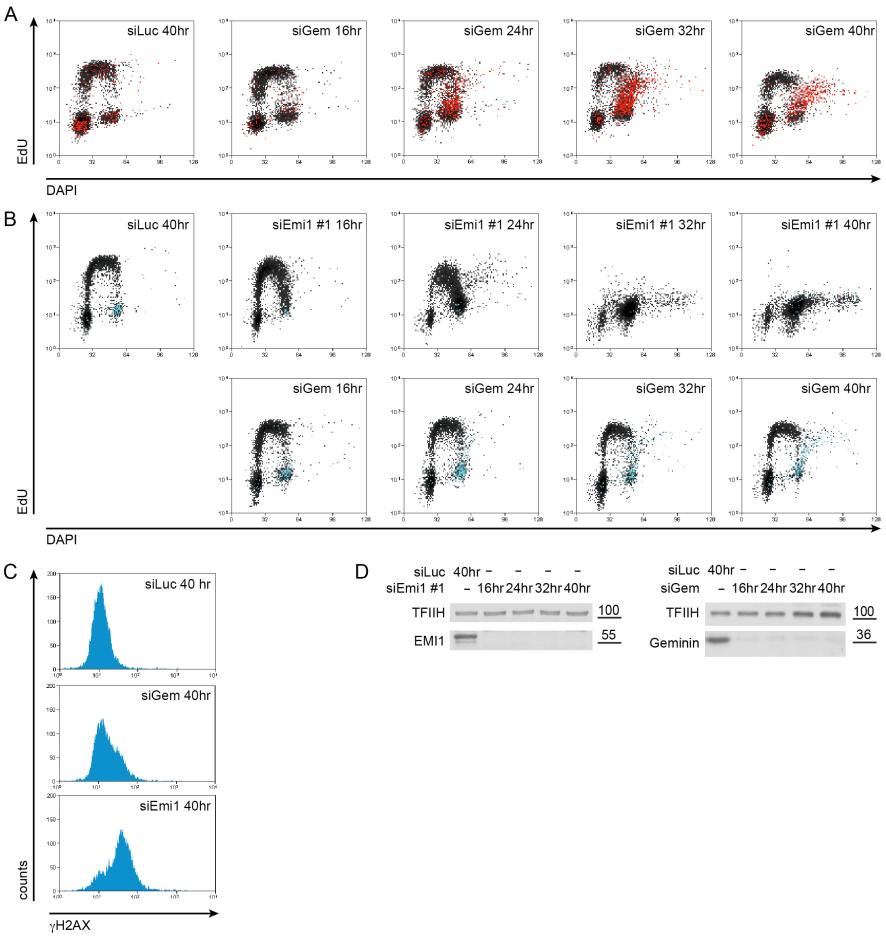

Supplemental Figure S7. Geminin-depletion does not visibly interfere with first S-phase completion and leads to reduced DNA damage during re-replication. (A) FACS analysis of DNA synthesis (EdU), DNA content (DAPI) and DDR activation (γH2AX) after mock- (siLuc) or Geminin depletion at the indicated time points in U2OS cells, using identical settings as in Fig. 1A. γH2AX-positive cells in red. (A) FACS analysis of DNA synthesis (EdU), DNA content (DAPI) and mitotic marker (H3-pS10) after mock- (siLuc) or Geminin depletion at the indicated time points in U2OS cells. H3-pS10-positive cells in cyan. (C) FACS analysis of DDR activation (γH2AX) after mock- (siLuc), Geminin- or Emi1 depletion at 40h. Cell cycle distribution (DNA content) at this time point can be seen in (B).

4. Discussion

Relevance of the biological question

The main aim of the work presented here is to understand, at a molecular level, how the cell deals with obstacles that impair its ability to efficiently and faithfully replicate their genome. DNA replication is, in fact, a crucial process, which involves the accurate duplication of the entire genetic information. As described in the introduction, numerous impediments may hinder DNA replication fork progression, leading to replication stress. In the last two decades, great attention has been given to replication stress, as this is regarded as an early, primary cause of tumorigenesis, and can be already frequently detected in hyper-proliferative pre-cancerous lesions. A second - perhaps counterintuitive - reason why it is of primary importance understanding how replication forks deal with genotoxic stress, is that interfering with DNA replication is a widely used strategy in cancer treatment, but the molecular mechanisms underlying sensitivity or resistance to these treatments are largely elusive.

Our lab, including the efforts presented in this thesis, has pioneered the use of single-molecule analysis of the replication process and the *in vivo* visualization of replication intermediates, to possibly improve our mechanistic understanding of replication stress. The microscopy-based techniques we exploited allowed us to study the replication dynamics and DNA structures forming during cancer-relevant replication stress. Data from our lab suggest that different chemical insults or the activation of proto-oncogenes, lead to stall of the replication fork, and the subsequent formation of a four-way junction structure - the reversed fork. This is relevant, as a comprehensive understanding of the factors involved in fork remodeling and metabolism, as well as their time and modes of action, can be instrumental to design better diagnostic and perhaps therapeutic approaches in the coming years.

Oncogene-induced replication stress

The initial part of this thesis was inspired by previous work published by our lab[25], showing that overexpressing CYCE or CDC25A in U2OS cells leads to frequent formation of reversed replication forks, which are processed by endonucleases MUS81/EME1 into DSB upon cell cycle checkpoint deregulation. This is as an important mechanistic aspect that may contribute to chromosomal instability in oncogene overexpressing cells and prompted us to extend our studies to other proto-oncogenes, in order to find the 'common denominator' that underlies oncogene-induced replication stress.

We thus decided to study aberrant activation of c-MYC and H-RAS, two well-studied oncogenes clearly contributing to tumourigenesis. Both of them are centrally positioned in the molecular circuitry regulating cell growth and as such they have very potent oncogenic activity.

To determine whether formation and endonucleolytic processing of reversed forks is a shared trait also by these two aggressive proto-oncogenes, we selected two highly proliferative cellular systems, U2OS and h-TERT immortalized RPE-1 cell lines. The first is a tumor cell line and as it has been used in CYCE and CDC25A overexpression, will serve as control to exclude cellular specific effects of replication stress. The second cell line is a primary cell line and represents a more physiological context to study the outbreak of tumorigenesis.

To overexpress c-MYC and H-RAS we explored transient transfection and transduction, two techniques that offer the relevant advantage of extending our studies to different kinds of cells. Although faster and simpler, transient transfection showed low efficiency of gene uptake and, since we want to investigate the early events of oncogene activation, it generally does not allow a controlled expression of the genes of interest. Therefore, we decided to stably integrate our genes of interest exploiting retroviral transduction. Once the retroviruses carrying the gene of interest have been produced, they were used to easily infect different target cells lines. To achieve a temporal control of c-MYC and H-RAS activity we used ER^{TAM}- 4-OHT system. Here, the gene is highly expressed under the control of the retroviral 5'LTR, but the protein translocates to the nucleus and is active only when the cells are exposed to 4-OHT. We characterized the efficiency and the fidelity of ER^{TAM}- 4-OHT system by analyzing mainly the activity of c-MYC-ER^{TAM} in RPE-1 cell line. Time-course immunofluorescence and quantitative real-time RT-PCR analysis revealed a significant increase of c-MYC-ER^{TAM} localization and activity in the nucleus compared to the EV control, even in the absence of 4-OHT, implying a technical defect of the ER^{TAM} system. The 'leakiness' in the nuclear translocation might arise from traces of estrogens in the reagents used to grow and manipulate the cells (e.g. traces of phenol red or inefficient removal of estrogens from serum). Another possibility is that the concentration of c-MYC-ER^{TAM} exceeds the one of HSP90, leaving many fusion proteins free to translocate in the nucleus. Collectively, these analyses showed that ER^{TAM} - 4-OHT is not a suitable experimental system for precise temporal control of the gene expression.

To overcome these technical drawbacks, we plan to exploit new overexpression methods. An attractive alternative could be tetracycline inducible expression, which has been shown to be very effective for *CYCE* and *CDC25A* expression[25]. One of the major benefits of the Tet-inducible system is that it allows a varied expression levels of the transgene and offers the possibility to rapidly and reversibly switch the transgene on or off at any time point. Another alternative could be the use of already existing human cancers that 'naturally' overexpress c-MYC or H-RAS. Despite appealing, however, this approach lacks the substantial advantage of inducing oncogene activation in a time-controlled manner, and thus to study early effects on DNA replication.

We plan to resume this part of the thesis as part of a new PhD project. In combination with our recent findings discussed bellow, we will investigate replication fork reversal and stability as

possible 'common denominator' mechanisms underlying replication stress by different oncogenes.

Function of HR factors at replication fork reversal

The second part of the thesis, recently accepted for publication in Nature Communications[113], focuses on the events occurring at the replication fork, when DNA replication is stalled by nucleotide depletion, leading to reversed fork formation and, in specific genetic background, to degradation of newly synthesized strands.

Our focus has been on the action of BRCA2, RAD51 and MRE11, recognized players of DSBs repair via HR. DSB repair requires end-processing and the formation of 3' ssDNA overhangs, for which MRE11 nuclease has been implicated. BRCA2 is recruited at sites of DSBs and stimulates the loading of RAD51 recombinase on ssDNA, thus initiating homology search. Recent studies revealed that these key HR factors play an unexpected function at forks experiencing replication stress upon nucleotide depletion: BRCA2 loads and stabilizes RAD51 filaments at stalled forks to protect the newly synthesized DNA from MRE11-mediated degradation[39,40]. This new function appears to be essential to ensure correct progression of DNA replication and maintain genome stability. Indeed, uncontrolled fork degradation leads to chromosomal instability and has been linked to lethality in BRCA2-defective mESCs, as well to sensitivity to chemotherapeutic treatments of BRCA-tumors that have bypassed the requirement for HR[101,102,108].

These discoveries, derived from the work of many different laboratories, inspired us to hypothesize that reversed forks, which accumulate in response to replication interference and very much resemble DSBs, might be the target of nucleolytic degradation in BRCA2-deficient cells.

Our data reveal that these previously reported fork resection events are indeed triggered by fork reversal, as - in the absence of BRCA2 protein - the unprotected regressed arms of reversed forks act as the entry point for MRE11 degradation. Importantly, we show that this processing occurs even in conditions of replication interference that do not completely stall replication fork progression (i.e. mild CPT treatments), which better reflect clinically relevant conditions of genotoxic stress. Three additional studies performed in different human cell lines (e.g. ovarian cancer cells PEO1 and FA cell line EUFA423) and in Xenopus laevis egg extracts using a wide range of genotoxic treatments (e.g. CPT, HU, aphidicolin) confirmed this key finding[98,114,115]. Altogether these studies identify the protection of reversed forks by BRCA2 and RAD51 nucleofilaments as a central and conserved mechanism to prevent unscheduled fork processing upon replication stress.

BRCA2 has been extensively described to act in complex with RAD51. The role of BRCA2 in fork protection was previously linked to loading and stabilization of RAD51 on the DNA. We now show that, differently from BRCA2, RAD51 is essential for the formation of reversed forks. In line with

this finding, depletion of RAD51 did not lead to fork degradation, but surprisingly abolished the degradation observed in BRCA2 deficient cells. These data suggest a dual role for RAD51 at stalled fork: first, RAD51 mediates the formation of reversed forks in a BRCA2-independent manner; subsequently, in complex with BRCA2, it protects these structures from deregulated nucleolytic processing. We were able to genetically separate these two RAD51 functions by studying fork remodeling in FA patient cells carrying the *RAD51*^{T131P} mutation. RAD51^{T131P} cannot form stable RAD51 filaments as it has deregulated ATPase activity[97]. Our data suggest that stable RAD51 nucleofilaments are required for the protection of reversed forks, but not for their formation, as RAD51^{T131P} cells can mediate fork reversal, but are unable to protect them from MRE11-dependent degradation. How these unstable RAD51 filaments can drive fork remodeling in a BRCA2-independent manner will need further *in vivo* and biochemical investigations. We hypothesize that RAD51 might be loaded on the DNA by other mediators, such as RAD51 paralogs, which regulate HR by protecting RAD51 filaments against antirecombinase activity[116] and remodel the filaments to stimulate strand exchange[117]. Intriguingly, these factors have been recently implicated in stalled replication fork stability[91], but their potential role in fork remodeling remains to be tested. Alternatively, this step might be carried out without any mediator, by only partial displacement of RPA with short and unstable RAD51 filamente, which may be sufficient to prime fork reversal. This hypothesis is supported by ssDNA curtain studies showing that RPA is in dynamic equilibrium between free and bound states and few RAD51 nucleation events can occur without any mediator resulting in filaments formation[118]. Moreover, based on data from our lab and others, the step of reversed fork formation is assisted by the combined activity of different fork remodeling factors, like ZRANB3[55,115], SMARCAL1[52,114,115] and HLTF[53,115], which might facilitate RPA displacement. Last but not least, previous studies have reported two distinct pathways of RAD51 assembly at the chromatin: BRCA2-independent during S-phase and BRCA2-dependent after IR[119]. Supported by our findings on the different nature of RAD51 filaments formed at the fork before fork reversal and on the regressed arm, it is conceivable that in the first step RAD51 does not strictly require a loader, because of the reported direct interaction with replication apparatus[120]. Conversely, at DSBs induced by IR and at regressed arms - which structurally resemble a DSB - *de novo* loading of RAD51 may strictly require BRCA2.

Similarities and differences between DSBs and regressed arms

It is possible that the MRN complex-dependent resection that typically occurs on DSB ends also takes place at regressed arm. A recent report showed *in vivo* that - as for DSBs - CtIP is required to initiate the MRE11-dependent degradation of the unprotected regressed arms and, because of its limited processivity, EXO1 contributes to extended fork degradation in BRCA-deficient cells. The role of DNA2 in this context seems somewhat limited but may deserve further investigation[98].

In the absence of RECQ1 - a fork remodeling enzyme which specifically restores normal forks from reversed ones[58] - the nucleolytic resection of regressed arms is mediated by the combined activity of WRN and DNA2, independently from CtIP, MRE11 or EXO1[57]. BOD1L loss is yet another condition where the uncontrolled resection of damaged forks and increased genomic instability is DNA2, but not MRE11 dependent.[93] Moreover, our fiber assay and EM experiments show that FA cells carryng RAD51^{T131P} show both MRE11- and DNA2-dependent degradation reversed forks (data not shown). Molecular determinants that channel the pathway towards one or the other processing pathway are not yet clear. The presence of ssDNA at the regressed arm, specific chromatin marks, or proteins bound to the end of the regressed arms - such as Ku70/80 - might influence the rate of resection and the type of nuclease recruited, similarly to what observed at DSBs[80].

In the context of replication fork stalling, similar to BRCA2, BRCA1 prevents MRE11-mediated degradation of reversed forks[98,115]. However, upon DSBs formation, BRCA1 is well-known to promote CtIP- and MRN-dependent resection to initiate HR[121]. BRCA1 plays a crucial role also in the pathway choice between HR and NHEJ, but the loss of the two antagonists in this decision, namely 53BP1 or RIF1 in BRCA1$^{-/-}$ cells did not limit the degradation of nascent strand by MRE11 upon HU fork stalling, suggesting a role for BRCA1 at stalled forks different from the one observed at DSB[102]. Further investigations are required to clarify the exact role and the dynamics of BRCA1 and other proteins shown to be required in stabilization of stalled forks, such as FANCD2[40,90], BOD1L[93] and WRNIP1[89].

Physiological relevance of fork reversal

The degradation of stalled forks in BRCA2 deficient cells has been shown to cause chromosomal instability. Preventing the degradation by inhibiting the activity of MRE11 or impairing its recruitment to the fork by PTIP or CHD4 downregulation rescues the chromosomal instability detected in HU-treated BRCA2-defective cells. Consistent with published data, we observe an increase of breaks and gaps when we treat BRCA2-deficient cells with HU, which decreases when MRE11 activity is inhibited or its recruitment is impaired by PTIP or, as we showed now, RAD52 downregulation. Surprisingly, however, if we prevent fork degradation by impairing fork reversal (e.g. ZRANB3 inactivation) we observed a further increase of chromosomal breakage in BRCA2-defective cells, which persisted also when inhibiting MRE11 activity or its recruitment by PTIP depletion. These data suggest that this chromosomal instability is not associated with forks resection, but most likely with defective repair of DSBs arising upon genotoxic stress in the absence of fork reversal. Thus, not all systems that prevent fork degradation in BRCA2-defective cells restore genome stability; in fact, we show that abolishing fork reversal during replication stress is detrimental for genome stability in BRCA2-defective cells.

PARP inhibitiors have long been known to aggravate chemosensitivity and genome instability of

BRCA-defective cells, mainly by exploiting their DSB repair defect[50] and are now either used in the clinic or are in the final phases of clinical trials for BRCA2 mutated breast (https://www.breastcancertrials.org) and ovarian cancer treatment. Recent reports showed that PARP inhibition or its depletion can also suppress the observed fork degradation in BRCA-defective cells[101,102] and the acquisition of PARP inhibitors and cisplatin resistance was associated with replication fork protection in Brca2-deficient tumor cells that do not develop Brca2 reversion mutations.

PARP inhibition was shown to lower the frequency of reversed forks by deregulating the RECQ1 activity and to promote replication-dependent chromosomal breakage in combination with genotoxic treatment (CPT). Consistent with the requirement of fork reversal to observe fork degradation (this thesis), we found that PARP inhibition also prevents fork degradation in BRCA2-depleted cells upon replication fork stalling, similar to RAD51 or ZRANB3 loss. We next assessed chromosomal instability by treating BRCA2-deficient cells with PARP inhibitors and HU and, as for ZRANB3 inactivation, we observed a further increase in genome instability compared to BRCA2-defective cells treated with HU only. Additional ZRANB3 loss in these conditions did not further increase chromosomal breaks, suggesting an epistatic relationship between these two ways of fork reversal impairment. Taken together these data strongly suggest that the synthetic lethality of PARP inhibition and BRCA2 defects upon replication stress reflects defective fork remodeling induced by PARP inhibition. These results provide additional evidence for the physiological role of global fork reversal and indicate the factors mediating the formation or stabilization of reversed forks as potential therapeutic targets against HR-defective tumors.

Connecting the dots

Initially we planned to study the role of HR factors in fork remodeling in the context of oncogene-induced replication stress. As the construction of a suitable system to overexpress c-MYC and H-RAS was still in progress, we exploited a series of reagents already present in the lab, allowing a finely-tuned tetracycline-dependent CYCE overexpression in U2OS. Preliminary experiments suggest that prolonged downregulation of BRCA2 *per se* resulted in reduced fork progression rate and DDR activation. In line with a recent report from Maria Jasin lab[108], accumulating DNA damage in these cells lead them to stall in G1 phase. Interestingly, when we activated the oncogene CYCE in BRCA2 downregulated cells, the G1 block was abolished and S phase cells displayed impaired DNA replication – as seen by compromised EdU incorporation, impaired completion of bulk DNA replication or extensive re-replication. I find these preliminary observations intriguing, especially in light of the recently published work. In my opinion these data would deserve attention and further investigation, in order to possibly link mechanistically the following series of recent observations:

(i) Reversed forks are formed in response to *CYCE* overexpression, as well as upon induction of re-replication events caused by origin licensing deregulation[25,26]. Preliminary experiments discussed in this thesis suggest that BRCA2 in these cells limits re-replication and replication stress.

(ii) Cyclin E overexpression has been shown to increase replication initiation and conflicts with transcription resulting in DNA damage that activates RAD51-mediated recombination[23].

(iii) It has been reported that DNA re-replication caused by deregulated origin firing, for example by CDT1 overexpression[109] or geminin inactivation[110], results in replication fork stalling and DSBs for which HR is a primary mechanism of repair[111].

(iv) The lab of Thanos Halazonetis has performed a screen in order to select factors implicated in DNA synthesis specifically in cells overexpressing CYCE and identified POLD3, a subunit of DNA polymerase delta, as well as HR factors, as strictly necessary for cell cycle progression and processive DNA synthesis. They propose that BIR repair of damaged replication forks observed in CYCE overexpressing cells results in segmental genomic duplication (particularly tandem head-to-tail duplications, which is frequently found in breast and ovarian cancer)[122]. Following up on this report, they found that RAD52 is required for G1-to-S-phase transition to facilitate the restart of collapsed forks in CYCE-overexpressing cells and propose that RAD52, together with POLD3, participates in BIR. Additionally, they identified MUS81, SLX4 and SMARCAL1 – fork remodeling and processing enzymes – as being required for S-phase progression in cyclin-E-overexpressing cells[123].

(v) Finally, as discussed above, we report that BRCA2 and RAD51 protect reversed forks from extensive nucleolytic degradation. Moreover, we found that RAD52 interacts with MRE11 to promote stalled fork degradation and chromosomal breakage in HU treated BRCA2-defective cells. Additionally, Alessandro Vindigni lab reported that the resection of the regressed arms establishes the substrate for MUS81 cleavage of the stalled forks in BRCA2-deficient cells to promote POLD3-dependent fork rescue.

Taken together, these data suggest that nucleotide depletion, replication/transcription conflicts, re-replication and/or increased DNA torsional stress induced by genotoxic treatments or oncogenes activation lead to the formation of reversed forks by the action of SMARCAL1, ZRANB3, HLTF and RAD51. Once formed, reversed forks are protected by BRCA2- and RAD51 to limit chromosomal instability. Loss of these factors will lead to RAD52-dependent recruitment of MRE11 at regressed arm, which is processed by MUS81 and SLX4 into DSB for a BIR repair

of the collapsed forks. In order to test this unified hypothesis we could assess resection of the stalled forks and DSB formation in CYCE overexpressing cells upon BRCA2 loss. The resection and chromatin instability should be rescued by mirin treatment.

If this is true, unscheduled processing of reversed forks could be proposed as 'common denominator' mechanism of tumorigenesis and as such, factors involved in its formation, stabilization and processing could represent new potential targets for therapeutic intervention in cancer cells that experience replication stress.

5. Materials and Methods

Oncogene-induced replication stress

Cell culture, treatments, and transfections

Human osteosarcoma (U2OS)-derived clones carrying inducible copies of *CYCE* and *CDC25A* were grown in DMEM supplemented with 10% FCS and 4 µg/ml tetracycline (Sigma-Aldrich, T7660). The overexpression of the oncogenes was induced by washing off tetracycline. Retinal pigment epithelium (RPE-1) cells were grown in DMEM and 10% FCS, while BJ foreskin fibroblasts (kindly provided by Fabrizio d'Adda di Fagagna, IFOM-IEO Campus, Milan, Italy) were maintained in MEM medium supplemented with 10% FCS, 10 mM NEAA, 1mM NaPyruvate and 2 mM Glutamine. During the retroviral transduction Phoenix-AMPHO cells and later U2OS and RPE-1 cells carrying *c-Myc-ER^{TAM}* or *H-Ras-ER^{TAM}* were grown in phenol free DMEM (Life Technologies, 21063-045) supplemented with 10% charcoal stripped FCS (Sigma-Aldrich, F6765). Where indicated the cells were treated with 100 nM 4-OHT (Sigma-Aldrich, T5648). The treatments was refreshed every day. Treatments with CPT (Sigma-Aldrich, C9911) were carried out at the final concentration of 25 nM.

Transient transfection and retrovirus transduction

For transient oncogene overexpression in U2OS cells, cells were transfected with pBabe (empty vector) or plasmid encoding Cdc25A (kindly provided by J. Lukas, Center for Protein Research, Copenhagen, Denmark) 24h before collection using FuGENE6 (Promega, E2313) according to the manufacturer's instructions. For depletion experiments, cells were transfected at indicated time points before oncogene induction with the indicated siRNA using Lipofectamine RNAiMax (Invitrogen, 13778-150) according to the manufacturer's instructions:

siLuc (40 nM; 5′-CGUACGCGGAAUACUUCGATT-3′);

siBRCA2 (48 h, 40 nM; 5′-UUGACUGAGGCUUGCUCAGUUTT-3′).

For virus production, about 1.5x10^6 Phoenix packaging cells were plated 2 days before transfection. The cells were transfected with 10 µg of pBabe (empty vector) and pBabe-puro-Myc-ER (kindly provided by Carla Grandori, Fred Hutchinson Cancer Research Center, Seattle, USA), pLNCX2 (empty vector) and pLNCX2-neo-RAS^{V12}-ER (kindly provided by Fabrizio d'Adda di Fagagna, IFOM-IEO Campus, Milan, Italy) and pLTR-CMV-GFP-puro (kindly provided by Raffaella Santoro, Department of Molecular Mechanisms of Disease, University of Zurich, Zurich, Switzerland) using the calcium phosphate coprecipitation method. For a 10 cm plate 438 µl of H_2O, 10 µg of DNA and 61 µl of 2 M $CaCl_2$ were mixed and added dropwise to 500 µl 2xHBS. The solution was incubated for 5 min added to the cells. The medium was refreshed 8h and 24h after the transfection. Two days after the transfection, the retrovirus-containing supernatants were

filtered through 0.45 µm syringe filters and used to infect U2OS and RPE-1 cells. For a more efficient infection, 8 mg/ml of polybrene was added to the filtered supernatant. The infection was repeated 3h after the first infection. Two rounds of infection were repeated on the next day. The cells were selected with 3 µg/ml puromycin (InvivoGen, ant-pr-1) or 3 mg/ml G418 (InvivoGen, ant-gn-1). For single clone isolation the cells were highly diluted, plated on a 10 cm dish and picked using cloning cylinders.

Western blotting

Cells were collected and lysed using 2x Laemmli buffer or NP-40 lysis buffer (HEPES 50 mM, NaCl 250 mM, EDTA 5 mM, NP-40 1%, DTT 1 mM, proteinase inhibitors (Roche)) for BRCA2 extraction. Protein amounts were normalized using known concentrations of BSA and protein absorbance was measured using Nanodrop technology. Precast gradient 4-15% SDS-gels were run at 180 V and proteins were either wet-blotted overnight (30 V, 4 °C) or for 2 h (100 V, 4 °C) at room temperature on Nitrocellulose blotting membranes (GE Healthcare). Membranes were blocked in 2% ECL (GE Healthcare) in 0.1% TBST (1xTBS supplemented with 0.1% Tween-20) for at least 30 min and incubated with primary antibodies over night at 4 °C or at room temperature for 4 h in blocking solution and secondary antibodies were added for 1 h at room temperature (in blocking solution). Membranes were washed 3 times with 0.1% TBST after primary and secondary antibody incubations and detected with ECL detection reagent (GE healthcare). Antibodies: c-MYC (Santa Cruz Biotechnology, N-262, sc-764, 1:500); H-RAS (Santa Cruz Biotechnology, C-20, sc-520, 1:500); BRCA2 (EMD Millipore, Ab-1, OP 95, 1:500); CycE (Santa Cruz Biotechnology, C-19, sc-198; 1:500); RPA2 (Calbiochem, NA19L, 1:1000); TFIIH (Santa Cruz Biotechnology, S-19, sc-293, 1:2000), GAPDH (Millipore, MAB374, 1:2000).

Extraction of cytoplasmic and nuclear proteins

Cells were collected (ca 5-10x10^6 cells) by trypsinization procedure and washed three times with ice cold PBS. The cells were centrifuged at 6000 rpm for 5 min at 4°C and 5x packed cell volume of cytoplasmic extract buffer (HEPES 10 mM pH 7.9, KCl 10 mM, EDTA 0.1 mM) was added to the pellet. The cells were incubated on ice for 5 min and then centrifuged at 3000 rpm for 5 min. The supernatant, which correspond to cytoplasmic extract, was collected. The pellet was resuspended in 100 µl of cytoplasmic buffer without NP-40 and centrifuged at 3000 rpm for 5 min. This procedure was repeated two times. A volume of nuclear buffer (HEPES 20 mM pH 7.9, NaCl 0.4 M, EDTA 1 mM, Glycerol 25%, Protease Inhibitors (Roche)) equal to volume of the pellet was added to the pellet and incubated on ice for 10 min. After the centrifugation at 14000 rpm for 5 min at 4°C, the supernatant (nuclear extract) was collected. Equal amount of cytoplasmic and

nuclear proteins were resolved by electrophoresis using SDS-PAGE electrophorisis and detected by western blotting with the indicated antibodies.

Quantitative real-time PCR

Total RNA was isolated from cells using the Oligotex mRNA Mini Kit (Qiagen). RNA of 500 ng was used for complementary DNA (cDNA) synthesis using Transcriptor First Strand cDNA Synthesis Kit (Roche). Quantitative real-time SYBR-Green-based PCR reactions were performed in triplicate and monitored with the Light Cycler 480 (Roche) system. The following primer pairs were used:

eIF4E:	forward 5' GATGGTATTGAGCCTATGTGG 3';
	reverse 5' CAATAAGGCACAGAAGTGTCTC 3'.
Nucleolin:	forward 5' AGAGCAATCAGGCTGGAGTTG 3';
	reverse 5' TTCAGTGGTATCCTCAGACAGGC 3'.
β-actin:	forward 5' CCAACCGCGAGAAGATGA 3';
	reverse 5' CCAGAGGCGTACAGGGATAG 3'.

Immunofluorescence and Flow cytometry

For single-cell immunostaining, cells were treated fixed with 4% formaldehyde/PBS for 15 min at room temperature (RT), permeabilized in 0.5% Triton X-100 for 10 min and stained for γH2AX (Millipore, Ser139, 05-636, 1:300), CDC25A (Santa Cruz Biotechnology, sc-7389, F-6, 1:300), c-Myc (Santa Cruz Biotechnology, N-262, sc-764, 1:100) and H-Ras (BD Transduction Laboratories, 610001, 1:100), detected by appropriate secondary antibodies, and mounted with Vectashield (Vector Laboratories). Cells were imaged using a microscope (model DMRB; Leica) equipped with a camera (model DFC360 FX; Leica). Images were taken at 60x, using Leica Application Suite 3.3.0.

For cell cycle analysis by propidium iodide staining cells were washed three times with ice-cold PBS (5 min, 400g, 4°C) and fixed with ice-cold 70% ethanol for 30 min. Subsequently the cells were washed with PBS, and the DNA was stained with 25 µg/ml propidium iodide (Sigma-Aldrich, 81845) and 100 µg/ml RNase A (Invitrogen, C35002) at RT for 1h. For flow cytometric analysis of γH2AX/EdU/DAPI, cells were labeled for 30 min with 10 µM EdU, harvested, and fixed for 15 min with 4% formaldehyde/ PBS. Cells were washed with 1% BSA/PBS, pH 7.4, permeabilized in 0.5% saponin/1% BSA/PBS and stained with anti- γH2AX antibody for 2h (Millipore, Ser139, 05-636, 1:500), followed by incubation with a suitable secondary antibody for 30 min. Incorporated EdU was labeled according to the manufacturer's instructions (Life Technologies, #C35002). For flow cytometric analysis for c-Myc/DAPI, prior the fixation, the cells were pre-extracted with 0.5% TritonX-100 for 10 min on ice. The cells were then fixed for 15 min with 4% formaldehyde/ PBS, washed with 1% BSA/PBS, pH 7.4, permeabilized with 0.5% saponin/1% BSA/PBS and stained

with anti-c-Myc antibody for 2h (Santa Cruz Biotechnology, N-262, sc-764, 1:125). In both assays the DNA was stained with 1 µg/ml DAPI. Samples were measured on a Cyan ADP flow cytometer (Beckman Coulter) and analyzed with Summit software v4.3 (Beckman Coulter).

DNA fiber spreading

Following the depletion of proteins of interest, cells were sequentially pulse-labeled with 30 µM CldU (c6891, Sigma-Aldrich) and 250 µM IdU (I0050000, European Pharmacopoeia) for 20 min each. The cells were collected and resuspended in PBS at 2.5×10^5 cells per ml. The labeled cells were diluted 1:5 (v/v) with unlabeled cells, and 2.5 µl of cells were mixed with 7.5 µl of lysis buffer (200 mM Tris-HCl, pH 7.5, 50 mM EDTA, and 0.5% (w/v) SDS) on a glass slide. After 9 min, the slides were tilted at 15–45°, and the resulting DNA spreads were air dried, fixed in 3:1 methanol/acetic acid overnight at 4 °C. The fibers were denatured with 2.5 M HCl for 1 h, washed with PBS (2x 3 min) and blocked with 0.2% Tween 20 in 1% BSA/PBS for 40 min. The newly replicated CldU and IdU tracks were labeled (for 2.5 h in the dark, at RT) with anti-BrdU antibodies recognizing CldU (Abcam, ab6326, 1:500) and IdU (BD, B44, 347580, 1:100), followed by 1 h incubation with secondary antibodies at RT in the dark: anti–mouse Alexa Fluor 488 (Invitrogen, A11001, 1:300) and anti–rat Cy3 (Jackson ImmunoResearch Laboratories, Inc., 712-166-153,1:150,). Images were acquired (IX81; Olympus; objective lenses: LC Plan Fluor 60x, 1.42 NA oil Olympus BX60 microscope) and analyzed using ImageJ software. The Mann–Whitney test was applied for statistical analysis using Prism (GraphPad Software).

6. References

1. Fragkos, M., Ganier, O., Coulombe, P. & Méchali, M. DNA replication origin activation in space and time. *Nat. Rev. Mol. Cell Biol.* **16,** 360–374 (2015).
2. Méndez, J. & Stillman, B. Chromatin association of human origin recognition complex, cdc6, and minichromosome maintenance proteins during the cell cycle: assembly of prereplication complexes in late mitosis. *Mol. Cell. Biol.* **20,** 8602–12 (2000).
3. Wold, M. S. Replication protein A: a heterotrimeric, single-stranded DNA-binding protein required for eukaryotic DNA metabolism. *Annu Rev Biochem* **66,** 61–92 (1997).
4. Burgers, P. M. J. Polymerase dynamics at the eukaryotic DNA replication fork. *J. Biol. Chem.* **284,** 4041–4045 (2009).
5. Fachinetti, D. *et al.* Replication Termination at Eukaryotic Chromosomes Is Mediated by Top2 and Occurs at Genomic Loci Containing Pausing Elements. *Mol. Cell* **39,** 595–605 (2010).
6. Nishiyama, A., Frappier, L. & Méchali, M. MCM-BP regulates unloading of the MCM2-7 helicase in late S phase. *Genes Dev.* **25,** 165–175 (2011).
7. Maric, M., Maculins, T., De Piccoli, G. & Labib, K. Cdc48 and a ubiquitin ligase drive disassembly of the CMG helicase at the end of DNA replication. *Science (80-.).* **346,** 1253596–1253596 (2014).
8. Priego Moreno, S., Bailey, R., Campion, N., Herron, S. & Gambus, A. Polyubiquitylation drives replisome disassembly at the termination of DNA replication. *Science (80-.).* **346,** 477–481 (2014).
9. Friedberg, E. C. A brief history of the DNA repair field. *Cell Res.* **18,** 3–7 (2008).
10. Lindahl, T. & Nyberg, B. Rate of Depurination of Native Deoxyribonucleic Acid. *Biochemistry* **11,** 3610–3618 (1972).
11. Ciccia, A. & Elledge, S. J. The DNA Damage Response: Making It Safe to Play with Knives. *Mol. Cell* **40,** 179–204 (2010).
12. Karakaidos, P. *et al.* Activation of the DNA damage checkpoint and genomic instability in human precancerous lesions. *Nature* 907–913 (2005). doi:10.1038/nature03492.1.
13. Bartkova, J. *et al.* DNA damage response as a candidate anti-cancer barrier in early human tumorigenesis. *Nature* **434,** 864–870 (2005).
14. Zeman, M. K. & Cimprich, K. A. Causes and consequences of replication stress. *Nat. Cell Biol.* **16,** 2–9 (2014).
15. Hamperl, S. & Cimprich, K. A. The contribution of co-transcriptional RNA:DNA hybrid structures to DNA damage and genome instability. *DNA Repair (Amst).* **19,** 84–94 (2014).
16. Mailand, N. Rapid Destruction of Human Cdc25A in Response to DNA Damage. *Science (80-.).* **288,** 1425–1429 (2000).

17. Bartkova, J. *et al.* Oncogene-induced senescence is part of the tumorigenesis barrier imposed by DNA damage checkpoints. *Nature* **444,** 633–637 (2006).
18. Di Micco, R. *et al.* Oncogene-induced senescence is a DNA damage response triggered by DNA hyper-replication. *Nature* **444,** 638–642 (2006).
19. Tsantoulis, P. K. *et al.* Oncogene-induced replication stress preferentially targets common fragile sites in preneoplastic lesions. A genome-wide study. *Oncogene* **27,** 3256–3264 (2008).
20. Miron, K., Golan-Lev, T., Dvir, R., Ben-David, E. & Kerem, B. Oncogenes create a unique landscape of fragile sites. *Nat. Commun.* **6,** 7094 (2015).
21. Hills, S. A. & Diffley, J. F. X. DNA replication and oncogene-induced replicative stress. *Curr. Biol.* **24,** 435–444 (2014).
22. Ekholm-Reed, S. *et al.* Deregulation of cyclin E in human cells interferes with prereplication complex assembly. *J. Cell Biol.* **165,** 789–800 (2004).
23. Jones, R. M. *et al.* Increased replication initiation and conflicts with transcription underlie Cyclin E-induced replication stress. *Oncogene* **32,** 3744–3753 (2013).
24. Bester, A. C. *et al.* Nucleotide deficiency promotes genomic instability in early stages of cancer development. *Cell* **145,** 435–446 (2011).
25. Neelsen, K. J., Zanini, I. M. Y., Herrador, R. & Lopes, M. Oncogenes induce genotoxic stress by mitotic processing of unusual replication intermediates. *J. Cell Biol.* **200,** 699–708 (2013).
26. Neelsen, K. J. *et al.* Deregulated origin licensing leads to chromosomal breaks by rereplication of a gapped DNA template. *Genes Dev.* **27,** 2537–2542 (2013).
27. Pratilas, C. A. & Solit, D. B. Targeting the mitogen-activated protein kinase pathway: Physiological feedback and drug response. *Clin. Cancer Res.* **16,** 3329–3334 (2010).
28. Barbacid, M. M. & M. RAS oncogenes: the first 30 years. *Nat. Rev. Cancer* 459–465 (2003).
29. Amati, B. & Land, H. Myc—Max—Mad: a transcription factor network controlling cell cycle progression, differentiation and death. *Curr. Opin. Genet. Dev.* **4,** 102–108 (1994).
30. Kress, T. R., Sabò, A. & Amati, B. MYC: connecting selective transcriptional control to global RNA production. *Nat. Rev. Cancer* **15,** 593–607 (2015).
31. Maya-Mendoza, A. *et al.* Myc and Ras oncogenes engage different energy metabolism programs and evoke distinct patterns of oxidative and DNA replication stress. *Mol. Oncol.* **9,** 601–616 (2015).
32. Dominguez-Sola, D. *et al.* Non-transcriptional control of DNA replication by c-Myc. *Nature* **448,** 445–451 (2007).
33. R Taub, I Kirsch, C Morton, G Lenoir, D Swan, S Tronick, S Aaronson, and P. L. Translocation of the c-myc gene into the immunoglobulin heavy chain locus in human

Burkitt lymphoma and murine plasmacytoma cells. *Proc. Natl. Acad. Sci.* **79,** 7837–7841 (1982).

34. Beroukhim, R. *et al.* The landscape of somatic copy-number alteration across human cancers. *Nature* **463,** 899–905 (2010).
35. O'Driscoll, M., Ruiz-Perez, V. L., Woods, C. G., Jeggo, P. A. & Goodship, J. A. A splicing mutation affecting expression of ataxia-telangiectasia and Rad3-related protein (ATR) results in Seckel syndrome. *Nat. Genet.* **33,** 497–501 (2003).
36. Flynn, R. L. & Zou, L. ATR: A master conductor of cellular responses to DNA replication stress. *Trends Biochem. Sci.* **36,** 133–140 (2011).
37. Se, C. R. ATM and ataxia telangiectasia. **6,** 0–6 (2005).
38. Ray Chaudhuri, A. *et al.* Topoisomerase I poisoning results in PARP-mediated replication fork reversal. *Nat. Struct. Mol. Biol.* **19,** 417–423 (2012).
39. Schlacher, K. *et al.* Double-strand break repair-independent role for BRCA2 in blocking stalled replication fork degradation by MRE11. *Cell* **145,** 529–542 (2011).
40. Schlacher, K., Wu, H. & Jasin, M. A Distinct Replication Fork Protection Pathway Connects Fanconi Anemia Tumor Suppressors to RAD51-BRCA1/2. *Cancer Cell* **22,** 106–116 (2012).
41. Branzei, D. & Foiani, M. Maintaining genome stability at the replication fork. *Nat. Rev. Mol. Cell Biol.* **11,** 208–219 (2010).
42. De Piccoli, G. *et al.* Replisome Stability at Defective DNA Replication Forks Is Independent of S Phase Checkpoint Kinases. *Mol. Cell* **45,** 696–704 (2012).
43. Hashimoto, Y., Chaudhuri, A. R., Lopes, M. & Costanzo, V. Rad51 protects nascent DNA from Mre11-dependent degradation and promotes continuous DNA synthesis. *Nat. Struct. Mol. Biol.* **17,** 1305–1311 (2010).
44. Berti, M. & Vindigni, A. Replication stress: getting back on track. *Nat. Struct. Mol. Biol.* **23,** 103–109 (2016).
45. Neelsen, K. J. & Lopes, M. Replication fork reversal in eukaryotes: from dead end to dynamic response. *Nat. Rev. Mol. Cell Biol.* **16,** 207–220 (2015).
46. Higgins, N. P., Kato, K. & Strauss, B. A model for replication repair in mammalian cells. *J. Mol. Biol.* **101,** 417–425 (1976).
47. Atkinson, J. & McGlynn, P. Replication fork reversal and the maintenance of genome stability. *Nucleic Acids Res.* **37,** 3475–3492 (2009).
48. Follonier, C., Oehler, J., Herrador, R. & Lopes, M. Friedreich's ataxia–associated GAA repeats induce replication-fork reversal and unusual molecular junctions. *Nat. Struct. Mol. Biol.* **20,** 486–494 (2013).
49. Zellweger, R. *et al.* Rad51-mediated replication fork reversal is a global response to genotoxic treatments in human cells. *J. Cell Biol.* **208,** 563–579 (2015).

50. Bryant, H. E. *et al.* Specific killing of BRCA2-deficient tumours with inhibitors of poly(ADP-ribose) polymerase. *Nature* **434,** 913–917 (2005).
51. Farmer, H. *et al.* Targeting the DNA repair defect in BRCA mutant cells as a therapeutic strategy. *Nature* **434,** 917–921 (2005).
52. Bétous, R. *et al.* SMARCAL1 catalyzes fork regression and holliday junction migration to maintain genome stability during DNA replication. *Genes Dev.* **26,** 151–162 (2012).
53. Kile, A. C. *et al.* Article HLTF ' s Ancient HIRAN Domain Binds 3 0 DNA Ends to Drive Replication Fork Reversal Article HLTF ' s Ancient HIRAN Domain Binds 3 0 DNA Ends to Drive Replication Fork Reversal. *Mol. Cell* **58,** 1090–1100 (2015).
54. Fugger, K. *et al.* FBH1 catalyzes regression of stalled replication forks. *Cell Rep.* **10,** 1749–1757 (2015).
55. Vujanovic, M. *et al.* Replication Fork Slowing and Reversal upon DNA Damage Require PCNA Polyubiquitination and ZRANB3 DNA Translocase Activity. *Mol. Cell* **67,** 882–890.e5 (2017).
56. Ahuja, A. K. *et al.* A short G1 phase imposes constitutive replication stress and fork remodelling in mouse embryonic stem cells. *Nat. Commun.* **7,** 10660 (2016).
57. Thangavel, S. *et al.* DNA2 drives processing and restart of reversed replication forks in human cells. *J. Cell Biol.* **208,** 545–562 (2015).
58. Berti, M. *et al.* Human RECQ1 promotes restart of replication forks reversed by DNA topoisomerase I inhibition. *Nat. Struct. Mol. Biol.* **20,** 347–354 (2013).
59. Hanada, K. *et al.* The structure-specific endonuclease Mus81 contributes to replication restart by generating double-strand DNA breaks. *Nat. Struct. Mol. Biol.* **14,** 1096–1104 (2007).
60. Couch, F. B. *et al.* ATR phosphorylates SMARCAL1 to prevent replication fork collapse. *Genes Dev.* **27,** 1610–1623 (2013).
61. Futreal, P. A. *et al.* BRCA1 and BRCA2 : different roles in a common pathway of genome protection. *Nature* **9,** 1–12 (2015).
62. Miki, Y. *et al.* Strong Candidate for the Breast and Ovarian Cancer Susceptibility Gene BRCA1. *Science (80-.).* **266,** 66–71 (1994).
63. Richard Wooster, Graham Bignell, Jonathan Lancaster, Sally Swift, Sheila Seal, Jonathan Mangion*, Nadine Collins, Simon Gregory, Curtis Gumbs, Gos Micklem, Rita Barfoot, Rifat Hamoudi, Sandeep Patel, Catherine Rices, Patrick Biggs, Yasmin Hashim, Amanda S, A. A. & M. R. S. Identification of the breast cancer susceptibility gene BRCA2. *Nature* **378,** 592 (1995).
64. Mavaddat, N. *et al.* Cancer Risks for BRCA1 and BRCA2 Mutation Carriers : Results From Prospective Analysis of EMBRACE. **105,** (2017).
65. Dhillon, K. K., Swisher, E. M. & Taniguchi, T. Secondary mutations of BRCA1/2 and drug

resistance. *Cancer Sci.* **102,** 663–669 (2011).

66. Helleday, T. The underlying mechanism for the PARP and BRCA synthetic lethality: Clearing up the misunderstandings. *Mol. Oncol.* **5,** 387–393 (2011).
67. Ray Chaudhuri, A. & Nussenzweig, A. The multifaceted roles of PARP1 in DNA repair and chromatin remodelling. *Nat. Rev. Mol. Cell Biol.* (2017). doi:10.1038/nrm.2017.53
68. Esashi, F., Galkin, V. E., Yu, X., Egelman, E. H. & West, S. C. Stabilization of RAD51 nucleoprotein filaments by the C-terminal region of BRCA2. *Nat. Struct. Mol. Biol.* **14,** 468–474 (2007).
69. Shibata, A. Mutat Res Fund Mol Mech Mutagen Regulation of repair pathway choice at two-ended DNA double-strand breaks. (2017).
70. Bunting, S. F. *et al.* 53BP1 inhibits homologous recombination in brca1-deficient cells by blocking resection of DNA breaks. *Cell* **141,** 243–254 (2010).
71. Callen, E. *et al.* 53BP1 mediates productive and mutagenic DNA repair through distinct phosphoprotein interactions. *Cell* **153,** 1266–1280 (2013).
72. Chapman, J. R. *et al.* RIF1 Is Essential for 53BP1 - Dependent Nonhomologous End Joining and Suppression of DNA Double-Strand Break Resection. *Mol. Cell* **49,** 858–871 (2013).
73. Lee, K. J. *et al.* Phosphorylation of Ku dictates DNA double-strand break (DSB) repair pathway choice in S phase. *Nucleic Acids Res.* **44,** 1732–1745 (2015).
74. Saredi, G. *et al.* H4K20me0 marks post-replicative chromatin and recruits the TONSL–MMS22L DNA repair complex. *Nature* **534,** 714–718 (2016).
75. Ferretti, L. P., Lafranchi, L. & Sartori, A. A. Controlling DNA-end resection: A new task for CDKs. *Front. Genet.* **4,** 1–7 (2013).
76. Lieber, M. R. The Mechanism of Double-Strand DNA Break Repair by the Nonhomologous DNA End-Joining Pathway. *Annu. Rev. Biochem.* **79,** 181–211 (2010).
77. Pawelczak, K. S., Bennett, S. M. & Turchi, J. J. Coordination of DNA-PK activation and nuclease processing of DNA termini in NHEJ. *Antioxid. Redox Signal.* **14,** 2531–43 (2011).
78. Jiang, W. *et al.* Differential phosphorylation of DNA-PKcs regulates the interplay between end-processing and end-ligation during nonhomologous end-joining. *Mol. Cell* **58,** 172–185 (2015).
79. Davis, A. & Chen, D. DNA double strand break repair via non-homologous end-joining. *Transl. Cancer Res.* **2,** 130–43 (2013).
80. Cannavo, E. & Cejka, P. Sae2 promotes dsDNA endonuclease activity within Mre11–Rad50–Xrs2 to resect DNA breaks. *Nature* **514,** 122–125 (2014).
81. Garcia, V., Phelps, S. E. L., Gray, S. & Neale, M. J. Bidirectional resection of DNA double-strand breaks by Mre11 and Exo1. *Nature* **479,** 241–244 (2011).

82. Heyer, W.-D., Ehmsen, K. T. & Liu, J. Regulation of Homologous Recombination in Eukaryotes. *Annu. Rev. Genet.* **44,** 113–139 (2010).
83. Lomonosov, M., Anand, S., Sangrithi, M., Lomonosov, M. & Anand, S. Stabilization of stalled DNA replication forks by the BRCA2 breast cancer susceptibility protein service Stabilization of stalled DNA replication forks by the BRCA2 breast cancer susceptibility protein. 3017–3022 (2003). doi:10.1101/gad.279003
84. Zhang, J. & Walter, J. C. Mechanism and regulation of incisions during DNA interstrand cross-link repair. *DNA Repair (Amst).* **19,** 135–142 (2014).
85. Howlett, N. G., Taniguchi, T., Durkin, S. G., D'Andrea, A. D. & Glover, T. W. The Fanconi anemia pathway is required for the DNA replication stress respone and for the regulation of common fragile site stability. *Hum. Mol. Genet.* **14,** 693–701 (2005).
86. Hussain, S. *et al.* Direct interaction of FANCD2 with BRCA2 in DNA damage response pathways. *Hum. Mol. Genet.* **13,** 1241–1248 (2004).
87. Wang, X., Andreassen, P. R. & Andrea, A. D. D. Functional Interaction of Monoubiquitinated Functional Interaction of Monoubiquitinated FANCD2 and BRCA2 / FANCD1 in Chromatin. *Mol Cell Biol* **24,** 5850–62 (2004).
88. Iannascoli, C., Palermo, V., Murfuni, I., Franchitto, A. & Pichierri, P. The WRN exonuclease domain protects nascent strands from pathological MRE11/EXO1-dependent degradation. *Nucleic Acids Res.* **43,** 9788–9803 (2015).
89. Leuzzi, G., Marabitti, V., Pichierri, P. & Franchitto, A. WRNIP 1 protects stalled forks from degradation and promotes fork restart after replication stress. *EMBO J.* **35,** 1–15 (2016).
90. Yang, Y. *et al.* FANCD2 and REV1 cooperate in the protection of nascent DNA strands in response to replication stress. *Nucleic Acids Res.* **43,** 8325–8339 (2015).
91. Somyajit, K., Saxena, S., Babu, S., Mishra, A. & Nagaraju, G. Mammalian RAD51 paralogs protect nascent DNA at stalled forks and mediate replication restart. *Nucleic Acids Res.* **43,** 9835–9855 (2015).
92. Klein, H. L. The consequences of Rad51 overexpression for normal and tumor cells. *DNA Repair (Amst).* **7,** 686–693 (2008).
93. Higgs, M. R. *et al.* BOD1L Is Required to Suppress Deleterious Resection of Stressed Replication Forks. *Mol. Cell* **59,** 462–477 (2015).
94. Dungrawala, H. *et al.* RADX Promotes Genome Stability and Modulates Chemosensitivity by Regulating RAD51 at Replication Forks. *Mol. Cell* **67,** 374–386.e5 (2017).
95. Ying, S., Hamdy, F. C. & Helleday, T. Mre11-dependent degradation of stalled DNA replication forks is prevented by BRCA2 and PARP1. *Cancer Res.* **72,** 2814–2821 (2012).
96. Karanja, K. K., Lee, E. H., Hendrickson, E. A. & Campbell, J. L. Preventing over-resection by DNA2 helicase/nuclease suppresses repair defects in Fanconi anemia cells. *Cell Cycle* **13,** 1540–1550 (2014).

97. Wang, A. T. *et al.* A Dominant Mutation in Human RAD51 Reveals Its Function in DNA Interstrand Crosslink Repair Independent of Homologous Recombination Article A Dominant Mutation in Human RAD51 Reveals Its Function in DNA Interstrand Crosslink Repair Independent of. *Mol. Cell* **59,** 478–490 (2015).
98. Lemaçon, D., Jackson, J., Quinet, A., Brickner, J. R. & Li, Shan, Stephanie Yazinski, Zhongsheng You, Grzegorz Ira, Lee Zou, Nima Mosammaparast, A. A. V. MRE11 and EXO1 nucleases degrade reversed forks and elicit MUS81- dependent fork rescue in BRCA2-deficient cells . *Nat. Commun.* **in press,** (2017).
99. Dungrawala, H. *et al.* The Replication Checkpoint Prevents Two Types of Fork Collapse without Regulating Replisome Stability. *Mol. Cell* **59,** 998–1010 (2015).
100. Bryant, H. E. *et al.* PARP is activated at stalled forks to mediate Mre11-dependent replication restart and recombination. *EMBO J.* **28,** 2601–2615 (2009).
101. Ding, X. *et al.* Synthetic viability by BRCA2 and PARP1/ARTD1 deficiencies. *Nat. Commun.* **7,** 12425 (2016).
102. Chaudhuri, A. R. *et al.* Replication fork stability confers chemoresistance in BRCA-deficient cells. *Nature* **535,** 382–387 (2016).
103. Guillemette, S. *et al.* Resistance to therapy in BRCA2 mutant cells due to loss of the nucleosome remodeling factor CHD4. *Genes Dev.* **29,** 489–494 (2015).
104. Lord, C. J. & Ashworth, A. Mechanisms of resistance to therapies targeting BRCA-mutant cancers. *Nat. Med.* **19,** 1381–1388 (2013).
105. Prakash, R., Zhang, Y., Feng, W. & Jasin, M. Homologous Recombination and Human Health: The Roles of {BRCA1,} {BRCA2,} and Associated Proteins. *Cold Spring Harb Perspect. Biol.* **7,** a016600 (2015).
106. Littlewood, T. D., Hancock, D. C., Danielianl, P. S. & Parker, M. G. A modified oestrogen receptor ligand-binding domain\nas an improved switch for the regulation of\nheterologous proteins. *Methods* **23,** 1686–1690 (1995).
107. Schlosser, I. *et al.* A role for c-Myc in the regulation of ribosomal RNA processing. *Nucleic Acids Res.* **31,** 6148–6156 (2003).
108. Feng, W. & Jasin, M. BRCA2 suppresses replication stress-induced mitotic and G1 abnormalities through homologous recombination. *Nat. Commun.* **8,** 525 (2017).
109. Liu, E. *et al.* The ATR-mediated S phase checkpoint prevents rereplication in mammalian cells when licensing control is disrupted. *J. Cell Biol.* **179,** 643–657 (2007).
110. Melixetian, M. *et al.* Loss of Geminin induces rereplication in the presence of functional p53. *J. Cell Biol.* **165,** 473–482 (2004).
111. Truong, L. N. *et al.* Homologous recombination is a primary pathway to repair DNA double-strand breaks generated during DNA rereplication. *J. Biol. Chem.* **289,** 28910–28923 (2014).

112. Davidson, I. F., Li, A. & Blow, J. J. Deregulated Replication Licensing Causes DNA Fragmentation Consistent with Head-to-Tail Fork Collision. *Mol. Cell* **24,** 433–443 (2006).
113. Mijic, S. *et al.* Replication fork reversal triggers fork degradation in BRCA2-defective cells. *Nat. Commun.* **in press,** (2017).
114. Kolinjivadi, A. M. *et al.* Smarcal1-Mediated Fork Reversal Triggers Mre11-Dependent Degradation of Nascent DNA in the Absence of Brca2 and Stable Rad51 Nucleofilaments. *Mol. Cell* **67,** 867–881.e7 (2017).
115. Taglialatela, A., Nanez, S. A., Huang, J. & Leuzzi, Giuseppe, B. L. and A. C. Restoration of replication fork stability and genome integrity in BRCA1- and BRCA2-deficient cells by inactivation of SNF2-family fork remodelers. *Mol. Cell* **in press,** (2017).
116. Liu, J. *et al.* Rad51 paralogues Rad55–Rad57 balance the antirecombinase Srs2 in Rad51 filament formation. *Nature* **479,** 245–248 (2011).
117. Taylor, M. R. G. *et al.* Rad51 Paralogs Remodel Pre-synaptic Rad51 Filaments to Stimulate Homologous Recombination. *Cell* **162,** 271–286 (2015).
118. Ma, C. J., Gibb, B., Kwon, Y., Sung, P. & Greene, E. C. Protein dynamics of human RPA and RAD51 on ssDNA during assembly and disassembly of the RAD51 filament. *Nucleic Acids Res.* **45,** 749–761 (2017).
119. Tarsounas, M., Davies, D. & West, S. C. BRCA2-dependent and independent formation of RAD51 nuclear foci. *Oncogene* **22,** 1115–1123 (2003).
120. Bailis, J. M., Luche, D. D., Hunter, T. & Forsburg, S. L. Minichromosome Maintenance Proteins Interact with Checkpoint and Recombination Proteins To Promote S-Phase Genome Stability. *Mol. Cell. Biol.* **28,** 1724–1738 (2008).
121. Bin Wang, Shuhei Matsuoka, Bryan A. Ballif, Dong Zhang, Agata Smogorzewska, Steven P. Gygi, S. J. E. Abraxas and RAP80 Form a BRCA1 Protein Complex Required for the DNA Damage Response. *Science (80-.).* **1,** 1194–1199 (2007).
122. Costantino, L. *et al.* Break-Induced Replication Repair of Damaged Forks Induces Genomic Duplications in Human Cells. *Science (80-.).* **343,** 88–91 (2014).
123. Sotiriou, S. K. *et al.* Mammalian RAD52 Functions in Break-Induced Replication Repair of Collapsed DNA Replication Short Article Mammalian RAD52 Functions in Break-Induced Replication Repair of Collapsed DNA Replication Forks. 1127–1134 (2016).

7. Acknowledgments

First and foremost I would like to thank Prof. Massimo Lopes for giving me the opportunity to pursue my PhD in his laboratory. It has been a challenging journey I am deeply grateful for his excellent scientific guidance, and particularly for his patience and support through tough times. I acknowledge the scientific freedom he has provided, which allowed me to develop my independent thinking.

I thank my PhD thesis committee members, Prof. Alessandro Sartori, and Prof. Martin Pruschy, for their valuable recommendations and suggestions during the course of this work. I am grateful also to the former member of my Phd committee, Prof. Fabrizio d'Adda di Fagagna, for his helpful inputs related to oncogene project during my first committee meeting and for openly sharing reagents.

I thank to our collaborators Dr. Pavel Jansack, Dr. Andre Nussenzweig and Arnab Chaudhuri for their valuable help and discussions. I would like to express my gratitude also to Center for Microscopy and Image Analysis of the University of Zurich for their amazing (literally 24/7) technical assistance.

Very special thank goes to Ralph Zellweger, Nagaraja Chappidi, Matteo Berti, Kurt Jacobs, Karun Mutreja, Sebastian Ursich, who contributed significantly to my work. Without you I would not be able to cross that finish line.

I am very grateful to all present and past Lopes lab members for sharing ideas and for helpful discussions throughout this time. In particular, I would like to thank Kai Neelsen for his guidance at the beginning of my PhD.

I would like to thank IMCR. It has been a wonderful place to work at and I particularly appreciate the willingness to share protocols, reagents, discussions, ideas, laughs and beers.

On a personal note, I extend my deepest regards to my family and Claudio Cantù for their unconditional support and love. You are my shelter and my force.

8. Curriculum vitae

PERSONAL INFORMATION

Name	Sofija Mijic
Date of birth	1. December 1987
Place of birth	Loznica, Serbia
Nationality	Switzerland

EDUCATION AND RESEARCH EXPERIENCE

March 2013 - present	**PhD in Cancer Biology** Supervisor: Prof. Massimo Lopes Thesis title: **The role of BRCA2 in the Maintenance of Genome Stability in Response to Replication Stress** Institute of Molecular Cancer Research University of Zürich Switzerland
August 2012 - December 2012	**Research Assistant** Konrad Basler Laboratory Institute of Molecular Life Sciences; University of Zürich Switzerland
May 2011- July 2012	**Master of Science in Biology, Molecular and Cellular Biology** Supervisor: Prof. Konrad Basler Thesis title: **Flac-ChIP: a novel method to investigate chromatin associated regulatory complexes in Drosophila melanogaster** Institute of Molecular Life Sciences, University of Zürich Switzerland
August 2010	**Summer internship** Supervisor: Dr. Daniel Bopp Project title: **Effect of missexpression of Tctra^{F} full-length and truncated Tctra$^{\Delta CAM}$ in T.casteneum and D.melanogaster** Institute of Molecular Life Sciences, University of Zürich Switzerland

2007-2012	**Bachelor of Science in Biology** Secondary Subject: Biochemistry Faculty of Sciences University of Zürich Switzerland
2003-2007	**High School Diploma** Liceo cantonale di Bellinzona Switzerland

TEACHING

Autumn Semester 2011	Practical course BIO 111: Molekulare und klassische Genetik Teaching theory and practical execution
Spring Semester 2014	Block course BIO 246: Genome Instability and Molecular Cancer Research Teaching and full time supervision of students in laboratory
Autumn Semester 2014	Practical course BIO 111: Molekulare und klassische Genetik Teaching theory and practical execution

COURSES AND CONFERENCES

April 2017	Talk Keystone Symposia meeting 'DNA Replication and Recombination' Santa Fe, New Mexico, USA
April 2016	Talk Genomic Integrity Forum 2016 EMBO YIP Sectorial meeting Seville, Spain
June 2016	Poster presentation 'At the Intersection of DNA Replication and Genome Maintenance: from Mechanisms to Therapy' Trieste, Italy
June 2015 '	StratCan Interactive Summer School in Cancer 2015 'Targeting DNA Repair in Cancer Saltsjöbaden, Stockholm

PUBLICATIONS

Mijic, Sofija; Zellweger, Ralph; Chappidi, Nagaraja; Berti, Matteo; Jacobs, Kurt; Mutreja, Karun; Ursich, Sebastian; Chaudhuri, Arnab Ray; Nussenzweig, Andre; Jansack, Pavel; Lopes, Massimo (2017). **Replication fork reversal triggers fork degradation in BRCA2-defective cells.** Nature Communications, accepted for pubblication.

Neelsen, Kai J; Zanini, Isabella M Y; Mijic, Sofija; Herrador, Raquel; Zellweger, Ralph; Ray Chaudhuri, Arnab; Creavin, Kevin D; Blow, J Julian; Lopes, Massimo (2013). **Deregulated origin licensing leads to chromosomal breaks by rereplication of a gapped DNA template.** Genes and Development, 27(23):2537- 2542.